2-9-2011

Human mitochondrial hotdog-fold thioesterase : hTHEM4 and hTHEM5

Hong Zhao

Recommended Citation

Zhao, Hong. "Human mitochondrial hotdog-fold thioesterase : hTHEM4 and hTHEM5." (2011). https://digitalrepository.unm.edu/chem_etds/9
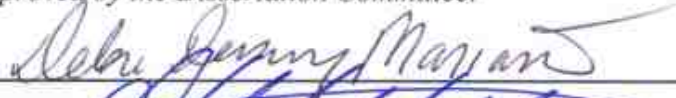
Hong Zhao

Candidate

Department of chemistry and chemical biology

Department

This dissertation is approved, and it is acceptable in quality and form for publication:

Approved by the Dissertation Committee:

_____, Chairperson

_____

_____

_____

_____

_____

_____

_____

HUMAN MITOCHONDRIAL HOTDOG-FOLD THIOESTERASE: hTHEM4 AND hTHEM5

BY

HONG ZHAO

B.S., Chemistry, Sichuan University, China, 2000
M.S., Chemistry, Sichuan University, China, 2003

DISSERTATION

Submitted in Partial Fulfillment of the
Requirements for the Degree of

Doctor of Philosophy

Chemistry

The University of New Mexico
Albuquerque, New Mexico

December, 2010

DEDICATION

To my parents, Shufen Zhang and Yinjiu Zhao, who always ask me how the experiment is going although they might not know too much about the enzyme, who have done so much for me in my life although I just did a little for them.

ACKNOWLEDGMENTS

I heartily acknowledge Dr. Debra Dunaway-Mariano, my research advisor, for opening a new scientific window for me, for continuing to encourage and support me through the years of research. Her guidance and professional style will remain with me as I continue my career.

I am so grateful to have worked and collaborated with several groups of outstanding scientists. Many thanks go to Dr. Patrick S Mariano, who has been giving me valuable advice and support for all these years. Many thanks go to Dr. Marco Bisoffi in the department of Biochemistry and Molecular Biology, University of New Mexico School of Medicine, for teaching me how to work on human cell line system, showing me the molecular biology research and provocative discussions. I am also grateful to Dr. Osnat Herzberg and Dr. Kap Lim, Dr. Manish Chandra in University of Maryland, who solved the structures of hTHEM4 and hTHEM5. In addition I would like to express my appreciation to Dr. Lusong Luo and his group at GlaxoSmithKline, who did the Akt1 activity experiment.

I also thank my committee member, Dr. Charles E Melancon for serving as committee member in the defense and taking time to read my dissertation. I would also like to thank all of the past and present members of Dr. Debra Dunaway-Mariano's group for their help and friendship.

And finally to my husband, Danqi, his support is the greatest gift of all.

HUMAN MITOCHONDRIAL HOTDOG-FOLD THIOESTERASE: hTHEM4 AND hTHEM5

BY

HONG ZHAO

ABSTRACT OF DISSERTATION

Submitted in Partial Fulfillment of the
Requirements for the Degree of
Doctor of Philosophy

Chemistry

The University of New Mexico

Albuquerque, New Mexico

December, 2010

Human Mitochondrial Hotdog-fold Thioesterase:
hTHEM4 and hTHEM5

Hong Zhao

B.S., Chemistry, Sichuan University, China, 2000

M.S., Chemistry, Sichuan University, China, 2003

Ph.D., Chemistry, University of New Mexico, 2010

ABSTRACT

Hotdog-fold acyl-CoA thioesterases (ACOTs) are found in all three kingdoms of life (Archaea, Bacteria and Eukarya). All the hotdog-fold thioesterases share common catalytic scaffold and function: hydrolysis of acyl-CoA or acyl-ACP (acyl carrier protein). However the biological roles that they perform vary greatly, different substrate specificity and catalytic efficiency assign unique set of biological functions to each of them, which is further defined by tissue distribution, cellular location, protein partners and regulators.

The focuses of my doctoral studies, described in this dissertation, are two members of the human hotdog-fold thioesterase superfamily: human THEM4 and human THEM5. The genes encoding hTHEM4 and hTHEM5 are two adjacent brothers in the chromosome 1q21.3. Expression of truncated hTHEM4(Δ39) in *E. coli* produced a homogenous product. In vitro activity analysis proved that hTHEM4 is a high activity,

broad substrate range, acyl-CoA thioesterase. In addition to hydrolysis of short and long chain acyl-CoAs (k_{cat}/K_M value: 10^4 to 10^6 $M^{-1}s^{-1}$), it also catalyzes the hydrolysis of myristoyl-ACP and palmitoyl-ACP. The X-ray structure of hTHEM4(Δ39) bound with an inert fatty acyl-CoA analog revealed that N-terminal domain is two separate helix inserts coupled with a disordered extended loop. In order to understand the relationship between hTHEM4 and Akt1, the effect of purified (fl)hTHEM4 and hTHEM4(Δ39) on the phosphorylation (activation) and activity of full-length and truncated Akt1 were tested at GlaxoSmithKline. The results showed that (fl) hTHEM4 has a small but significant direct effect on Akt1 catalytic activity, and also on Akt1 activation at both Thr308 (by PDK1) and Ser473 (by mTORC2). The co-immunoprecipitation experiment was also carried out to investigate the physical association between hTHEM4 and Akt1. Taken together, hTHEM4 and Akt1 are associated with each other, and the effect (inhibition or activation) is concentration-dependent.

The full-length hTHEM5 was expressed in HEK 293T cells at a high level compared to that observed for the hTHEM4. The hTHEM5(Δ40) X-ray structure depicts essentially the same active site observed for hTHEM4, and no features that we recognize which might explain the difference in expression level in transfected HEK 293T cells. Interestingly, the in vitro kinetic studies carried out with hTHEM5(Δ40) showed a similar substrate specificity profile, yet a 100-fold drop in k_{cat}. The cellular location imaging of hTHEM5 in transfected HEK 293T cells using hTHEM5-GFP and (Δ32)-hTHEM5-GFP fusions showed specific mitochondrial location of hTHEM5-GFP and a distributive location of the (Δ32)-hTHEM5-GFP.

In parallel with the biological function study, a structure-function analysis of hTHEM4 and hTHEM5 mechanisms of catalysis and substrate recognition was also carried out. Structure guided site directed mutagenesis and steady-state kinetic analysis of the purified mutants has been done to identify the enzyme residues that contribute to substrate binding and catalysis. Single turnover experiment in $H^{18}O$ was done to define the role of the active carboxylate residue (nucleophilic vs base).

TABLE OF CONTENTS

LIST OF FIGURES

LIST OF TABLES

CHAPTER ONE

INTRODUCTION

1.1 Overview of Acyl-CoA Thioesterase and Fatty Acid Metabolism

Acyl-CoA thioesterases, also known as acyl-CoA hydrolases, are a group of enzymes that hydrolyze CoA thioesters, such as acyl-CoAs (saturated, unsaturated, branched chain), bile acid-CoAs, and CoA esters of prostaglandins, to produce the corresponding free acids and coenzyme A. Therefore, these enzymes are putative regulators of the cellular levels of CoA thioesters, free acids and CoAs. Acyl-CoA thioesterases are found in both prokaryotes and eukaryotes. In mammalian cells, these enzymes are localized in distinct cellular organelles including the mitochondria, peroxisomes, cytosol and endoplasmic reticulum (*1,2*).

The concentrations of long-chain acyl-CoAs are in the range 0.2-3.1 mM within mitochondria (*3,4*), 0.4 mM within peroxisomes (*3*) and 30-90 µM in the cytosol (*3,5*). The total CoASH (free CoASH plus CoASH thioesters) concentration has been estimated to be 0.14 mM in the cytosol, 0.7 mM in peroxisomes and over 5 mM in mitochondria (*3*). The changes in cellular free CoASH, long-chain acyl-CoA, peroxisomal β-oxidation and cellular acyl-CoA thioesterases are strikingly coordinated thereby connecting the acyl-CoA thioesterases to the metabolism of fatty acids (*6*).

Mitochondria are sometimes described as " cellular power plants" because they supply energy to the cell by generating adenosine triphosphate (ATP) through the oxidation of the organic metabolites via the citric acid cycle. Key to this process is β-

oxidation of the fatty acids, which are present as fatty acyl-CoA adducts exemplified by palmitoyl-CoA. The β-oxidation of fatty acids involves three stages (see Figure1.1) including the (1) activation of fatty acids in the cytosol. (2) transport of fatty acids into mitochondria (carnitine shuttle). (3) β-oxidation in the mitochondrial matrix. During the β-oxidation process, the fatty acyl-CoAs are broken down in mitochondria and/or peroxisomes to generate acetyl-CoA (see Figure 1.2) (*7*). Acetyl-CoA will then enter the citric acid cycle, which is of central importance in all living cells that use oxygen as part of cellular respiration (see Figure 1.3) (*8*). In eukaryotic cells, the citric acid cycle takes place in the matrix of the mitochondria. The requirement for free CoASH within mitochondria is very high as it is a critical intermediate in not only the citric acid cycle but also in β-oxidation and other metabolic pathways. Therefore, a readily available supply of CoASH is essential for optimal mitochondrial function.

The free fatty acids liberated from the acyl-CoAs and acyl-ACPs (acyl carrier proteins) by the action of thioesterases are also implicated in several essential biological processes. Fatty acids are transported across the inner mitochondrial membrane by the protein UCP3 and then esterified with CoASH by the membrane bound fatty acyl-CoA synthetase so that they enter the mitrochondrial matrix for oxidation in the form of fatty acyl-CoA thioesters. The fatty acyl-CoA thioesterase governs the concentrations of free CoASH and free fatty acids inside the mitochondrion by hydrolyzing the fatty acyl-CoA thioesters.
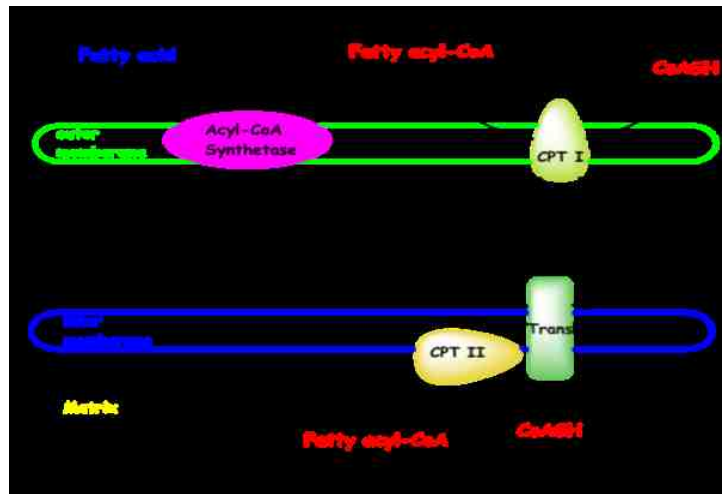
Figure 1.1 Three stages of the β-oxidation of fatty acids in mitochondrial matrix
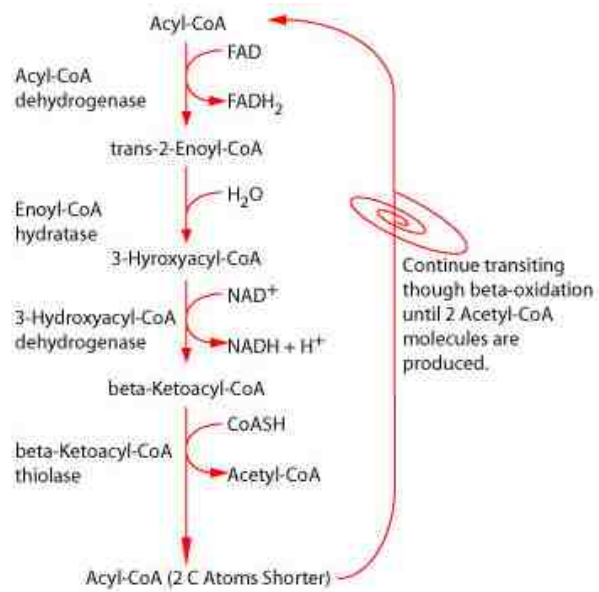
Figure 1.2 The mitochondrial fatty acid β-oxidation of saturated fatty acids
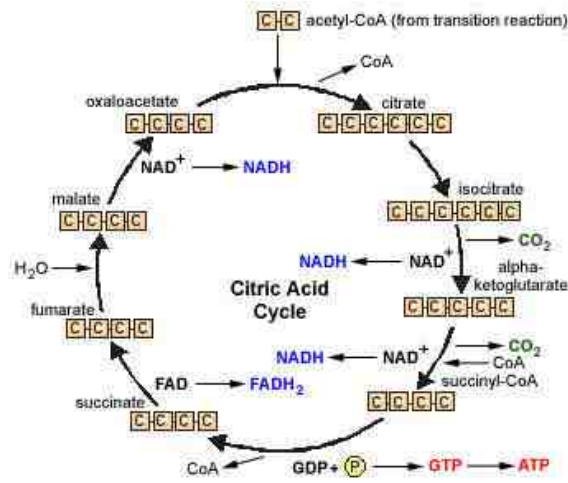
Figure 1.3 The citric acid cycle

Peroxisomes are involved in the metabolism of a variety of lipids, including very long chain fatty acids, dicarboxylic fatty acids, bile acid intermediates, prostaglandins, leukotrienes, thromboxanes, pristanic acid and xenobiotic fatty acids (*9,10*). Two different sets of enzymes catalyze β-oxidation of CoA esters of very long straight chain fatty acids, prostaglandins, and dicarboxylic fatty acids and the oxidation of branched-chain fatty acids and bile acids. Continuous β-oxidation depends on the availability of acyl-CoA, NAD, free CoASH and carnitine. Therefore acyl-CoA thioesterases play an important role in controlling both acyl-CoA and CoASH levels within the peroxisome.

The cytosol consists mostly of water containing dissolved ions, small molecule metabolites, and large water-soluble macromolecules (such as proteins and tRNAs). In prokaryotes, metabolism takes place in the cytosol and only a few metabolic reactions occur within the membrane and periplasmic space. While many metabolic pathways still occur in the cytosol of eukaryotes, others operate within organelles. Acyl-CoA thioesterases, particularly the brain thioesterases purified from the cytosol of rat (*11,12*)

4

and human (*13*) show very high activity towards arachidonoyl-CoA. As arachidonic acid is the substrate for enzymatic production of prostaglandins, leukotrienes and thromboxanes, and steroids, acyl-CoA thioesterases play an important role in regulating these pathways. Free fatty acids or acyl-CoA esters can bind to fatty acid-binding proteins present in the cytosol of many different tissues. This provides a mechanism for intracellular lipid trafficking. Fatty acid ω-oxidation produces dicarboxylic acids in the cytosol, which can be transformed to CoASH esters in the endoplasmic reticulum and chain-shortened by peroxisomal β-oxidation prior to excretion.

1.2 Type I and Type II Acyl-CoA Thioesterases (ACOTs)

Two types of acyl-CoA thioesterases (ACOTs for human; Acots for rhodent) have been identified thus far. Type I ACOTs have been found in animals only, while Type II variants are present in most living organisms (*14*). Type I ACOTs are believed to contain an α/β hydrolase catalytic domain in the C-terminal region, with a Ser-Asp-His catalytic triad. Type II thioesterases possess the so-called "hot-dog" fold (*15*). Type I ACOTs are found in a mouse gene cluster comprised of six genes encoding acyl-CoA thioesterase with locations in cytosol (Acot1), mitochondria (Acot2), and peroxisomes (Acot3-6), while the corresponding human gene cluster contains only four thioesterase proteins (ACOT1, ACOT2, ACOT4 and ACOT6). Human ACOT1 and ACOT2 share similar characteristics with the corresponding mouse genes. Human ACOT4 carries the activities of three mouse peroxisomal ACOTs (Acot3, 4, and 5). Human ACOT6 is not known to be a full length active protein since translation of the its gene begins from a

methionine present at the end of exon 2. Despite the fact that there are three exons encoding *ACOT*, the mouse Acot6 is expressed as a truncated 46-kDa protein (*16*). A unique feature of rodent type-I Acots is their ability to be upregulated by peroxisome proliferating agents. For example, Neuman et al. demonstrated that an increase in liver Acot2 mRNA transcription occurs in rodents administered with di(2-ethylhexyl)phthalate (DEHP) (*17*). This discovery enabled the over-expression of the protein and its characterization. However, this upregulatory effect has not yet been observed in humans (*18, 19*).

Type II ACOTs (ACOT7, ACOT8, ACOT9, ACOT11, ACOT12 and ACOT13) contain one or two "hot-dog" fold domains. ACOT7/Acot7 is the most extensively studied acyl-CoA thioesterase, because of its specificity for arachidonoyl-CoA and purported role in inflammation. The *Acot7* gene is expressed as multiple isoforms in a tissue-specific manner. The expression in tissues other than the brain and testis is likely to have an impact on fatty acid metabolism (*20, 21*). Research aimed at the identification of individuals with specific acyl-CoA thioesterase deficiencies among clinical patients with suspected mitochondrial fatty acid oxidation disorders revealed that lowered levels of thioesterase activity in the human skin fibroblasts correlate with lowered levels of ACOT7 (*22*). ACOT8 (first known as PTE-2) is ubiquitously expressed and it is induced at the mRNA level by treatment with the peroxisome proliferator and by fasting. The recombinant Acot8 from mouse showed highest activities against CoA thioesters of the primary bile acids choloyl-CoA and chenodepxycholoyl-CoA that are present in peroxisome. The catalytic activity is inhibited by free CoASH, suggesting that

intraperoxisomal free CoASH levels regulate the activity of this enzyme. The acyl-CoA specificity of recombinant Acot8 closely resembles that of the enzyme purified from mouse liver peroxisomes. This observation suggests that Acot8 is the major acyl-CoA thioesterase in peroxisomes and Acot8 may function as a key regulator of peroxisomal lipid metabolism (*23*).

Two isoforms of the murine 48-kDa enzymes, named Acot9 (encoded by the X chromosome) and Acot 10 (encoded by chromosome 15), contain a 20-amino acid N-terminal mitochondrial targeting sequence, The mitochondrial location of these proteins was confirmed by using immunofluorescence and confocal microscopy (*24*). ACOT11/Acot11 (also known as BFIT, them1) can be induced in mouse brown adipose tissue (BAT) by exposure to warm temperatures. This up-regulation could serve several possible purposes including (1) to cause an increase in nonesterified fatty acids available to release inhibition placed upon thermogenin (UCP1), (2) to serve to decrease cellular levels of esterified FAs thereby slowing β-oxidation and futile ATP generation, and (3) to bring about regulation of mitochondrial levels of CoASH (*25*).

Human ACOT12, cloned and expressed in insect cells, consists of two hotdog fold domains and a C-terminal steroidogenic acute regulatory protein-related lipid transfer (START) domain. The enzyme exhibits high specificity towards acetyl-CoA and it is activated by ATP and inhibited by ADP (*26*). ACOT13 (human thioesterase superfamily member 2:hTHEM2) and mouse Acot13 have been reported to bind medium to long chain acyl-CoAs tightly but to display low catalytic turnover with these substrates (*27, 28*).

7

1.3 Properties of Mammalian ACOTs

1.3.1 Substrate Specificity of Mammalian ACOTs

Studies of the substrate specificities of acyl-CoA thioesterases showed that saturated and unsaturated, short, medium and long-chain acyl-CoAs, and branched-chain acyl-CoAs serve as substrates for these enzymes (*23, 24, 27, 28, 29, 30*).

Table 1.1 Summary of substrate specificity of mammalian ACOTs

ACOTs	Preferred Substrate
ACOT1,	Long-chain saturated acyl-CoAs (C12~C20), K_m is 2~4 μM
ACOT2	Long-chain unsaturated acyl-CoAs: C16:1, C18:1 and C18:1 trans. Typical K_m for ACOT2 is 4~6μM. No detectable activity with acyl-CoAs of eight carbon atoms or shorter.
ACOT4	Dicarboxylyl-CoA: Succinyl-CoA (K_m=13.3±1.32 μM) Glutaryl-CoA (K_m=37.2±9.05μM)
ACOT6	Methyl-branched acyl-CoAs: phytanoyl-CoA, Pristanoyl-CoA
ACOT7	Unsaturated long-chain acyl-CoA: Arachidonoyl-CoA
ACOT8	Branched-chain acyl-CoA: choloyl-CoA, chenodeoxycholoyl-CoA, 4,8-Dimethyl nonanoyl-CoA
ACOT9	Myristoyl-CoA
ACOT12	Short-chain acyl-CoA: acetyl-CoA
ACOT13	Long-chain acyl-CoA: Myristoyl-CoA, arachidonoyl-CoA

1.3.2 Subcellular Localization and Tissue Distribution of Mammmmalian ACOTs

The specific cellular localization and tissue distribution appears to determine the different biological functions of the ACOTs. ACOT1, ACOT6, ACOT7 (isoforms) ACOT12 and ACOT13 are located in the cytosol, whereas ACOT4 and ACOT8 are peroxisomal proteins. ACOT2, ACOT7 (one isoform) and ACOT9 are found in mitochondria. In addition, ACOTs are found mostly in brain (ACOT7, ACOT9), liver (ACOT12), kidney (ACOT4, ACOT13) and testis tissues, and some are specifically located in white (ACOT6) and brown adipose tissue (ACOT11).

ACOTs that are found in tissues, like kidney and liver, are closely related to fatty acid oxidation. Brain and testis contain by far the highest ACOT activities. The long-chain acyl-CoA hydrolyzing activity in brain is much higher than any other organ in the body (*31, 32, 33*). Adipose tissue contains a hormone-sensitive lipase (HSL), which is activated by PKA-dependent phosphorylation. The activation process increases the release of fatty acids into the blood, which in turn leads to increased oxidation of fatty acids in other tissues, such as muscle and liver. In the liver, the net result of increased acetyl-CoA levels is the production of ketone bodies, which occurs under conditions where carbohydrates and gluconeogenic precursors in the liver are not sufficient to enable increased glucose production. Fatty acids that are produced in response to glucagon or epinephrine will be completely oxidized. Since PKA also phosphorylates acetyl-CoA carboxylase, the synthesis of fatty acid is thereby inhibited.

1.3.3 Putative Cellular Functions Other Than Metabolism of Fatty Acids

Many significant advances have been made in the functional characterization of type-I and -II human ACOTs in recent years. Elucidation of the roles played by these enzymes has revealed that they are associated with lipid biosynthesis via allosteric regulation of enzymes, regulation of ion channel opening, signal transduction, budding and fusion of intracellular membranes, and regulation of gene transcription via nuclear receptors. Evidence also exits suggesting that ACOTs may be linked to neurodegenerative diseases, epilepsy, obesity and inflammation. An example of this is found in the role played by Acot7 in brain function. Analysis of acyl-CoA thioesterases within the developing mouse brain revealed that the expression of *Acot7* increases during the period starting from day twelve during embryogenesis and ending at day seven following birth. After this period, expression of this protein declines until it reaches *ca.* 70% of the highest expression level (*34*). This expression occurs only in brain cells that have differentiated into the neuronal lineage, a finding that is consistent with the results of earlier studies that characterized Acot7 as being exclusively localized to neurons (*35*).

1.3.4 Structure of Mammalian Acyl-CoA Thioesterases

Mammalian ACOTs belong to either the α/β hydrolase or the hotdog-fold family. All type-I ACOTs contain a N-terminal β-sandwich domain and a C-terminal α/β hydrolase catalytic domain. Type-II ACOTs differ in their domain content and organization. The most simple member ACOT13, consists of a single hot-dog domain

while ACOTs7-10 have two tandem double hot-dog domains, in which two pairs of hot-dog domains are fused. Finally, ACOTs11 and 12 possess an additional C-terminal START domain and two tandem double hot-dog fold domains.

The crystal structure of ACOT2, determined by Tong L. and coworkers (*36*), Shows the presence of two domains, including a C-terminal domain, which has a α/β hydrolase fold that positions the catalytic triad Ser294-His422-Asp388. Its N-terminal domain contains a seven-stranded β-sandwich, which has some distant structural homologs in other proteins (Figure 1.4), that does not contribute any catalytic active site residues. It is possible that the N-terminal domain plays a role in regulating the specificity for acyl-CoA substrates, although this has not been formally probed.
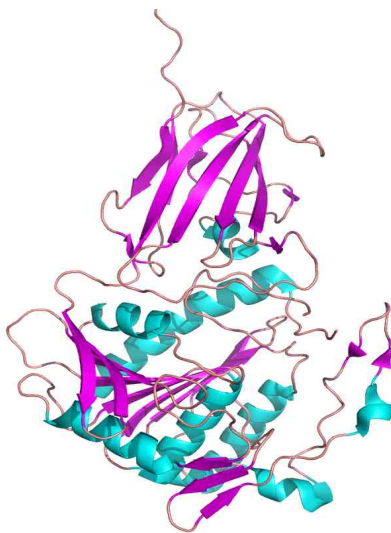
Figure 1.4 The crystal structure of ACOT2. The N-terminal domain is located at the top of the illustration.

The structures of Type II ACOTs have not been fully characterized since the X-ray structures of only ACOT13 (also known as hTHEM2) and ACOT7 have been determined. The apo structure of ACOT13, reported in 2006(*37*), shows that it is comprised of four monomers, each containing a single hotdog domain, which are organized into a back-to-back tetramer. Later (*27*), the structure of ACOT13, complexed with the inert substrate analog undecan-2-one-CoA, was reported (Figure 1.5). This structure enabled characterization of the substrate binding sites and catalytic residues, which were evaluated using site directed mutagenesis techniques.
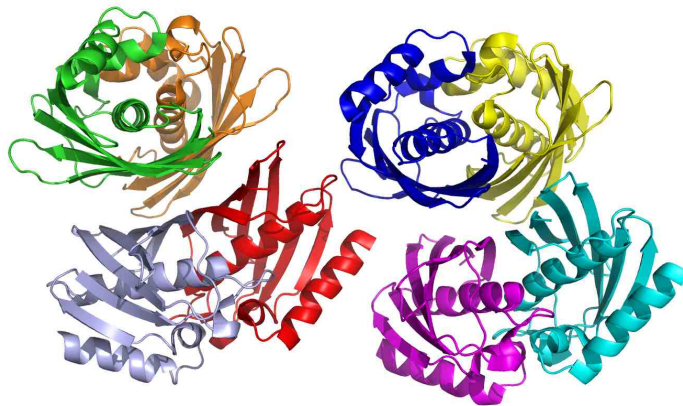
Figure 1.5 The X-ray crystal structure of ACOT13 (hTHEM2) showing the two tetramers observed in the asymmetric cell. The individual subunits are separately colored (37).

The crystal structure of the mouse acyl-CoA thioesterase 7 (ACOT7) was determined in 2007 (*38*). The engineered N- and C-terminal double hotdog fold domains of this protein, produced in *E. coli,* were crystallized separately for structure determination and a model of the structure of the full-length enzyme was generated

using chemical cross-linking, mass spectrometry, and molecular modeling observations. The quaternary structure of ACOT7 features a trimer of hotdog fold dimers. Both domains are required for activity, but only one of two possible active sites in the dimer is functional. Asn24 and Asp213 (from N- and C-domains, respectively) were identified as important catalytic residues through the use of site-directed mutagenesis.

1.4 Statement of Doctoral Research Goals

Human thioesterase superfamily member 4 (hTHEM4) and member 5 (hTHEM5) are new members of the type II ACOTs. Each has a special domain organization comprised of an unknown N-terminal domain and a hotdog fold domain. hTHEM4, also known as the Akt1 C-terminal regulatory protein, and hTHEM5 are paralogs whose encoding genes are neighbors on the human chromosome. The focus of my doctoral studies, described in this dissertation, was the cellular location, X-ray structure, chemical and biological function, catalytic mechanisms, and regulation of the two hotdog thioesterases hTHEM4 and hTHEM5.

References

1. Hunt, M.C. and Alexson, S.E. (2002). The role Acyl-CoA thioesterases play in mediating intracellular lipid metabolism. Prog. Lipid Res. 41,99-130.

2. Kirkby, B., Roman N., Kobe, B., Kellie, S., Forwood, J.K. (2010). Functional and structural properties of mammalian acyl-coenzyme A thioesterases. Prog. Lipid Res. doi:10.1016/j.plipres.2010.04.001.[Epub ahead of print].

3. Horie, SC., Isobe, M., Suga, T. (1986). Changes in CoA pools in hepatic peroxisomes of the rat, under various conditions. J. Biochem. 99,1345-52.

4. Alexson, S.H.E., Nedergaard, J., Cannon, B. (1985). Inhibition of acetyl-carnitine oxidation in rat brown-adipose-tissue mitochondria by erucoyl-carnitine is due to sequenstration of CoA. Biochim Biophys Acta. 834, 149-58.

5. Deeney J.T., Tornheim, K., Korchak, H.M., Prentki, M., Corkey, B.E. (1992). Acyl-CoA eaters modulate intracellular Ca^{2+} handling by permeabilized clonal pancreatic β-cells. J. Biol Chem. 273, 26383-7.

6. Berge, R.K., Aarsland A. (1985) Correlation between the cellular level of long-chain acyl-CoA, peroxisomal beta-oxidation, and palmitoyl-CoA hydrolase activity in rat liver. Are the two enzyme systems regulated by a substrate-induced mechanism?. Biochim Biophys Acta. 837(2), 141–151.

7. Picture downloaded from http://www.reactome.org

8. Picture downloaded from http://student.ccbcmd.edu

9.Van, Veldhoven PP., Mannaerts GP. (1999) Role and organization of peroxisomal beta-oxidation. Adv Exp Med Biol. 466, 261-72.

10. Hashimoto T. (1999) Peroxisomal beta-oxidation enzymes. Neurochem Res 24, 551-63.

11. Yamada J, Furihata T, Tamura H, Watanabe T, Suga T. (1996) Long-chain acyl-CoA hydrolase from rat brain cytosol: purification, characterization, and immunohistochemical localization. Arch Biochem Biophys. 326,106–114.

12. Broustas CG, Hajra AK.(1995) Purification, properties, and specificity of rat brain cytosolic fatty acyl coenzyme A hydrolase. J Neurochem. 64(5), 2345–2353.

13. Yamada J, Kurata A, Hirata M Taniguchi T, Takama H, Furihata T, Shiratori K, Iida N, Takagi-Sakuma M, Watanabe T, Kurosaki K, Endo T, Suga T. (1999) Purification, molecular cloning, and genomic organization of human brain long-chain acyl-CoA hydrolase. J Biochem. 126(6),1013-9.

14. Mandel, R. C., Tweel, B., Tong L. (2009) Crystal structure of human mitochondrial acyl-CoA thioesterase (ACOT2). Biochem Biophys Res Commun. 385(4), 630-3.

15. Huhtinen K., O'Byrne, J., Lindquist, Per J.G., Contreras, A.J., Alexon S.E.H. (2002) The peroxisome proliferator-induced cytosolic Type I acyl-CoA thioesterase (CTE-I) is a serine-histidine-aspsrtic acid α/β hydrolase. J Biol Chem 277, 3424-3432.

16. Hunt, M.C., Rautanen, A., Westin, A.K.M., Svensson, T., Alexon, S.E.H. (2006) Analysis of the mouse and human acyl-CoA thioesterase (ACOT) gene clusters shows that convergent, functional evolution results in a reduced number of human peroxisomal ACOTs. FASEB J 20, 1855-1864.

17. Neuman, I., Maloberti, P., Lisdero, C., Colonna, C., Peralta, J., Poderoso, J. J., Podesta, E.J. (2002) β-Adrenergic stimulation controls the expression of a thioesterase

specific for very-long-chain fatty acids in perfused hearts. Biochem Biophys Res Commun. 299(1),135-41.

18. Yamada, J. (2005) Long-chain acyl-CoA hydrolase in the brain. Amino Acids. 28(3), 272-8.

19. Mandard, S., Müller M., Kersten, S. (2004) Review: peroxisome proliferator-activated receptor α target genes. Cell Mol Life Sci. 61, 393-416.

20. Hunt, M.C., Yamada, J., Maltais, L.J., Wright, M., Podesta, E.J., Alexson, S.E.H. (2005) A revised nomenclature for mammalian acyl-CoA thioesterse/hydrolases. J Lipid Res. 46, 2029-32.

21. Hunt, M.C., Greene, S., Hultenby, K., Svensson, L.T., Engberg, S., Alexson, S.E.H. (2007) Alternative exon usage selectively determines both tissue distribution and subcellular localization of the acyl-CoA thioesterse 7 gene products. Cell Mol Life Sci. 64,1558-70.

22. Hunt, M.C., Ruiter, J., Mooyer, P., van Roermond, C.W., Ofman, R., Ijlst, L., Wanders, R.J. (2005) Identification of fatty acid oxidation disorder patients with lowered acyl-CoA thioesterase activity in human skin fibroblasts. Eur J Clin Invest. 35(1), 38-46.

23. Hunt, M.C., Solaas, K., Kase, B.F., Alexson, S.E.H. (2002) Characterization of an acyl-CoA thioesterase that functions as a major regulator of peroxisomal lipid metabolism. J Biol Chem. 277(2), 1128-38.

24. Poupon, V., Begue, B., Gagnon, J., Dautry-Varsat, A., Cerf-Bensussan, N., Benmerah, A. (1999) Molecular cloning and characterization of MT-ACT48, a novel mitochondrial acyl-CoA thioesterase. J Biol Chem. 274(27), 19188-94.

25. Adams, S.H., Chui, C., Schilbach, S.L., Yu, X.X., Goddard, A.D., Grimaldi, J.C., Lee, J., Dowd, P., Colman, S., Lewin, D.A. (2001) BFIT, a unique acyl-CoA thioesterase induced in thermogenic brown adipose tissue: cloning, organization of the uman gene and assessment of a potential link to obesity. Biochem J. 360, 135-42.

26. Suematsu, N., Isohashi, F. (2006) Molecular cloning and functional expression of human cytosolic acetyl-CoA hydrolase. Acta Biochim Pol. 53(3), 553-61.

27. Cao, J., Xu, H., Zhao, H., Gong, W.M., Dunaway-Mariano, D. (2009) The mechanisms of human hotdog-fold thioesterase 2 (hTHEM2) substrate recognition and catalysis illuminated by a structure and function based analysis. Biochemistry. 48(6), 1293-304.

28. Wei, J., Kang, H.W., Cohen, D.E. (2009) Thioesterase superfamily member 2 (Them 2)/ acyl-CoA thioesterase 13 (Acot13): a homotetrameric hotdog fold thioesterase with selectivity for long-chain fatty acyl-CoAs. Biochem J. 421, 311-22.

29. Jones, J. M., Gould, S.J. (2000) Identification of PTE2, a human peroxisomal long-chain acyl-CoA thioesterase. Biochem Biophys Res Commun. 275, 233-40.

30. Westin, M.A.K., Hunt, M.C., Alexson, S.E.H. (2005) The identification of a succinyl-CoA thioesterase suggests a novel pathway for succinate production in peroxisomes. J Biol Chem. 280(46), 38125-32.

31. Kurooka, S., Hosoki, K., Yoshimura, Y. (1972) Some properties of long fatty acyl-Coenzyme A thioesterase in rat organs. J Biochem. 71(4), 625-34.

32. Anderson, A.D., Erwin, V.G. (1971) Brain acyl-coenzyme A hydrolase: distribution, purification and properties. J Neurochem. 18(7), 1179-86.

33. Knauer, T.E. (1979) Factors affecting the activity and stability of the palmitoyl-coenzyme A hydrolase of rat brain. Biochem J. 179(3), 515-23.

34. Yamada, J., Kuramochi, Y., Takagi, M., Suga, T. (2004) Expression of acyl-CoA hydrolase in the developing mouse brain. Neurosci Lett. 355(1-2), 89-92.

35. Kuramochi, Y., Takagi-Sakuma, M., Kitahara, M., Emori, R., Asaba, Y., Sakaguchi, R., Watanabe, T., Kuroda, J., Hiratsuka, K., Nagae, Y., Suga, T., Yamada, J. (2002) Characterization of mouse homolog of brain acyl-CoA hydrolase: molecular cloning and neuronal localization. Brain Res Mol Brain Res. 98(1-2), 81-92.

36. Mandel, C.R., Tweel, B., Tong, L. (2009) Crystal strucuture of human mitochondrial acyl-CoA thioesterase (ACOT2). Biochem Biophys Res Commun. 385, 630-3.

37. Cheng, Z.J., Song, F., Shan, X.Y., Wei, Z.Y., Wang, Y.L., Dunaway-Mariano, D., Gong, W.M. (2006) Crystal structure of human thioesterse superfamily member 2. Biochem Biophys Res Commun. 349, 172-7.

38. Forwood, J.K., Thakur, A.S., Guncar, G., Marfori, M., Mouradov, D., Meng, W.N., Robinson, J., Huber, T., Kellie, S., Martin, J.L., hUME, D.A., Kobe, B. (2007) Structural basis for recruitment of tandem hotdog domains in acyl-CoA thioesterase 7 and its role in inflammation. Proc Natl Acad Sci USA, 104(25), 10382-7.

CHAPTER TWO

CHARACTERIZATION OF HUMAN THIOESTERASE

SUPERFAMILY MEMBER 4 (HTHEM4)

2.1 Introduction

Hotdog-fold acyl-CoA thioesterases (ACOT) are found in all three kingdoms of life (Archaea, Bacteria and Eukarya). Typically *ca.*10 different hotdog-fold thioesterases exist per organism, all of which share a common catalytic scaffold and a common chemical function involving catalysis of the hydrolysis of acyl-CoA or acyl thioesters of the acyl carrier protein (ACP). However, the biological roles that these thioesterase perform vary greatly. The differences in substrate specificities and catalytic efficiencies result in a unique set of biological functions for each, which is further defined by tissue distributions, cellular locations, protein partners and regulators. hTHEM4, also known as the carboxyl-terminal modulator protein (CTMP), is a two-domain protein made up of 240 amino acids. The C-terminal domain (*ca.* 100 amino acids) is homologous to the phenylacetyl-CoA thioesterase (PaaI) of *E. coli*. On the other hand, the N-terminal domain has no known counter part in living organisms. Our attention was first drawn to hTHEM4 by a report that it is a regulator of protein kinase B α (also known as Akt1 or PKBα) (*1*) and that epigenetic down-regulation of hTHEM4 transcription is a common aberration in glioblastmas (*2*). Whereas the connection between Akt1/PKBα activity and cancer is well known (*3*), the link between the hotdog-fold thioesterase hTHEM4 and Akt1/PKBα activity is not known.

2.1.1 Domain Structure of hTHEM4

The gene coding for the human hotdog thioesterase hTHEM4 is located at chromosome 1q21 and contains six coding exons. Sequence analysis suggests that hTHEM4 is comprised of an unknown N-terminal domain and a C-terminal hotdog fold domain (Figure 2.1). The C-terminal domain (residues 100-240) shares 17% sequence identity with the bacterial hotdog fold phenylacetyl-CoA thioestase PaaI (Figure 2.2).

Figure 2.1 Domain structure of hTHEM4

Figure 2.2 Sequence alignment of hTHEM4 (100-240 residues) and the E.coli hotdog thioesterase PaaI.

20

2.1.2 Biological Significance of hTHEM4

hTHEM4 is also known as the carboxyl-terminal modulator protein CTMP. In the original study describing CTMP published in 2001, Hemmings and co-workers reported evidence from *in vivo* studies that hTHEM4 binds to the C-terminal regulatory domain of Akt1/PKBα and that it negatively regulates Akt1/PKBα *in vivo*. In addition, these workers reported that hTHEM4 forms an endogenous complex with Akt1/PKBα at the plasma membrane and that the effect of its binding is to reduce Akt1/PKBα phosphorylation at Ser473, resulting in a decrease in Akt1/PKBα activity. Further exploration of the effect of hTHEM4 on downstream effectors of Akt1/PKBα revealed that (1) coexpression of hTHEM4 (Flag-CTMP) completely abolish the inhibitory effect of Akt1/PKBα on c-*fos*-mediated transcription, (2) over-expression of hTHEM4 reduced phosphorylation of glycogen synthase kinase-3β (GSK-3β) on Ser9, a known Akt1/PKBα -mediated phosphorylation event, and (3) over-expression of hTHEM4 reverted the phenotype of AKT8 cells (CCL64 cells stably expressing *v-Akt1/PKBα*), inhibited the uncontrolled proliferation induced by *v-Akt1/PKBα*, and abolished or delayed the tumor growth in mice injected with AKT8 cells (*1*).

It has long been known that Akt1/PKBα plays a key role in cell proliferation, cellular survival, and transformation. Indeed, Akt1/PKBα has emerged as a central player in tumorgenesis (*3*). Hence, elucidating the molecular details of the modulation effect of hTHEM4 on Akt1/PKBα is an important goal. Since 2001, a number of publications have appeared describing hTHEM4 in the context of cancer, neurological disorders, diabetes, or cell apoptosis. For example, one study led to a successful lung cancer gene therapy in mice, in which the overexpression of exogenous hTHEM4 was utilized to inhibit

Akt1/PKBα (*4,5*). Another investigation of hTHEM4 expression in a variety of glioblastoma cells (*2,6*) demonstrated that at least a 50% decrease in hTHEM4 mRNA levels relative to non-neoplastic brain tissue takes place, supporting the proposed inhibitory effect of hTHEM4 on Akt1/PKBα activity. It was also found that a reduced mRNA level is related to the hypermethylation of the hTHEM4 promoter, thus, suggesting that the epigenetic down-regulation of hTHEM4 transcription might be a common aberration in glioblastomas. In contrast to the original suggestion (*1*) that Akt1/PKBα recruits hTHEM4 to the membrane and in this manner becomes resistant to activation by phosphorylation, Ono et al. (*7*) reported that hTHEM4 associates with and recruits Akt1/PKBα to the membrane where it is activated by phosphorylation catalyzed by upstream kinases.

In addition, the possible role of hTHEM4 in neurological disorders has been probed. Specifically, analysis of the coding sequences of hTHEM4 in Focal Cortial Dysplasias (FCD), using Taylor-type ballon cells (FCD$_{IIb}$), revealed a C to G polymorphism at the nucleotide position 113 of exon 2, which results in a serine to cysteine amino-acid exchange (Ser38Cys) in the protein product (*8*). Although Ser38 in hTHEM4 is an kinase phosphorylation site (*9*), which might link this mutant with the pathogenic role of activated Akt1/PKBα, further investigations were unable to produce evidence for the involvement of hTHEM4 in FCD$_{IIb}$ (*8*). In recent work (*10*), it has been shown that global ischemia triggers the expression and activation hTHEM4 in selectively vulnerable hippocampal neurons by binds to and inhibiting Akt1/PKBα activity and that hTHEM4 is essential to ischemia-induced neuronal death.

2.1.3 Mitochondrial Location of hTHEM4 and its Role in Cell Apoptosis

hTHEM4 residues 1-32 [MLRSCAARLRTLGALCLPPVGRRLPGSEPRP] are predicted by MitoProt II (*11*) to comprise a mitochondrial localization sequence (MLS). This prediction was experimentally verified by Hemmings and co-workers (*12*) who found that hTHEM4 exhibits a dual sub-mitochondrial localization as a membrane-bound pool and a free pool of mature (the MLS is removed by proteolysis) in the inter-membrane space. Evidence was presented that suggests that induction of apoptosis by administration of actinomycin D causes the release of mature hTHEM4 into the cytosol and that in this local hTHEM4 delays Akt1/PKBα phosphorylation and sensitizes apoptosis of the cell.

Park and Hemmings and coworkers also reported (*13*) that hTHEM4 binds to the leucine zipper/EF-hand-containing trans membrane-1 protein, which is integral to the mitochondrial inner membrane. In addition, these workers (*9*) showed that phosphorylation of hTHEM4 at Ser37/Ser38 prevents its mitochondrial localization. In the cytoplasm, hTHEM4 associates with the heat shock protein 70 (Hsp70), thus, preventing the formation of complexes between Hsp70 and the apoptotic protease activating factor I and sensitizing the cell toward apoptosis.

2.1.4 Objectives

The studies of the biological function(s) hTHEM4 reported to date have consisted of *in vivo* investigations carried out in mice or in cultured human cells. The findings have provided evidence for links between hTHEM4 and both cancer and cell apoptosis. Nevertheless, two aspects of this work are noteworthy. Firstly, many of the results arising

in these efforts are conflicting, even those published by the same research group. Secondly, the fact that hTHEM4 is a member of the hotdog fold thioesterase family and, therefore, is equipped with the typical constellation of catalytic residues for thioesterase activity has been overlooked and consequently not factored into consideration of the role(s) it plays in the cell. The initial objectives of the doctoral studies described in this dissertation are to (1) determine if hTHEM4 catalyzes acyl-CoA hydrolysis by isolating the enzyme and testing it against a panel of potential thioester substrates, (2) elucidate the mechanism by which hTHEM4 catalyzes thioester hydrolysis and (3) determine the structure of hTHEM4.

2.2 Experimental

2.2.1 Materials

Commercial Materials. Restriction enzymes (NdeI, XhoI, BamHI) and T4 DNA ligase were purchased from Invitrogen (Carlsbad, CA). P*fu Turbo* DNA polymerase was from Strategene (Cedar Creek, TX). Oligonucleotide primers were custom-synthesized by Invitrogen. Competent *Escherichia coli* cells (BL21 Star™ (DE3) One Shot) were obtained from Invitrogen, and the pET23a (+) and pET14b vector were purchased from Novagen. Butyryl-CoA, hexanoyl-CoA, decanoyl-CoA, lauroyl-CoA, myristoyl-CoA, palmitoyl-CoA, stearoyl-CoA and arachidonoyl-CoA were purchased from Sigma-Aldrich (St. Louis, MO). All other chemicals were purchased from Sigma-Aldrich except where noted.

Synthetic Substrates and Inhibitors. 3-Hydroxyphenylacetyl-CoA, 2-Hydroxybenzoyl-CoA and 4-hydroxybenzoyl-CoA, were synthesized by using previously

reported methods (*14,15*). The inhibitor hexyl-CoA was prepared by reacting 1-iodohexane with CoA. 1-Iodohexane (50 mg) was dissolved in ethanol (3 mL) and benzene (400 µl) and then added drop-wise to a stirred solution of 30 mg of coenzyme A lithium salt in 3.5 mL deionized H_2O. The pH was maintained between 7 and 8 by the addition of 1.0 M LiOH in deionized water. The mixture was stirred for an additional 16 h with the pH maintained at 7 -8, and extracted three times with ethyl acetate. The water fraction was concentrated by lyophilization and then chromatographed on a Sephadex-G15 (Amersham Pharmacia) column with deionized water as the eluant. Column fractions were analyzed by using HPLC (High Performance Liquid Chromotography) equipped with a Beckman Ultrasphere C-18 reverse-phase column. The fractions containing pure hexyl-CoA were pooled and concentrated by using lyophilization. The yield is *ca.*15% and the structure of the product was confirmed by using MS (mass spectroscopy) analysis. The inhibitor undecan-2-one-CoA was prepared by reacting 1-bromoundecan-2-one with CoA. 1-Bromoundecan-2-one was prepared by employing the following procedure. Bromine (1.28 g, 8 mmol) was added to a solution of undecan-2-one (1.36 g, 8 mmol) in anhydrous methanol (20 mL). After 15 min, when the solution color had changed to pale yellow, water (30 mL) and concentrated H_2SO_4 (2 mL) were added and the mixture was stirred at room temperature for 1 h. Ether extraction and concentration of the ethereal extracts gave a yellow oil which was subjected to silica gel chromatography (1:4 dichloromethane/hexane) and low temperature re-crystallization from pentane to give the pure *bromoketone*. The 1-bromoundecan-2-one (108 mg) was dissolved in ethanol (3 mL) and benzene (400 µL) and then added dropwise to a stirred solution of 68 mg of coenzyme A lithium salt in 3.5 mL deionized H_2O. G15 Column

25

chromatography gave fractions containing pure undecan-2-one-CoA that were pooled and concentrated by lyophilization. The yield is *ca.*13% and the structure of the product was confirmed by using MS and H-NMR. The theoretical molecular weight of undecan-2-one-CoA is 935.2 compared to the observed mass of 934.2. ^{1}H NMR (in D_2O) is: δ0.855 (s, 3H), 0.888 (t, 3H), 0.985 (s, 3H), 1.278 (m, 14H), 1.584 (m, 2H), 2.675 (m, 3H), 3.242 (q, 1H), 3.382 (t, 2H), 3.567 (m, 3H), 3.635 (m, 1H), 3.906 (m, 1H), 4.091 (s, 1H), 4.308 (s, 1H), 4.657 (s, 1H), 6.28 (d, 1H), 8.465 (s, 1H), 8.721 (s, 1H).

2.2.2 hTHEM4 Cloning and Expression in Eukaryotic Cells.

This work was carried out under the direction of Professor Marco Bisoffi of the UNM Medical School.

EGFP-hTHEM4 fusion protein cloning, transfection, growing and imaging

To obtain a fluorescence fusion protein for *in vivo* imaging, the gene encoding hTHEM4 was cloned into pEGFP-N1 vector (BD Bioscience Clontech). Transfections were performed using the Lipofectamine 2000 reagent (Invitrogen), for a standard 24-well cell culture plate (2 cm^2 surface area per well), 1 μg of plasmid DNA was added to 50 μL of Opti-MEM I Reduced Serum Medium (Invitrogen) and mixing was followed by the addition of solution containing 2 μL of Lipofectamine 2000 and 50 μL of Opti-MEM I Reduced Serum Medium. The solution was incubated for 20 min at room temperature before adding it to the well. The cells were incubated at 37°C in a 5% CO_2 incubator for 48 h prior to testing for transgene expression.

After 48 h post-transfection cells were observed directly by the Zeiss LSM 510 microscope system, for evidence of the expression of hTHEM4 gene. Specifically, the

different views of EGFP-N1 transfected cells (vector control) and EGFP-hTHEM4 transfected cells were compared.

pcDNA 3.1/myc-HisA-hTHEM4 construction

To overexpress hTHEM4 in the HEK 293 cell line for the determination of its physiological characteristics, the gene encoding hTHEM4 was cloned into the pcDNA 3.1/myc-HisA vector (Invitrogen) by using the cloning sites BamHI and AgeI. The sequence was confirmed by DNA sequencing at the Health Sciences Center Facility in the University of New Mexico. Transfections were performed using the same procedure as that employed for the EGFP-hTHEM4 fusion construct. HEK 293 cells were grown in minimal essential medium eagle (MEME, Sigma), supplemented with 10% fetal bovine serum (FBS, Hyclone), under a 5% CO_2 atmosphere at 37 °C. Protein expression was monitored after 48 h by Western Blot of the whole cell extract using commercial anti-C-terminal His-tag antibody (Invitrogen, 46-0693) and anti-hTHEM4 antibody (Abnova, H00117145-B01).

pcDNA 4/HisMax TOPO expression

hTHEM4 was also cloned by using the pcDNA4/HisMax TOPO TA Expression Kit (Invitrogen K864-20). The feature of this vector is that the human cytomegalovirus (CMV) promoter in pcDNA4 allows high-level expression of the PCR product, and the recombinant protein expression is further enhanced by the presence of the QBI SP163 translational enhancer. The PCR product was expressed as a fusion to the N-terminal

Xpress(DLYDDDDK) epitope and a polyhistidine (6xHis) tag for detection and purification.

2.2.3 Cloning, Expression and Purification of hTHEM4 in *E. coli*

Full-length hTHEM4

Full-length hTHEM4 gene was ligated into pET-14b vector (N-terminal His$_6$ tag) and then transformed into BL21 (DE3) competent cells. The cells incubated at 20 °C and 200 RPM for 8 h, then induced with 0.4 mM IPTG. After 12 h, the cells were harvested by centrifugation at 4°C and 6500 RPM. The 10 g of cell paste was suspended in 100 mL of ice-cold lysis buffer (50 mM NaH$_2$PO$_4$, 200 mM NaCl, 10 mM imidazole, 1 mM PMSF; pH 8.0), passed through a French press at 1200 PSIG, and then centrifuged at 48000 × g and 4 °C for 30 min. The supernatant was loaded onto a Ni-NTA Agarose column (QIAGEN, 25 mL) pre-equilibrated with the lysis buffer. The column was washed with 300 mL buffer of 50 mM NaH$_2$PO$_4$/200 mM NaCl /80 mM imidazole (pH 8.0) and then the column was eluted with 200 mL of 50 mM NaH$_2$PO$_4$/200 mM NaCl /250 mM imidazole (pH 8.0). The fractions were analyzed by SDS-PAGE, and the desired fractions were combined, dialyzed into Hepes pH 7.5 buffer and stored at -80 °C. The yield for full-length hTHEM4 is low because of a low expression level.

Truncated form I: hTHEM4 (39)-minus the first 39 amino acids

The truncated gene was prepared using a PCR based strategy with the full-length gene serving as template and commercial custom oligonucleotides as primers. The

truncated gene was ligated into the pET-23a vector, which introduces a C-terminal His_6 tag. The plasmid was transformed into BL21-codon plus (DE3) RIL competent cells for over-expression. The cells were grown as described above and harvested by centrifugation. The suspended cells were lysed by using a French press, and following centrifugation of the lysate, the supernatent was loaded onto a Ni-NTA Agarose column (QIAGEN, 25 mL), pre-equilibrated with the lysis buffer. The column was washed with 300 mL of 50 mM NaH_2PO_4/500 mM NaCl /80 mM imidazole (pH 8.0) and then the column was eluted with 200 mL of 50 mM NaH_2PO_4/500 mM NaCl /250 mM imidazole (pH 8.0). The fractions were analyzed by SDS-PAGE, and then the desired fractions were combined and concentrated using Centricon (10 kDa, Pall Filtron) at 4 ^{o}C. Yield: 35 mg protein/ gm wet cell.

Truncated form II: hTHEM4 (T) C-terminal thioesterase domain

The hTHEM4 C-terminal thioesterase domain (removal of the first 100 amino acids) was prepared by generation of a truncated gene using a PCR based strategy as described in the previous section. To improve solubility, the His_6-MBP TEV cleavable vector was chosen as expression vector. The recombinant plasmid carrying the truncated gene was transformed into BL21 (DE3) competent *E. coli* cells. The His_6-MBP-h_4 (T) fusion protein lysis solution was subjected to Ni-NTA column chromatography. His_6-TEV protease was added to the pooled fractions which were then incubated overnight at 4 °C. The progress of the cleavage reaction was monitored by using SDS-PAGE. The resulting solution was loaded onto a second Ni-NTA column in order to separate the desired protein (without His tag) from the uncleaved protein.

2.2.4 Native Molecular Weight Determination of hTHEM4

The association states of full hTHEM4 and truncated hTHEM4 (Δ39) were determined by using the Biophysics Resource of Keck Facility at Yale University, which employed HPLC (High Performance Liquid Chromotography) SEC (Size Exclusive Chromotography) (LS) Light Scattering (RI) Refractive Index analysis to determine the native molecular weights of hTHEM4 in solution.

2.2.5 Steady-State Kinetic Studies and Substrate Screening

Enzymatic Assays. Reactions were monitored at 25 °C and pH 7.5 by measuring the 412 nm absorbance of 5-thio-2-nitrobenzoate formed by the reaction of DTNB with the CoA anion liberated from the acyl-CoA substrates (short, medium and long chain, saturated and unsaturated aliphatic acyl-CoAs and aromatic acyl-CoAs). Reactions were initiated by adding hTHEM4 to assay solutions composed of substrate (at varying concentration: 1-10 fold K_m), DTNB (2 mM), KCl (0.2 M) and 50 mM K^+Hepes (pH 7.5) contained in quartz cuvettes (1 cm light path). The kinetic parameters V_{max} and K_m were determined from initial velocity data, measured as a function of substrate concentration, by using equation (1) and KinetAsyst (IntelliKinetics, PA),

$$V = V_{max} [A] / ([A] + K_m) \qquad (1)$$

where [A] is the substrate concentration, V is the initial velocity, V_{max} is the maximum velocity and K_m is the Michaelis constant. The reported error was computed by using data fitting. The k_{cat} was calculated from the ratio of V_{max} and the total enzyme concentration.

The enzyme concentration was determined using the Bradford method.

2.2.6 Substrates and Assays for Determination of Acyl-ACP Hydrolysis Activity

Preparation of Myristoyl-ACP (Palmitoyl-ACP).

Myristoyl-holo-acyl carrier protein (ACP) was synthesized by reacting the *apo* human cytosolic ACP with myristoyl-CoA, catalyzed by the human phosphopantetheinyl transferase (PPTase). The human cytosolic ACP fragment and PPTase plasmids were gift from Dr. Stuart Smith, Children's Hospital Oakland Research Institute, Oakland, CA. The two apoproteins were purified by using the earlier described method (*16,17*). The reaction mixture, containing 60 μM apo-ACP, 150 μM acyl-CoA and 2 μM PPTase in 20 mL of 20 mM Tris/1mM $MgCl_2$ (pH 7.0; 25 °C) was allowed to stand for 3 h. Concentrated acyl-ACP was prepared using a PALL 10K centrifuge device and product formation was verified by using TOF MS ES+. Apo-ACP (MW in Da) calculated: 13067, observed: 13066 and 13143 (posttranslational modified form); Myristoyl-ACP calculated: 13618, observed: 13617 and 13694 (posttranslational modified form); Palmitoyl-ACP calculated: 13646, observed: 13643 and 13720 (posttranslational modified form).

Hydrolysis reaction of myristoyl-ACP catalyzed by (Δ39) hTHEM4.

The (Δ39) hTHEM4 catalyzed hydrolysis reaction was monitored by using HR-MS. A 200 μL reaction solution containing 44 μM myristoyl-ACP, 10 μM (Δ39) hTHEM4, 50 mM HEPES and 100 mM NaCl at pH 7.5 was incubated at 37 °C for 1 h. A control reaction that lacked the (Δ39) hTHEM4 was also performed. The reaction rate was monitored at 37 °C by using the DTNB assay (see above).

2.2.7 Determination of Inhibition Constants

Competitive inhibition constants K_i for undeca-2-one-CoA and other inert substrate analog/product inhibitors was determined by measuring the initial velocity of hTHEM4 catalyzed substrate hydrolysis as a function of substrate concentration (K_m to $10K_m$) and inhibitor concentration (0, $1K_i$ and $2K_i$ μM). The initial velocity data were fitted to equation (2) using KinetAsyst (IntelliKinetics, PA),

$$V = V_{max} [A] / ([A] + K_m (1 + [I]/K_i)) \qquad (2)$$

where [A] is the substrate concentration, V is the initial velocity, V_{max} is the maximum velocity, K_m is the Michaelis constant, K_i is the competitive inhibition constant and [I] is the inhibitor concentration.

The myristoyl-CoA substrate inhibition constant was determined by measuring the initial velocity of (Δ39)hTHEM4 catalyzed myristoyl-CoA hydrolysis in triplicate for solutions initially containing (Δ39)hTHEM4 (0.02 μM), myristoyl-CoA (2 - 100 μM), DTNB (2 mM), KCl (0.2 M) and 50 mM K^+HEPES (pH 7.5, 25 ^{o}C). The initial velocity data were fitted to equation (3) using y= m1*m0/(m2+m0*(1+m0/m3)),

$$V=V_{max} [S]/(K_m+ [S](1+[S]/K_I)) \qquad (3)$$

where [S] is the substrate concentration, V is the initial velocity, V_{max} is the maximum velocity, K_m is the Michaelis constant, K_i is the substrate inhibition constant. Fitting kinetic data into equation: m1*m0/(m2+m0*(1+m0/m3)). m1=V_{max}; m2=K_m; m3=K_I.

2.2.8 Crystallization and X-ray Structure Determination and Modeling Studies

X-ray structure determinations were made by Professor Osnat Herzberg and her coworkers at the University of Maryland. Crystals of hTHEM4 (Δ39) were obtained by

32

vapor diffusion in hanging drops at room temperature. The reservoir solution contained 11 % w/v PEG 3350 and 0.1 M ammonium phosphate monobasic. The protein sample, kept in 0.2 M NaCl and 50 mM Hepes, pH 7.5, was mixed with the inhibitor undecan-2-one-CoA to a final protein concentration of 8 mg/mL and inhibitor concentration of 4 mM. Equal volumes of the protein solution and reservoir solution were equilibrated with the reservoir solution. Needle-like crystals appeared within three days (approximate dimensions 0.8 x 0.02 x 0.02 mm^3). The crystals were transferred to a mother liquor solution supplemented with 20% glycerol and flashed-cooled in propane cooled with liquid nitrogen.

X-ray diffraction data were collected at the GM/CA-CAT 23-ID Beam Line at the Advanced Photon Source, Argonne National Laboratory. The Beam Line was equipped with a MAR 300 CCD detector. Data were processed by using the program CrystalClear (Rigaku). The lattice parameters and the space group indicated that the crystals contained 49% solvent and two molecules in the asymmetric unit.

PSI-BLAST (*18*) showed that the closest hTHEM4 sequence homolog in the PDB is a protein from *Rhodococcus* sp. with a hotdog fold (E score of 10^{-7}, PDB entry code 2OV9, determined by the Midwest Center for Structural Genomics), although the function of this protein has not yet been defined. This structure was used as the search model to determine the hTHEM4 structure by employing the molecular replacement method. The PSI-BLAST sequence alignment spanned the hTHEM4 residues 142-231 corresponding to the majority of the *Rhodococcus* thioesterase hotdog core fold (residues 121-208) with 33 % amino acid identity. The N-terminal region of hTHEM4 (residues 39–120) has no identifiable homolog in the library of known structure.

Molecular replacement was performed with the PHASER program (*19,20*) and the dimeric *Rhodococcus* sp. thioesterase search model was truncated to include the entire hotdog core fold (residues 101-209). A single solution was readily obtained, with the dimer occupying the crystal asymmetric unit. The initial model was energy minimized with Refmac (*21*) followed by a non-crystallographic averaging and solvent-flattening using Resolve (*22*).

Building of the missing N-terminal polypeptide chain was accomplished by using repeated cycles of model building with Coot (*23*) and phase improvement with Resolve (*22)*.

2.2.9 Site-Directed Mutagenesis

Site directed mutagenesis was carried out using a PCR-based strategy with the WT-hTHEM4 (Δ39)/ pET-23a (+) plasmid as template, commercial primers and dNTP (Invitrogen), P*fu Turbo* DNA polymerase, and the Techgene thermal cycler manufactured by TECHNE (Princeton, NJ). The PCR products were treated with DpnI to remove the wild type plasmid before transformation into competent *Escherichia coli* cells (BL21 Star™ (DE3) One Shot). The sequence of the mutated gene was confirmed by employing DNA sequencing carried out by the DNA Sequencing Facility of the Health Sciences Center at the University of New Mexico. The plasmid was prepared using a QIAprep Spin Miniprep Kit (Qiagen). The hTHEM4 mutants were purified to homogeneity (monitored by SDS-PAGE) in a yield of *ca.* 7 mg of protein/g of wet cells by the same procedure used to purify the wild-type enzyme.

2.2.10 ^{18}O Incorporation Experiment from ^{18}O enriched Water under Single Turnover and Multiple Turnover Conditions.

Single turnover reaction. A 500 μL solution of 1.05 mM wild-type hTHEM4 (Δ39) in 50 mM Na$^+$Hepes (pH 7.5, 0.2 M NaCl) was lyophilized to form a powder to which was added 240 μL of 97% H$_2$^{18}O (Aldrich). After 15 min incubation at 25 °C, the solution was assayed to ensure that full activity of the enzyme was retained. Next, 10 μL of 20 mM benzoyl-CoA in H$_2$^{18}O solution was added giving a final enzyme concentration of 2.1 mM, and a final substrate concentration of 0.8 mM ([E]:[S]=2.6:1). After incubation at room temperature for 15 min, the solution was filtered by centrifugation at 1,4000 rpm for 30 min at 4 °C using a 10kDa Amicon ultra 0.5 centrifugal filter (Sigma-Aldrich). The filtrate was acidified by adding 10 μL of 6 N HCl and extracted four times with 1 mL portions of ethyl acetate. The ethyl acetate extracts were combined, dried over anhydrous sodium sulfate and concentrated *in vacuo* to give a solid that was dissolved in 80 μL of absolute methanol and subjected to GC-MS analysis with a Agilent Technologies 5975C VL MSD and 6850 Network GC System.

Multiple turnover reaction. The procedure described above was repeated for a reaction of 168 μM wild-type hTHEM4 (Δ39) and 0.8 mM benzoyl-CoA [E]:[S]=1:4.76. A control reaction included 2.1 mM D161L/T177V hTHEM4 (Δ39).

2.3 Results and Discussion

2.3.1 Expression of hTHEM4 in HEK 293 Cells

EGFP-hTHEM4 transfected HEK 293 cells were observed directly by using a Zeiss LSM 510 microscope system. By comparing different views of EGFP-N1

transfected cells (Figure 2.3) and EGFP-hTHEM4 transfected cells (Figure 2.4) a low level of EGFP-hTHEM4 gene expression was observed to have taken place. The over-expressed cytoplasmic GFP (green) "lights up" the cells whereas the GFP-hTHEM4 (green) "lights up" a smaller population of cells because of its low expression level.
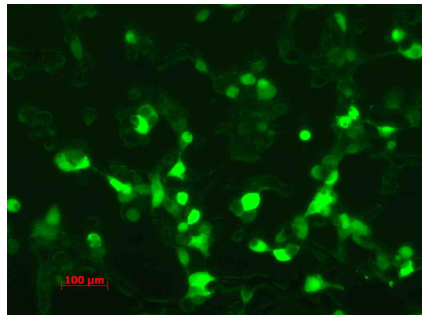
Figure 2.3 EGFP-N1 vector transfected HEK293, 48 h post-transfection
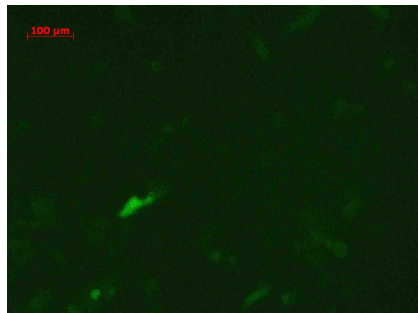
Figure 2.4 EGFP-hTHEM4 plasmid transfected HEK293, 48 h post-transfection

Attempts at detection of the full-length hTHEM4 (theoretical mass is 28274 Da) expression using pcDNA3.1 or pcDNA4, transfected in HEK 293 cells, using Western blot analysis (anti-THEM4 antibody or anti-Xpress antibody) did not yield positive results (see Figure 2.5 the last two lanes in Western Blot). A low level of expression

36

against a background of the endogenously expressed enzyme made detection using the anti-THEM4 antibody difficult. Likewise, the low level of hTHEM4 gene expression made detection by the anti-epitope (anti-Xpress) antibody ineffective.

One reason for low hTHEM4 expression might be that an increased level of thioesterase activity is toxic to the cell. To test this possibility, the expression levels of genes encoding the catalytically inactive hTHEM4 D161N and D161A mutants were examined (Figure 2.5). Significant expression of the wild type gene was not detected, however, this was not the case with the D161N mutant. No expression was observed for the D161A mutant a result that might be due to a folding problem. Whereas the wild-type and D161N hTHEM4 are easily produced in transformed *E. coli* cells, no protein product is observed in the case of the D161N hTHEM4 mutant gene clone. The L17R hTHEM4 mutant gene was also explored because it is commercially sold form and enhanced expression of this mutant (note that the mutation is located in the MLS) might explain why other groups were successful in observing *hTHEM4* over expression in transfected HEK293 cells (ref). Indeed, the L17R hTHEM4 mutant gene is expressed at a level that is even higher than that of the D161N hTHEM4 mutant gene (Figure 2.5).
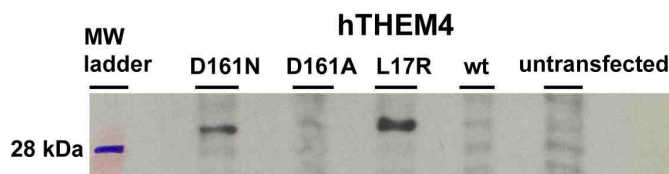
Figure 2.5 Western blot of whole cell extract of different hTHEM4 constructs expressed in HEK293 cells: Xpress-pcDNA4.0 vector, 24 h after transfection, employing the anti-Xpress antibody.

2.3.2 Expression of hTHEM4 in *E. coli*

The full-length hTHEM4 gene was also expressed in *E. coli* and then purified by using Ni-NTA column chromatography. The Commassie blue stained SDS-PAGE gel and the corresponding Western blot result are shown in Figure 2.6.
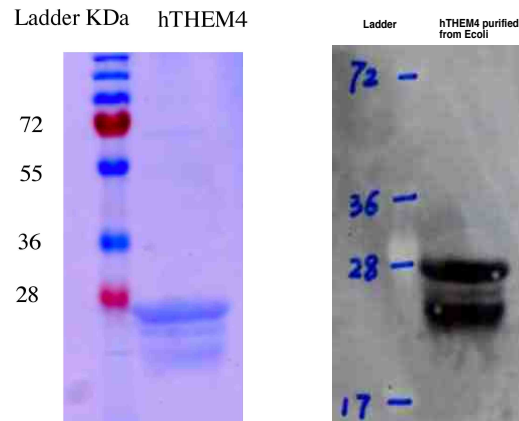
Figure 2.6 The Commassie blue stained SDS-PAGE (left) of recombinant His$_6$-hTHEM4 purified from *E. coli.* Western Blot (right): Anti-THEM4 antibody.

Purified hTHEM4 is separated into two fractions by SDS-PAGE, both of which bind the hTHEM4 antibody. This suggests that the full-length hTHEM4 is truncated by proteolytic cleavage within the N-terminal domain. Then N-terminal sequence analysis of the two proteins extracted from the bands (carried-out by Dr. Brian Martin of the NIH) was confirmatory in that the protein from the upper band sequence begin with GSSHHHHHHS, which is the correct sequence for hTHEM4. The lower band sequence starts at FSSEEVILKD, showing that the first 35 amino acids have been removed. The first 39 amino acids of hTHEM4 comprise the mitochondria localization sequence that is

predicted to be unstructured (*i.e*, not "folded"). This is consistent with the observed tendency of this region to undergo proteolytic cleavage.

hTHEM4 N-terminal truncation mutants were then prepared. One truncation mutant lacks the first 39 amino acids and the other lacks the first 100 amino acids, which comprise the entire N-terminal domain. The theoretical masses of these two truncates are 24063 Da and 15614 Da, respectively. Both proteins were purified by Ni-NTA column chromatography. The SDS-PAGE gels of the purified proteins are shown in Figure 2.7 and Figure 2.8.
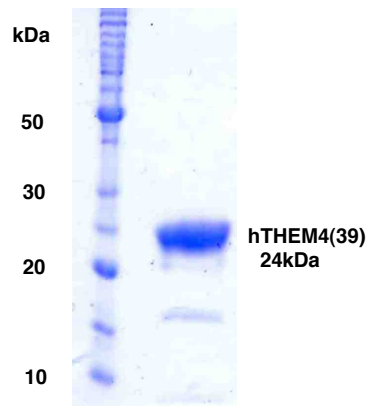
Figure 2.7 Right lane: Commassie blue stained SDS-PAGE gel of hTHEM4 (39)-His$_6$ expressed in E. coli and subjected to Ni-NTA column purification. Left lane: molecular weight standards.
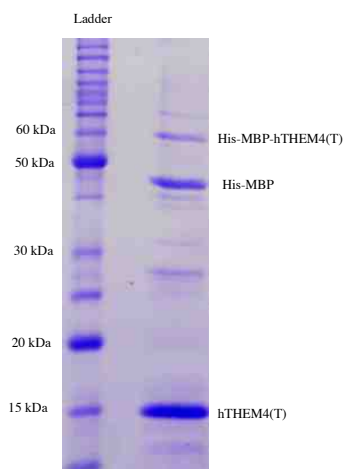
Figure 2.8 Commassie blue stained SDS-PAGE gel of double tagged construct: His$_6$ and the maltose binding protein (MBP) fusion adduct with the hTHEM4 C-terminal domain construct (residues 140-240) following Ni-NTA column purification, proteolytic cleavage of the MBP by TEV, loading onto Ni-NTA column again and Sephadex G-75 size exclusive column chromatography. Left lane: molecular weight standards.

The split of hTHEM4 protein product expressed in E. coli.

Inspection of the gel from SDS-PAGE chromatography of hTHEM4 (full-length) and hTHEM4 (Δ39) (see Figures 2.6 and 2.7) reveals the presence of protein fragments of 22 kDa, 16 kDa, 14 kDa and 8 kDa masses. Furthermore ES-MS analysis of the full-length hTHEM4 reveals the presence of a protein with a mass of 16662 Da, instead of 29292 Da (theoretical MW). Other truncated constructs including hTHEM4 (Δ35) minus the first 35 amino acids, hTHEM4 (Δ50) minus the first 50 amino acids, and the hTHEM4 N-terminal domain comprised of residues 1-119 amino acids were prepared. The 35 and 50 amino acid truncated hTHEM4 could be over-expressed in *E. coli*, but the N-terminal domain could not be. SDS-PAGE chromatography of hTHEM4 (Δ35) and hTHEM4 (Δ50) revealed that fragmentation had occurred in a similar manner as those

observed with other constructs. The results suggest that the N-terminal domain of hTHEM4 does not assume a compact and stable fold. It is not clear whether the fragmentation of the protein is a result of spontaneous hydrolysis or the action of a contaminating protease (despite the inclusion of protease inhibitors in the cell lysis buffer).

2.3.3 Native Molecular Weight of hTHEM4

Analysis of the association state of full-length hTHEM4 and truncated hTHEM4 (Δ39) showed that each is dimer in solution (Figure 2.9, 2.10 and Table 2.1). The dimer is known to be the minimal functional unit for hot-dog thioesterase activity and typically the tetramer or hexamer is the quaternary structure observed.
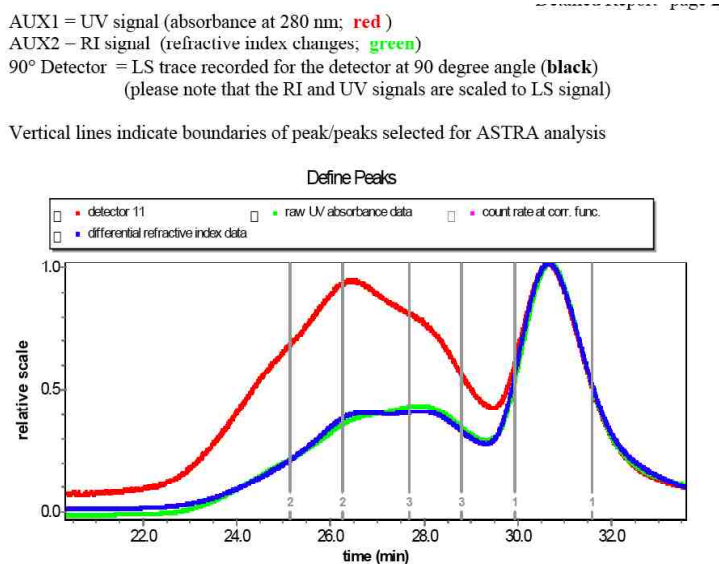
Figure 2.9 Peak ID Plot of full length hTHEM4: Major peak elution at 29.940-31.585 min, which suggests the dimer state. Other two minor peaks at 27.667-28.791 min and 25.137-26.261 min, which is corresponding to tetramer and hexamer separately.

AUX1 = UV signal (absorbance at 280 nm; **red**)
AUX2 = RI signal (refractive index changes; **green**)
90° Detector = LS trace recorded for the detector at 90 degree angle (**black**)
       (please note that the RI and UV signals are scaled to LS signal)

Vertical lines indicate boundaries of peak/peaks selected for ASTRA analysis
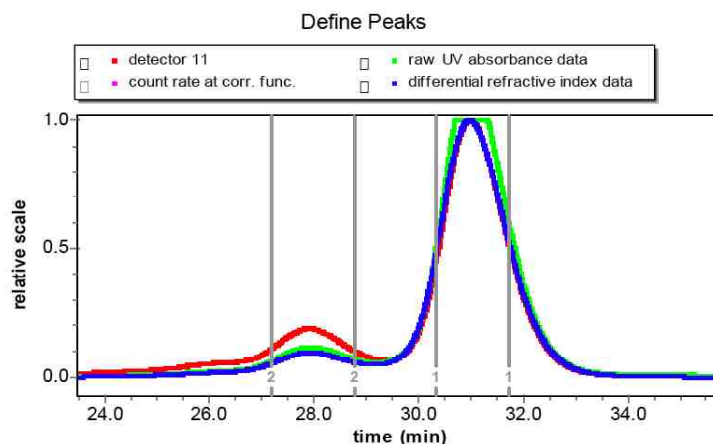
Figure 2.10 Peak ID Plot of Truncated hTHEM4(Δ39): Major peak elution at 29.940-31.585 min, which means formation of dimer. Minor peak is at 27.199-28.761 min, which is corresponding to the formation of tetramer.

Table 2.1 Results of SEC-LS/RI/UV analysis from ASTRA (reports for major peaks of selected analyses)

RUN	PEAK Elution at UV trace (mL)	MW (kDa) Calculated by ASTRA Average for the major peak (Mw)	MW (kDa) Calculated by ASTRA range of Mw observed	Sequence Predicated MW for monomer (kDa)	Oligomeric association
Full length hTHEM4	15.33	61	60-66	29	dimer
hTHEM4 (Δ39)	15.49	50	47-52	24	dimer

2.3.4 Catalytic Activity and Substrate Screening

Both full-length hTHEM4 and truncated proteins were tested for their ability to catalyze hydrolysis of myristoyl-CoA. The results shown in Table 2.2 demonstrate that full-length hTHEM4 and hTHEM4 (Δ39) are highly active catalysts whereas the MBP-hTHEM4 C-terminal domain fusion protein is 10,000-fold less active. The hTHEM4 C-terminal domain, without the fused MBP, had limited solubility and no detectable catalytic activity. This result suggests that the N-terminal domain acts to stabilize and/or solubilize the C-terminal "thioesterase" domain.

Table 2.2 Steady-state kinetic constants for hTHEM4 (full-length and truncated mutants) catalyzed hydrolysis of myristoyl-CoA at pH 7.5 and 25°C determined using the DTNB spectrophotometric assay.

Enzyme	$k_{cat}(s^{-1})$	K_m (μM)	k_{cat}/K_m ($M^{-1}s^{-1}$)
hTHEM4 (full-length)	2.26±0.04	1.17±0.08	1.9×10^6
hTHEM4 (Δ 39)	4.20±0.10	2.40±0.10	1.7×10^6
His$_6$-MBP-hTHEM4 (T)	0.12±0.01	6.19±1.25	2.0×10^4
hTHEM4 (T)	nd*	nd*	

* Activity is too low for the reliable determination of kinetic constants.

Table 2.3 Steady-State Kinetic Constants for the hTHEM4 (D39)-Catalyzed Hydrolysis of Acyl-CoA Thioesters Measured at pH 7.5 and 25°C using the DTNB spectrophotometric assay.

Substrate	k_{cat} (s^{-1})	K_m (µM)	k_{cat}/K_m (M^{-1}s^{-1})
Acetyl-CoA	$(5.5\pm0.3)\times10^{-1}$	22.6±3.2	2.4×10^4
n-Propionyl-CoA	$(2.4\pm0.1)\times10^{-1}$	87.9±1.0	2.8×10^3
n-Butyryl-CoA	$(2.2\pm0.1)\times10^{-1}$	15.8±2.0	1.4×10^4
Hexanoyl-CoA	1.2 ± 0.03	12.7±0.9	9.4×10^4
Octanoyl-CoA	2.4±0.03	8.3±0.3	2.9×10^5
Decanoyl-CoA	2.2±0.1	6.1±0.4	3.6×10^5
Lauroyl-CoA	4.7±0.2	3.3±0.5	1.4×10^6
Myristoyl-CoA	4.2±0.1	2.4±0.1	1.7×10^6
Palmitoyl-CoA	3.9±0.1	2.6±0.1	1.5×10^6
Stearoyl-CoA	4.9±0.2	5.1±0.5	9.6×10^5
Oleoyl-CoA	2.8±0.03	5.2±0.1	5.3×10^5
Arachidonoyl-CoA	1.0±0.05	8.6±0.2	1.1×10^5
Isobutyryl-CoA	0.5±0.03	103.3±8.0	4.9×10^3
Succinyl-CoA	0.1±0.003	153±11	6.5×10^2
3-HPA-CoA	4.1±0.1	48.2±3.3	8.5×10^4
2-HBA-CoA	$(3.4\pm0.2)\times10^{-1}$	41.6±2.3	8.2×10^3
4-HBA-CoA	$(2.9\pm0.2)\times10^{-1}$	28.5±3.9	1.0×10^4

The acyl-CoAs listed in Table 2.3 were tested as substrates for hTHEM4 (Δ 39) in order to define the hTHEM4 substrate range. Using the substrate k_{cat}/K_m value as the measure of substrate activity the results show that the medium-to-long chain fatty acyl-CoAs constitute the most active substrates of those tested (k_{cat}/K_m=1x10^5 to 1x10^6 M^{-1}s^{-1}). The aromatic substrates tested, 4-hydroxylbenzoyl-CoA, 2-hydroxylbenzoyl-CoA and 3-hydroxylphenylacetyl-CoA, are ~10-fold less active. The activity towards short chain, nonpolar acyl-CoA metabolites is even lower, however still within a physiologically relevant range. The polar acyl-CoA thioester, succinyl-CoA, was the least active substrate tested (k_{cat}/K_m=6.5 x10^2 M^{-1}s^{-1}). The substrate specificity profile shows that hTHEM4 is a high activity, low specificity acyl-CoA thioesterase which prefers medium to long chain fatty acyl-CoAs as substrates.

2.3.5 Hydrolysis of Myristoyl-ACP Catalyzed by hTHEM4 (Δ39).

The high catalytic activity observed for hTHEM4 with acyl-CoA thioesters does not rule out the possibility that hTHEM4 targets acyl-ACPs for hydrolysis. The cytosolic fatty acid synthase (FAS) and mitochondrial FAS function to produce fatty acids in their respective compartments. Thioesterases promote release of the fatty acid products formed from fatty acyl-ACP upon completion of chain extension (*24,25,26*). They are also known to play housekeeping roles in which they cause release of the ACP from a fatty acyl-ACP, which has prematurely terminated chain elongation (*27*). Recently, Professor Stuart Smith kindly provided our laboratory with clones of the human cytosolic FAS ACP domain, engineered as an independent protein with pantetheine transferase (PPTase) that catalyzes charging of the ACP with CoA to form the holo-ACP (i.e., the ACP with

its panthetheine arm). PPTases are typically promiscuous and, as such, will catalyze the transfer of an acyl-pantetheine unit to the ACP if provided with an acyl-CoA reactant in place of CoA. Our previous experience with the engineered ACP (*28*) suggests that the expression of its encoding gene *in E. coli* results in the native "apo" form (calculated: 13067 Da, ES-MS observed: 13066 Da) accompanied by a slightly higher molecular weight species (13143 Da) that has apparently undergone some form of posttranslational modification (most likely phosphorylation) that adds *ca.*76 Da to the overall mass (13143 Da). Nevertheless, both forms are biochemically active (*i.e.*, they are charged with an acyl-pantetheine unit in the presence of PPTase and in the presence of the thioesterase they undergo hydrolytic deacylation).

In order to test the activity of hTHEM4 (Δ39) towards the engineered cytosolic myristoyl-ACP (prepared as described in the Experimental), we used ES-MS to monitor the reaction. As shown in Figure 2.11, the mass spectrum of the reaction solution (44 μM myristoyl-holoACP in 50mM HEPES and 100mM NaCl buffer at pH 7.5 and 37 $^{\circ}$C) prior to the addition of hTHEM4 (Δ39) (lane A) contains two peaks at 13617 Da (myristoyl-holoACP; calculated 13618 Da) and 13693 Da (the posttranslational modified counterpart of myristoyl-holoACP). A control experiment was carried out by incubating a solution not containing hTHEM4(Δ39) (lane B). In this case, no change took place in the mass spectrum compared to the material in lane 1. Following 1 h incubation with 10 μM hTHEM4(Δ39) the mass spectra revealed (lane C) that holo-ACP (calculated 13408, observed: 13406 and 13483 (modified form)) is formed. The molecular weight difference is 210 Da, which shows that enzyme hydrolyzes the myristoyl-holo-ACP to form completely the holo form.

Reaction rates were monitored by using the DTNB assay at 37 °C(measuring the 412 nm absorbance of 5-thio-2-nitrobenzoate formed by reaction of 0.3 mM DTNB, the concentration of DTNB is lower than that used in the assay used to monitor hydrolysis of acyl-CoAs, with the free thiol of the holo-ACP). The concentration of myristoyl-holoACP (determined by using the BCA assay) was 10-80 μM and 0.257 μM of hTHEM4(Δ39) was used in each assay solution. The background reading for substrate alone is *ca.* 30%. Thus, rates were determined by incubating the 0.3mM DTNB buffer with myristoyl-holoACP at 37 °C first for 2 min and then adding the hTHEM4(Δ39) to initiate the reaction.The results give $k_{cat} = 0.06$ s^{-1}, $K_m = 12$ μM, $k_{cat}/K_m = 5 \times 10^3$ M^{-1}s^{-1}.
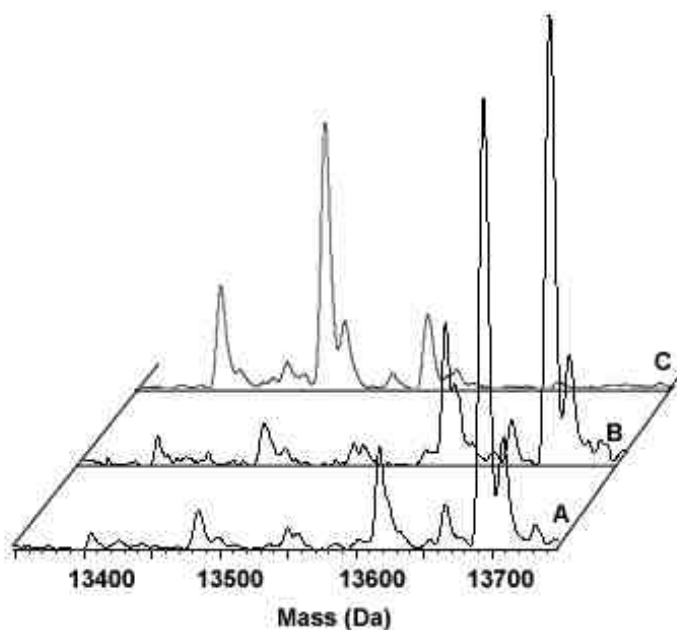
Figure 2.11 Mass spectra diagram of hydrolysis of Myristoyl-holo-ACP catalyzed by (Δ39) hTHEM4.Lane A, Myristoyl-holo-ACP sample (MW 13617, 13693(modified form); Lane B, Control reaction: without (Δ39) hTHEM4, incubated at 37 °C for 1 hour (no change: MW peak @ 13617 and 13693 Da); Lane C, Reaction run

with (Δ39) hTHEM4, incubated at 37 °C for 1 hour, product is holo-ACP (MW13405.5, 13483 Da).

2.3.6 Product and Substrate Analog Inhibition

a. Evaluation of Inert Substrate Analogs as Inhibitors

In order to carry out structure-function analysis of hTHEM4, the X-ray structure of the enzyme, complexed with either substrate or an inert substrate analog, was required. Despite the removal of the catalytic residues by using site directed mutagenesis (see below), the enzyme retained residual catalytic activity, which precluded co-crystallization with the substrate. An alternative approach which was pursued involved preparation of inert analogs of the fatty acyl-CoA substrate that could be used to co-crystallize with hTHEM4 or, alternatively, to soak into apo-hTHEM4 crystals. Two strategies that had previously proved effective for obtaining structures of the hotdog thioesterases with a bound substrate analog involve modification of the substrate thioester group by replacement of the C=O with a CH_2 group or insertion of a CH_2 group between the C=O and the sulfur atom (*14,15*). Owing to chain length limitations set by solubility issues, the two analogs chosen were undecan-2-one-CoA and hexyl-CoA. Each has a shorter chain length than that of the most active substrate myristoyl-CoA. Nevertheless, based on the k_{cat}/K_m values measured for hexanoyl-CoA and decanoyl-CoA (Table 2.3), they were expected to be sufficient reporters of interactions that lead to productive substrate binding. Undecan-2-one-CoA and hexyl-CoA were prepared by using methods described in the Experimental section. The intersecting initial velocity plot measured for undecan-2-one-CoA inhibition of (Δ39) hTHEM4 catalysis (Figure 2.12) showed that it serves as a competitive inhibitor ofthe substrate n-decanoyl-CoA, indicative of inhibitor binding at

the substrate binding site. Data fitting defined K_i= 0.8 ± 0.3 µM, indicative of very tight

binding that is needed for successful co-crystallization with hTHEM4. Hexyl-CoA

proved to be a competitive inhibitor (Figure 2.13), however it had a comparatively low

binding affinity (K_i = 8.4 ± 0.2 µM).
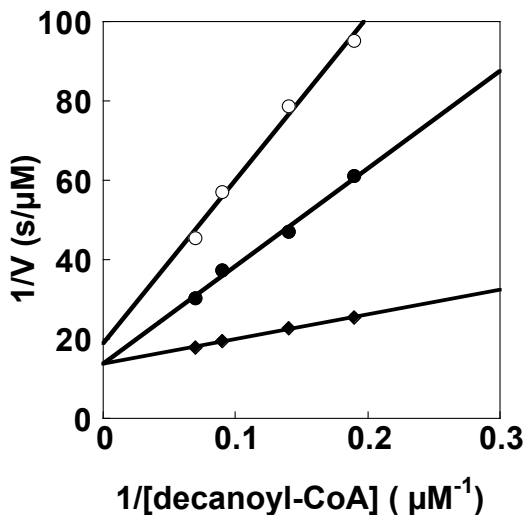
Figure 2.12 Double reciprocal plot of the initial reaction velocity (V) vs the

concentration of the n-decanoyl-CoA substrate. Reaction solutions initially contained 5

to 15µM n-decanoyl-CoA, 0.02µM (Δ39) hTHEM4, 2mM DTNB (pH 7.5, 25oC) and

0.0 (◆), 2.5(●) and 5.0(○) µM undeca-2-one-CoA. Data fitting defined Ki= 0.8 ± 0.3

µM.
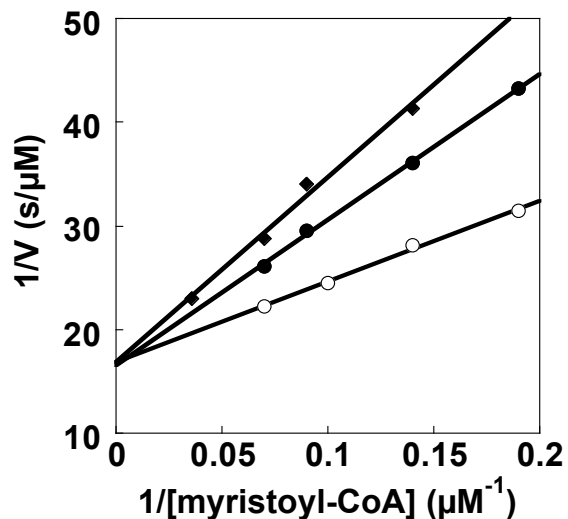
Figure 2.13 Lineweaver-Burk plot of hexyl-CoA inhibition of hTHEM4 (Δ39) catalyzed hydrolysis of myristoyl-CoA. Reaction solutions initially contained 5 to 28 μM myristoyl-CoA, 0.02μM (Δ39) hTHEM4, 2mM DTNB (pH 7.5, 25°C) and 0.0(○), 5.0 (●) and 10.0 (■)μM hexyl-CoA. Data fitting defined $K_i = 8.4 \pm 0.2$ μM.

b. Product inhibition

Because hTHEM4 thioesterase activity is highly efficiency and it has low substrate specificity, control of substrate targeting must rely on feedback inhibition and/or another form of regulation (compartmentalization; transcriptional or translational regulation). To test if regulation takes place by feedback inhibition, CoASH and several aliphatic carboxylic acids were probed as inhibitors of (Δ39) hTHEM4 catalysis.

Because the DTNB-based kinetic assay that is used to measure the initial velocities of (Δ39)hTHEM4 catalyzed acyl-CoA thioester hydrolysis is not compatible with experiments using exogenous CoASH as a product inhibitor, an alternate assay

method was employed. Accordingly, 4-HBA-CoA was used as substrate because its hydrolysis results in a decrease in absorbance at 300 nm ($\varepsilon = 11.8$ mM^{-1} • cm^{-1}). As a result, the hydrolysis reaction can be continuously monitored by using UV-spectroscopy. 4-HBA-CoA serves as a slow substrate of (Δ39)hTHEM4 with $k_{cat} = 2.9 \pm 0.2 \times 10^{-1}$ s^{-1} and $K_m = 29 \pm 4$ µM. The initial velocity data measured for (Δ39)hTHEM4 catalyzed 4-HBA-CoA hydrolysis in the presence and absence of CoASH is presented in the form of a Lineweaver-Burk plot in Figure 2.14. A clear slope effect is displayed, which defines $K_{is} = 81.0 \pm 0.2$, and a very small intercept effect is seen (most likely within the error of data collection), which corresponds to a $K_{ii} = 474.0 \pm 0.8$ µM. It is unlikely that CoASH serves as a feedback inhibitor because the K_m values of the fatty acyl-CoA substrates are *ca.*50-fold smaller than that of CoASH K_i.
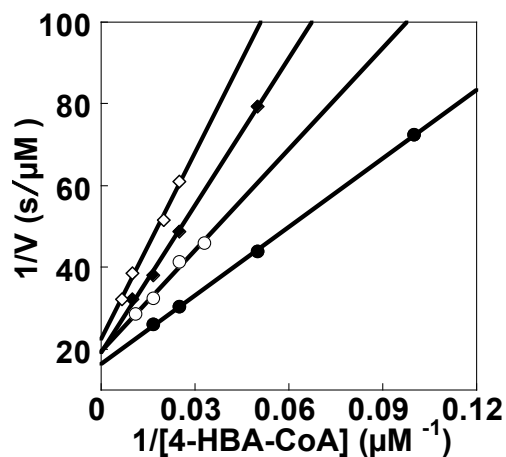
Figure 2.14 Double reciprocal plot of the initial reaction velocity (V) vs the concentration of the 4-HBA-CoA substrate. Reaction solutions initially contained 10 to 150 µM 4-HBA-CoA, 0.3µM (Δ39) hTHEM4, (pH 7.5, 25°C) and 0(●), 50(○), 100 (■)

and 150 ($\square$)µM CoA, monitored by 300nm direct assay. Data fitting defined $K_{is}= 81.0 \pm$ 0.2 µM and $K_{ii} = 474.0 \pm 0.8$ µM.

Next, product inhibition by the 4-hydroxybenzoate, hexanoate, octanoate (25 mM stock solution prepared in 30% aq. ethanol) and lauroate (50 mM stock solution prepared in 50% aq. ethanol) was determined by measuring the initial velocity of (Δ39) hTHEM4 catalyzed hydrolysis of 4.2 μM lauroyl-CoA (~K_m level) in solutions containing DTNB (1 mM), KCl (0.2 M) and 50 mM K$^+$HEPES (pH 7.5; 25 $^\circ$C) in the absence and presence of increasing concentrations of inhibitor up to 2-5 mM. The K_i value was estimated from the concentration of inhibitor that decreased the initial velocity by half. If no inhibition was observed, K_i was assumed to be greater than the value of the highest inhibitor concentration tested. The results, shown in Table 2.4, indicate that the carboxylate products bind very weakly to the enzyme and, therefore, likely do not regulate hTHEM4 through feedback inhibition.

Table 2.4. Carboxylate product inhibition constants determined for inhibition of (Δ39) hTHEM4 catalyzed hydrolysis of lauroyl-CoA at pH 7.5 and 25 $^\circ$C using the DTNB assay.

Carboxylic acid	K_i
4-hydroxybenzoate	~2mM
hexanoate	>2mM
octanoate	>2mM
lauroate	~1mM

c. Substrate inhibition

Many fatty acyl-CoA thioesterases are strongly inhibited at substrate concentrations above 10-20 µM. This phenomenon is often ascribed to the formation of micelles caused by the long hydrocarbon chains paired with the polar CoA unit. However, sometimes enzyme inhibition by fatty acyl-CoAs occurs at concentrations well below the critical micelle concentrations (CMC), which suggests they play a regulatory role rather than displaying nonspecific effects caused by their detergent properties. The CMC of a series of saturated fatty acyl-CoAs has been reported (*29*). The CMC of lauroyl-CoA is 1130 µM, myristoyl-CoA is 210 µM, palmitoyl-CoA is 42 µM. The effects of ionic strength and temperature on CMC were also reported (*30*), showing that the CMC values do not vary that greatly with changes in these parameters.

hTHEM4 is inhibited by myristoyl-CoA at concentrations above 10 µM, a value that is 21-fold lower than the myristoyl-CoA CMC. Therefore, it is doubted that inhibition in this case is a result of micelle formation. In order to accurately define the substrate steady-state kinetic constants k_{cat} and K_m and the substrate inhibition constant K_I, initial velocities of hTHEM4(Δ39) catalyzed myristoyl-CoA hydrolysis reactions were measured over an expanded concentration range. the data obtained were fitted to equation 3 (for details see the Experimental section) to define $k_{cat} = 0.084\pm0.003$ s^{-1}, $K_m=$ 2.55 ±0.33 µM and $K_I = 272 \pm 52$ µM. Myristoyl-CoA substrate inhibition can be explained based on analysis of the X-ray structure of the complex between hTHEM4(Δ39) and the tight binding inhibitor undecan-2-one-CoA (see Figure 2.21 in the section below). Two inhibitor ligands are seen to bind the acyl site, one productively and the other nonproductively (backwards). The large solvent exposed acyl binding site is

hydrophobic and this property attracts the fatty acyl tail of the substrate regardless of its overall orientation. Binding in the nonproductive mode is likely to inhibit either binding in the productive mode or release of the fatty acid product once catalytic turnover has occurred.

Table 2.5 The initial velocities determined for (0.02 μM) hTHEM4(Δ39) catalyzed hydrolysis of myristoyl-CoA measured over a large range of myristoyl-CoA concentrations (2-100 mM) at pH 7.5 and 25 ^{o}C using the DTNB assay. The velocities were measured in triplicate and the average of the three values are reported.

[substrate] μM	2.0	4.0	6.0	8.0	10.0	12.0
Velocity μM/s	0.0357	0.0495	0.0598	0.0654	0.0649	0.0641
[substrate] μM	15.0	30.0	60.0	80.0	100.0	
Velocity μM/s	0.0661	0.0705	0.0682	0.0613	0.0605	
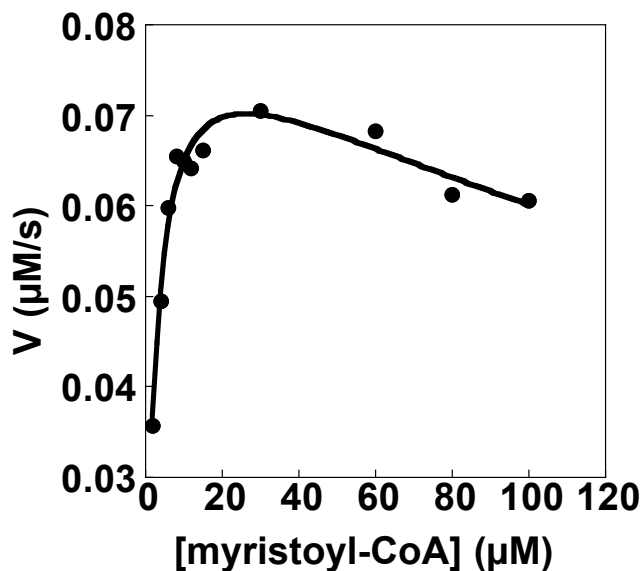
Figure 2.15. A plot of the data reported in Table 2.5. The curve represents fit to equation 3 (see Experimental).

2.3.7 hTHEM4 Structure-Function Analysis

hTHEM4 crystallization and X-ray structure Determination.

Using the (Δ39) hTHEM4 and undecan-2-one-CoA that was supplied, Osnat Herzberg and her coworkers succeeded in crystallizing (Δ39) hTHEM4 bound with undecan-2-one-CoA and determining the X-ray structure of the complex. Their findings are presented below and the structure refinement summary is given in Table 2.6.

Table 2.6 Summary of X-ray data collection and structure refinement.

Data collection	
Space group	$P2_12_12_1$
Cell dimension (Å)	$a = 56.6, b = 58.8, c = 135.4$
Wavelength (Å)	0.9202
Resolution (Å)	2.3
No. of observed reflections	85,318
Completeness (%)[a]	99.8 (99.9)
No. of unique reflections	20,650
R_{merge}[b]	0.086 (0.331)
$<I/\sigma(I)>$	9.5 (3.4)
Redundancy	4.1 (4.2)
Refinement	
No. of reflections used	20,649
No. of protein atoms	2,903
No. of UDC atoms	120
No. of water atoms	213
R_{cryst}[c]	0.198 (0.264)
R_{free}[d]	0.255 (0.330)
RMSd from ideal geometry	
Bond length (Å)	0.006
Bond angle (°)	1.3
Average B factor (Å^2)	
Protein	34
UDC	38
Water	40
Ramachandran plot (%)[e]	91.4, 8.6, 0.0, 0.0

[a]The values in parentheses are for the highest resolution shell, 2.38-2.30 Å.

$^b R_{merge} = \sum_{hkl} [(\sum_j | I_j - <I> |) / \sum_j | I_j |]$.

$^c R_{cryst} = \sum_{hkl} | |F_o| - |F_c| | / \sum_{hkl} |F_o|$, where F_o and F_c are the observed and calculated structure factors, respectively.

$^d R_{free}$ is computed from 1,001 randomly selected reflections omitted from the refinement.

^{e}Ramachandran plot categories are most favored, allowed, generously allowed, and disallowed (*31, 32*).

Overall structure. The crystal structure of the hTHEM4, bound with undecan-2-one-CoA, was determined at 2.3Å resolution. It is a homodimer (subunits are labeled as A&B) with two undecan-2-one-CoA ligands bound to the respective substrate-binding sites (Figure 2.16). The extending acyl fragment (model as C_9-(C=O)-C-S-C-C-N) of one substrate is found in the subunit A channel. Each subunit consists of a core hotdog fold and N-terminal residues 40-120 that adopt a novel fold. The hotdog-fold contains a six-stranded β-sheet that cradles a central α-helix. The N-terminal region does not form a compact independent domain but, rather, it contains two α-helices (α1 and α2) and largely irregular loop-like folding (residues 43-98 and 106-120 in subunit A, residues 43-81 and 106-120 in subunit B) along with two disordered regions (residues 99-105 in subunit A, and residues 82-105 in subunit B).
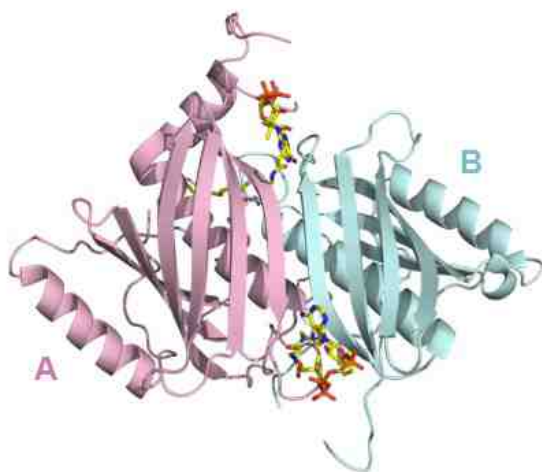
Figure 2.16 Overall structure of hTHEM4 (Δ39). The subunits are colored in pale green and pink. The undecan-2-one-CoA ligand is shown in stick with carbon atoms colored yellow, oxygen atoms red, nitrogen atoms blue and phosphorous atoms orange.
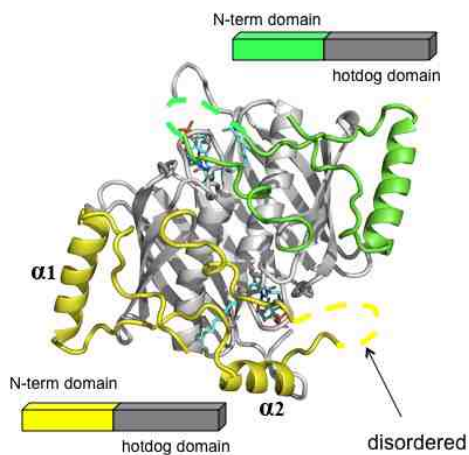
Figure 2.17 The hTHEM4 (Δ39) dimer. The N-terminal domains are shown in yellow and green. The undecan-2-one-CoA ligand shown in stick with the carbon atoms colored cyan, oxygen atoms red, nitrogen atoms blue and phosphorous atoms orange.

N-terminal domain folding The N-terminal region (Figure 2.17) flanks the hotdog fold core domain such that α1 is located nearly parallel to the edge β-strands of the hotdog fold on the β-sheet face, which is opposite from the face that interacts with the hotdog α

58

helix. Residues 72-76 of the loop and the ensuing helix α2 pack above the active site and deepen the channel that accommodates the acyl side chain of the substrate. As mentioned above, α2 is ordered only in one of the dimer subunits (subunit A in Figure 2.16). In addition to the flexibility of α2 and its association with the active site, the amino acid sequence alignment among all eukaryotic hTHEM4 homologs shows that residues that form the irregular structure are not well conserved whereas those that form the main α-helix (α1) are stringently conserved. This observation suggests that the α1 might be a recognition unit for targeting a specific partner for THEM4s. Alternatively, this observation suggests that the widest sequence divergence of the loop linker and α2 might be involved in recognition of a cellular target that is unique to each family member.

Acyl-CoA binding site. Two molecules of the undecan-2-one-CoA are positioned remotely at opposite ends of the dimer interface. The adenine, ribose and phosphate groups of the inhibitor are exposed to solvent and the acyl chain is threaded through a channel formed by the two hotdog-fold α helices as well as loop regions and N-terminal α2. The undecan-2-one-CoAs define two active sites of the hTHEM4 dimer. The binding mode that exposes the nucleotide moiety to solvent and wedges the pantetheine unit between the dimer subunits is similar to that seen in other hotdog acyl-CoA thioesterases. The pantetheine is positioned at the entrance to a tunnel that becomes increasingly hydrophobic as the acyl chain is threaded through it. The nucleotide moiety of undecan-2-one-CoA bends at the β-phosphate group in the bound state so that the adenine stacks above the β-sheet. The whole nucleotide unit resides on the protein surface where it appears to bind to electropositive side chains. Close interactions occur between Arg206

and Lys 207 and the phosphoryl groups, and a hydrogen bond exists between an N atom of the adenine moiety and the side chain of Asn 183 (see Figure 2.18). The undecane side chain of the inhibitor is threaded through the active site channel in a nearly extended conformation in the subunit that reveals a well defined α2 helix (subunit A) but it curls when α2 is disordered in subunit B, presumably to enhance hydrophobic interactions and avoid exposure to solvent. The central α helix of hTHEM4 begins with the conserved sequence HGG, and the undecan-2-one-CoA binds close to His 152 of the HGG sequence, Gly 146 from one subunit, and Asp 161 and Thr 177 from the partner subunit. Asp 161 is located close to the CoA sulfur atom, suggesting that it is a key catalytic residue (see Figure 2.19).
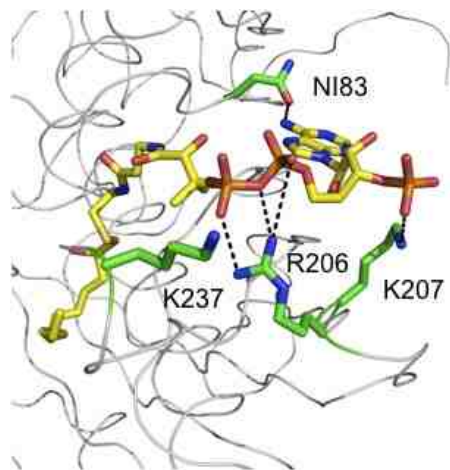
Figure 2.18 The hTHEM4 CoA binding site.
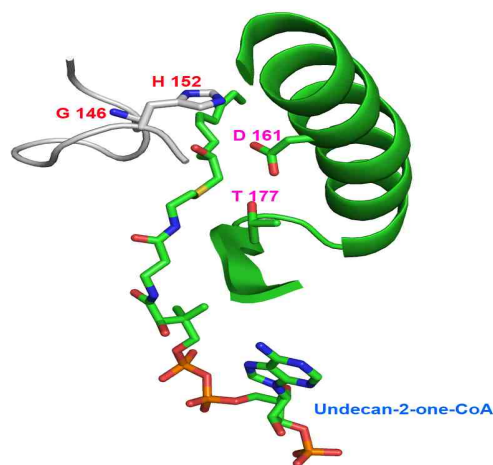
Figure 2.19 Putative hTHEM4 active site: G146, H152, D161 and T177

It is interesting to note that the electron density map in the subunit A channel contains a density indicating binding of an unknown compound that has a long extended shape. This density matches the fragment C_9-(C=O)-C-S-C-C-N, which threads in the opposite direction to undecan-2-one-CoA in the extending pocket formed by α2 helix and close loops of the N-terminal domain covering the core hotdog domain (see Figure 2.20 and Figure 2.21).
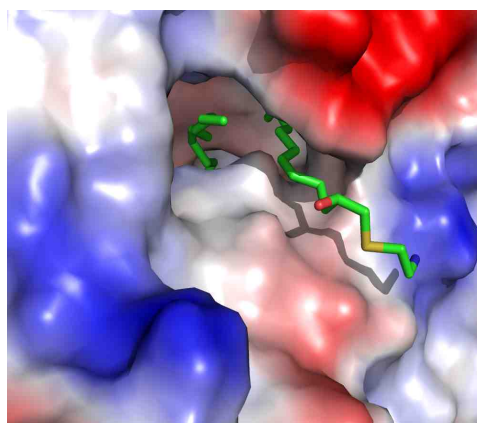
Figure 2.20 The C_9-(C=O)-C-S-C-C-N fragment shown in stick in relation to the terminal region of the undecan-2-one-CoA ligand (also shown in stick).
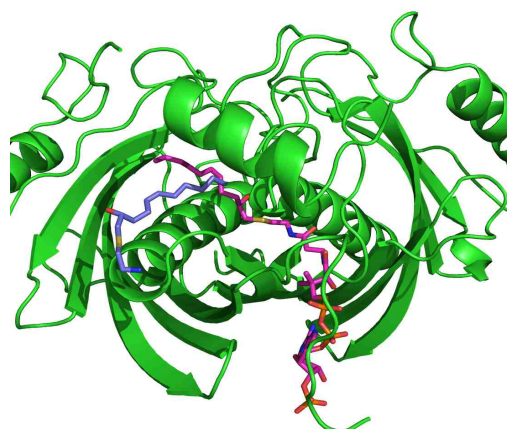
Figure 2.21 The extra fragment (carbon atoms colored purple) binding in the extending pocket, opposite to the undecan-2-one-CoA (carbon atoms colored magenta).

2.3.7 Determination of the Contributions of Active Site Residues to Catalysis

The active site residues of special interest include Asp161, Glu145, His152, Gly146, Thr177 and Tyr184. Residues Asp161, His152, Gly146 and Thr177 are well conserved among all the THEM4s and human THEM5 (sequence alignment see Figure 2.22).

Figure 2.22 Sequence alignment of all THEM4s and the human THEM4 paralog hTHEM5.

Conservative replacement of the Asp161 with Asn results in only a 60-fold reduction in the k_{cat} value (Table 2.7), which suggests that Asp161 functions as the general base in catalysis. Whereas the side chain of Asn cannot function as a catalytic base, it can position the water nucleophile through a hydrogen bond interaction. Glu replacement of Asp161 reduces the k_{cat} value 42-fold and increases the K_m value 20-fold, indicating that a side chain that extends the carboxylate group can still function but not as well as that in the native enzyme. Whereas substitution of the Asp161 with Ala results in no expression, Val replacement was successful. The kinetic constants measured for the Asp161Val mutant show an increased K_m value (262-fold) and a reduced k_{cat} value (210-fold). The activity of the Asp161Val mutant shows that the Asp161 contributes significantly to but is not essential for catalytic efficiency. This eliminates the possibility that this enzyme relies on Asp161 to function as a nucleophile and suggests that it is more likely to functions as a general base.

The Thr177 side chain hydroxyl group is located on the same side of the O=C-CH_2S (3.1 Å from the CH_2) of undecan-2-one-CoA as is the Asp161 carboxylate group and, in fact, it engages in a hydrogen bond interaction with the Asp161 carboxylate (2.9 Å). The k_{cat} values of the Thr177Ser and Thr177Val mutants are reduced 28-fold and 60-fold, respectively, from that of the wild-type enzyme (Table 2.7). The K_m values, however are unchanged. This suggests that the Thr177 hydroxyl group is important for catalytic turnover but possibly not for substrate binding. Probable roles for the Thr177 hydroxyl group are to assist Asp161 in its function as base and stabilize the CoAS- anion leaving group. If the water nucleophile binds between the Asp161 and His152 (see below), then the most likely role that Thr177 plays is to stabilize the CoAS- anionic

leaving group. The His152 ring is positioned over the carbonyl group of the undecan-2-one-CoA moiety and the His152 N3 is within hydrogen bonding distance (3.4 Å) of the Asp161 carboxylate group. However, unless N3 rather than the N1 of His152 carries the hydrogen, the close positioning may not result in interaction with the Asp161. Replacement of His152 with Phe and Ala results in 140-fold and 105-fold reductions in k_{cat}, respectively (Table 2.7). This result suggests that that the His152 ring is not simply playing a space filling role and that it may in fact be assisting the Asp161 in its role as a base.

The backbone amide NH of Gly146 is located 5.1 Å from the undecan-2-one-CoA carbonyl oxygen. Gly146 is located at the N-terminus of the central helix, a position in the 4-HBA-CoA thioesterase that is known to polarize the substrate thioester C=O by donation of a hydrogen bond from the backbone amide NH of this residue (*31,32*). Since the position of the undecan-2-one-CoA O=C-CH$_2$S moiety is only an approximation of the position that the substrate O=C-S group might assume in the enzyme substrate complex, it is possible that Gly146 functions to polarize the substrate O=C-S, thereby activating it for nucleophilic attack by water.

One highly unique feature of the hTHEM4 catalytic site is that Glu154, located on the central helix-loop of the opposing subunit, does not project into the catalytic site but rather its side chain is oriented in the other direction. In other hotdog thioesterases that belong to the same clade as hTHEM4 (the type AB clade represented by the *Arthrobacter* 4-HBA-CoA thioesterase (*34*)) a Gln or Asn residue is located on the loop and participates in catalysis. To test whether the hTHEM4 Glu154 is in fact not involved in catalysis, as the conformation of its side chain seen in the X-ray structure would suggest,

64

the Glu154Ala mutant was prepared and evaluated. There was no significant change

observed in catalytic efficiency (Table 2.7) and, thus, it is possible to conclude that

Glu154 plays no role in catalysis.

Table 2.7 Steady-State Kinetic Constants for the hTHEM4 mutants-Catalyzed Hydrolysis of Myristoyl-CoA Measured at pH 7.5 and 25°C

Enzyme	k_{cat} (s^{-1})	$K_m (\mu M)$	k_{cat} / K_m (M^{-1}s^{-1})
WT	4.2±0.1	2.4±0.1	1.7×10^6
D161V	0.02±0.00	493±137	48.2
D161E	0.10±0.01	45±3	2.3×10^3
D161N	0.07±0.01	335±93	2.0×10^2
E145A	2.6±0.1	2.0±0.1	1.3×10^6
T177A	0.07 ±0.01	4.0±1.0	1.8×10^4
T177S	0.15 ±0.01	2.0±0.4	6.4×10^4
Y184A	0.07±0.01	3.6 ±0.3	2.0×10^4
Y184F	4.0 ±0.4	2.2±0.5	1.9×10^6
H152A	0.04±0.01	62±4	6.7×10^2
H152F	0.03 ±0.01	1.1±0.1	2.7×10^4
R206A	1.5±0.1	4.2 ±0.6	3.6×10^5
R186A	6.1±0.7	5.7±1.5	1.1×10^6
N183A	5.0±0.4	4.3±0.9	1.2×10^6
K207A	1.5±0.3	2.8±1.3	6.7×10^5
K237A	2.9±0.1	1.6±0.1	1.8×10^6
D161L:T177V	0.02±0.01	336±65	49.9

Tyr184 is conserved among the THEM4s of human, chimpanzee, mouse and rat.

This position is occupied in dog, cow, horse and human THEM5 by Phe. The Tyr ring is

seen to buttress the terminal region of the pantetheine arm of the undecan-2-one-CoA, however, no direct interaction between the Tyr ring hydroxyl group and the ligand exists. The catalytic efficiency of the Tyr184Phe mutant is not significantly different from that of the wild-type enzyme whereas the k_{cat} value measured for the Tyr184Ala mutant is reduced 60-fold (Table 2.7). This result suggests that the Tyr184 functions in a space-filling role only.

The catalytic mechanism that we propose for hTHEM4 catalysis is depicted in Figure 2.23. In the pathway, Asp161 functions as general base to position and activate the water molecule for attack on the substrate carbonyl group. N3 of the His152 imidazole ring forms a hydrogen bond with the water nucleophile, orienting it for attack at the substrate carbonyl group. The backbone amide NH of Gly146 activates the substrate C=O for nucleophilic attack by forming a hydrogen bond with the oxygen atom. The Thr177 hydroxyl group forms a hydrogen bond with the thiolate leaving group, thus facilitating its departure. It is interesting to note that the double mutant D161L/T177A retains some activity.
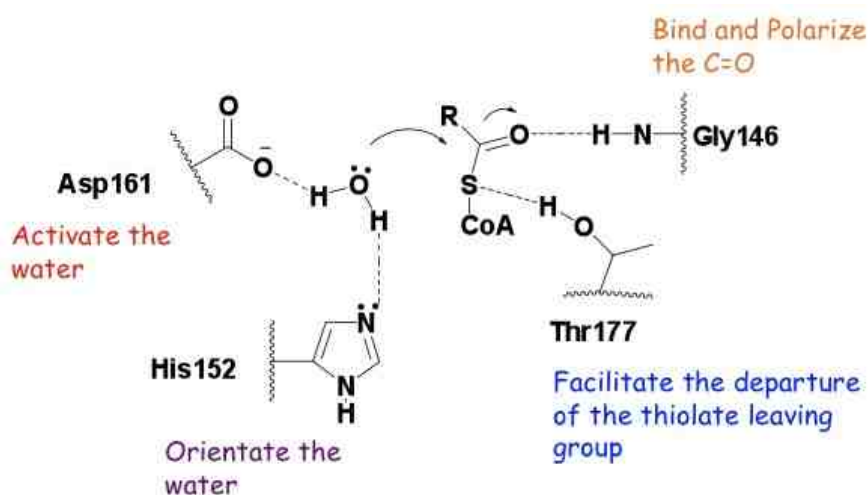
Figure 2.23 The proposed catalytic mechanism of hTHEM4

66

CoA binding site. The nucleotide unit of the undecan-2-one-CoA bound to (Δ39)hTHEM4 (Figure 2.16) resides at the entrance of the active site. The surface residues Asn183, Arg206, Arg186, Lys207 and Lys237 are observed to interact with the nucleotide moiety (Figure 2.18). To test the contribution that these residues make to substrate binding, each was separately replaced with Ala. The substrate specificity constants, included in Table 2.7, for the Ala mutants indicate that no one residue plays a significant role in catalysis. The fact that hTHEM4 accepts both acyl-CoAs and acyl-ACPs as substrates indicates that the enzyme can accept both the CoA nucleotide and ACP domains. However, the substrate specificity constant measured for myristoyl-CoA is much greater than that measured for myristoyl-ACP, a finding that indicates that a nucleotide is better accommodated by the enzyme than is the ACP.

In conclusion, the observations made in this effort suggest that the energy associated with substrate binding to hTHEM4 is largely derived from the substrates pantetheine unit (which fits snuggly in a tunnel; Figure 2.24)) and its fatty acyl side chain (which binds in a nonpolar channel; Figure 2.25). The size and polarity of the substrate acyl group determine the substrate specificity constant (Table 2.3). Moreover, desolvation of the nonpolar fatty acyl side chain and the nonpolar binding site no doubt contributes to substrate binding and, based on inspection of the k_{cat} values, it also contributes to catalytic efficieny.
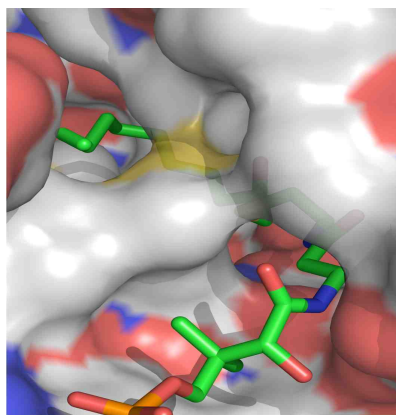
Figure 2.24 Pantoate chain binding tunnel   **Figure 2.25** Acyl chain binding pocket
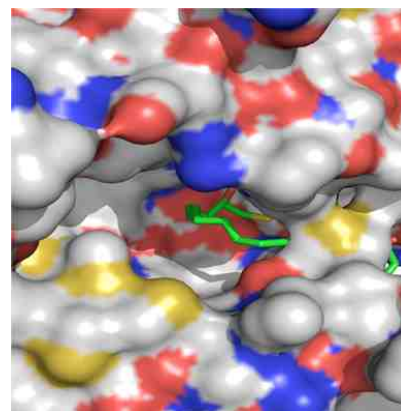
2.3.8 ^{18}O Incorporation into Product Benzoate during Wild-type Thioesterase Catalyzed Hydrolysis in ^{18}O enriched Water under Single Turnover and Multiple Turnover Conditions.

If the hTHEM4 thioesterase catalyzed hydrolysis proceeds via a general base mechanism, *i.e.* it involves direct attack of an activated water molecule on the thioester carbonyl carbon, 97% of the final product should be ^{18}O labeled under single turnover conditions when 97% ^{18}O-riched water is used as solvent for the catalytic reaction. On the other hand, the ^{18}O-incorporation outcome of a process promoted by nucleophilic catalysis is more difficult to predict, since both carbonyl groups in the mixed-anhydride intermediate can be attacked by water in the ensuing step that forms product. If the former Asp161 carbonyl group is attacked by water, the carboxyl group of the benzoic acid product would not contain any ^{18}O label. In contrast, if the benzoyl carboxyl group issite of water attack, the benzoic acid product would contain the ^{18}O label in its carboxyl group.

68

The mass spectrum of the benzoic acid standard (Figure 2.26) contains a parent ion (M*) peak at 122 m/z, and ion fragment peaks at (M*-OH) 105 m/z, (M*-COOH) at 77 m/z and an unassigned fragment peak at 51 m/z. The parent ion (M*) and parent ion fragment (M*-OH) contain oxygen from the carboxylic acid group and, as a result, can be used to measure ^{18}O incorporation. When a single turnover experiment was carried out in normal water, the product mass spectrum was identical to that of the standard benzoic acid (Figure 2.27). The mass spectrum of the product arising from a control reaction in $H_2{}^{18}O$ containing 168 µM wild-type hTHEM4 (Δ39), 2.1 mM D161L/T177V enzyme and 0.8 mM benzoyl-CoA showed 6% of the 122 m/z parent ion peak and 94% of the 124 m/z (contains one ^{18}O atom) parent ion. Thus, 6% ^{16}O containing product constitutes the "background" level of ^{16}O in corporation under these experimental conditions (Figure 2.28). The mass spectrum of the benzoic acid that results from a single turnover reaction carried out in $H_2{}^{18}O$ was observed to contain 6.4% of the 122 m/z peak and 93.6% of the 124 m/z peak (average value obtained fro duplicate reactions). This result indicates that the benzoic acid product contains one ^{18}O atom per carboxylic acid group (Figure 2.29) and suggests the operation of the general base mechanism. However, it is also consistent with a hydrolysis mechanism that proceeds via the anhydride intermediate in which attach occurs exclusively at the benzoyl carbonyl carbon. Therefore, these observations can not be used to rule out the possibility that Asp161 functions in a nucleophilic catalytic role in the enzymatic reaction.
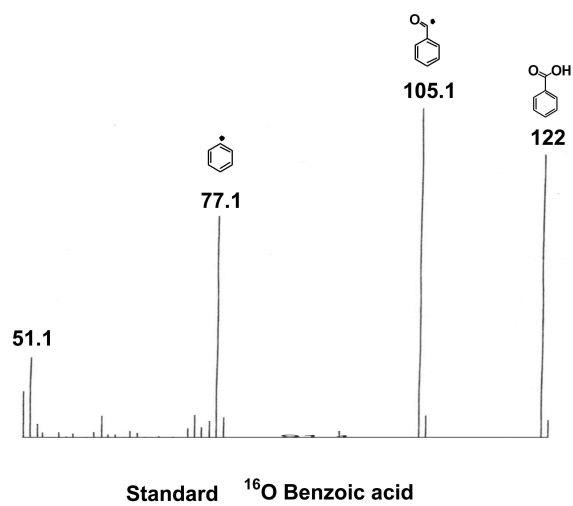
Figure 2.26 GC-MS spectrum of benzoic acid standard
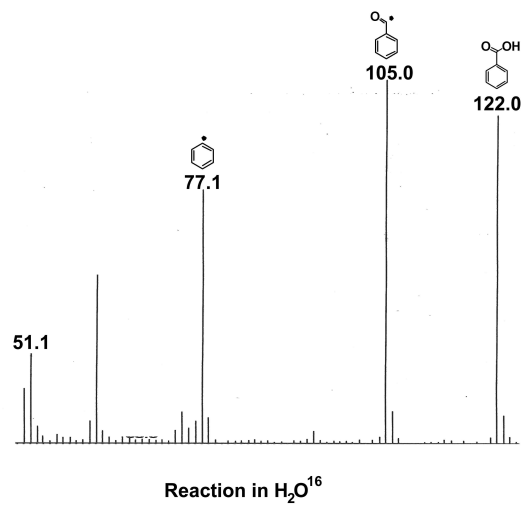
Figure 2.27 GC-MS spectrum of product of hTHEM4 (Δ39) hydrolyzing benzoyl-CoA in normal water.

Reaction in H_2O^{18} (multi-turnover as control)
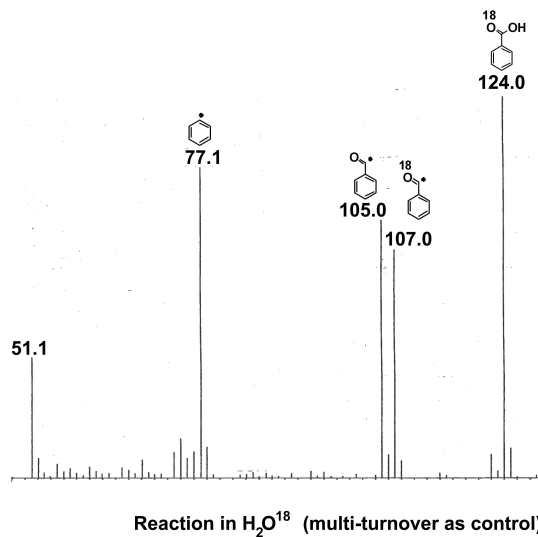
Figure 2.28 GC-MS spectrum of product resulting from reaction containing 168μM wild-type hTHEM4 (Δ39), 2.1 mM D161L/T177V enzyme and 0.8 mM benzoyl-CoA in $H_2^{18}O$

Reaction in H_2O^{18} (single turnover)
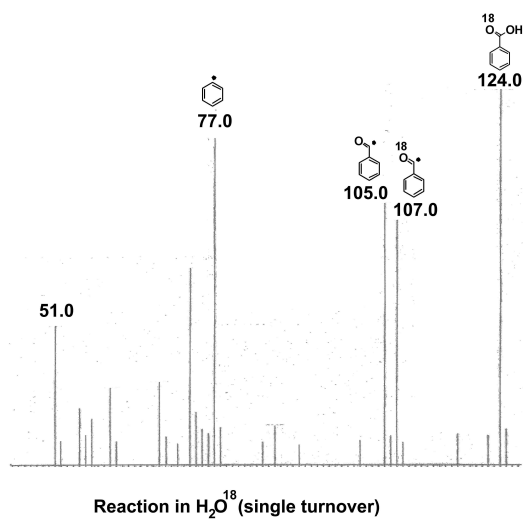
Figure 2.29 GC-MS spectrum of product of hTHEM4 (Δ39) hydrolyzing benzoyl-CoA in $H_2^{18}O$, under single turnover condition.

2.4 Conclusions

In conclusion, hTHEM4 is a broad-range, catalytic efficient acyl-CoA thioesterase with activity that extends to fatty acylated-ACP. The crystal structure of hTHEM4 indicates that it possesses a conserved hot-dog fold domain and an unusual fold domain containing two α-helices and largely irregular loop-like folding, which was predicted but not proved to have a regulatory role.

hTHEM4 is toxic to cells when the coding gene is transfected into a mammalian cell line for expression. Based on the results of Hemming, reported in 2009, that suggest that hTHEM4 is located in the mitochondria inter membrane space (IMS) (*12*), we propose that upon induction of cell apoptosis, hTHEM4 is released into cytoplasm where it promotes apoptosis with a concomitant delay/inhibition of PKB activation (associate with activated PKB or inhibit its 2 kinases). This proposal will be discussed in the next chapter. The high activity and broad specificity of hTHEM4 suggests that once it is released into the cytoplasm it hydrolyzes the fatty-acyl CoAs (and fatty-acyl ACPs), consequently, releasing long chain fatty acids which are known to be toxic to the cell. This process may also contribute to cell death.

References

1. Maira, S. M., Galetic, I., Brazil, D. P., Kaech, S., Ingley, E., Thelen, M., and Hemmings, B. A. (2001) Carboxyl-terminal modulator protein (CTMP), a negative regulator of PKB/Akt and v-Akt at the plasma membrane, *Science 294*, 374-380.

2. Knobbe, C. B., Reifenberger, J., Blaschke, B., and Reifenberger, G. (2004) Hypermethylation and transcriptional downregulation of the carboxyl-terminal modulator protein gene in glioblastomas, *J Natl Cancer Inst 96*, 483-486.

3. Testa, J. R., and Bellacosa, A. (2001) AKT plays a central role in tumorigenesis, *Proc Natl Acad Sci U S A 98*, 10983-10985.

4. Hwang SK, Kwon JT, Park SJ, Chang SH, Lee ES, Chung YS, Beck GR Jr, Lee KH, Piao L, Park J, Cho MH.(2007) Lentivirus-mediated carboxyl-terminal modulator protein gene transfection via aerosol in lungs of K-ras null mice.Gene Ther. 14(24):1721-30.

5. Hwang SK, Lim HT, Minai-Tehrani A, Lee ES, Park J, Park SB, Beck GR Jr, Cho MH.(2009) Repeated aerosol delivery of carboxyl-terminal modulator protein suppresses tumor in the lungs of K-rasLA1 mice. Am J Respir Crit Care Med. 179(12):1131-40.

6. Knobbe, C. B., Trampe-Kieslich, A., and Reifenberger, G. (2005) Genetic alteration and expression of the phosphoinositol-3-kinase/Akt pathway genes PIK3CA and PIKE in human glioblastomas, *Neuropathol Appl Neurobiol 31*, 486-490.

7. Ono, H., Sakoda, H., Fujishiro, M., Anai, M., Kushiyama, A., Fukushima, Y., Katagiri, H., Ogihara, T., Oka, Y., Kamata, H., Horike, N., Uchijima, Y., Kurihara, H., and Asano, T. (2007) Carboxy-terminal modulator protein induces Akt phosphorylation and activation, thereby enhancing antiapoptotic, glycogen synthetic, and glucose uptake pathways, *Am J Physiol Cell Physiol 293*, C1576-1585.

8. Schick, V., Majores, M., Engels, G., Spitoni, S., Koch, A., Elger, C. E., Simon, M., Knobbe, C., Blumcke, I., and Becker, A. J. (2006) Activation of Akt independent of PTEN and CTMP tumor-suppressor gene mutations in epilepsy-associated Taylor-type focal cortical dysplasias, *Acta Neuropathol 112*, 715-725.

9. Piao L, Li Y, Yang KJ, Park KA, Byun HS, Won M, Hong J, Kim JL, Kweon GR, Hur GM, Seok JH, Cho JY, Chun T, Hess D, Sack R, Maira SM, Brazil DP, Hemmings BA, Park J. (2009) Heat shock protein 70-mediated sensitization of cells to apoptosis by carboxy-terminal modulator protein. BMC Cell Biol. 10:53.

10. Miyawaki, T., Ofengeim, D., Noh, K.M., Latuszek-Barrantes, A., Hemmings, B.A., Follenzi, A., Zukin, R.S. (2009) The endogenous inhibitor of Akt, CTMP, is critical to ischemia-induced neuronal death. Nat Neurosci. 1, 494-500.

11. Claros. M.G., Vincens. p.(1996) Computational method to predict mitochondrially imported proteins and their targeting sequences. Eur. J. Biochem. 241*,* 779-786.

12. Parcellier, A., Tintignac, L.A., Zhuravleva, E., Cron, P., Schenk, S., Bozulic, L., Hemmings, B.A. (2009) Carboxy-terminal modulator protein (CTMP) is a mitochondrial protein that sensitize cells to apoptosism. Cell Signal, 21(4), 639-50.

13. Piao L, Li Y, Kim SJ, Sohn KC, Yang KJ, Park KA, Byun HS, Won M, Hong J, Hur GM, Seok JH, Shong M, Sack R, Brazil DP, Hemmings BA, Park J.(2009) Regulation of OPA1-mediated mitochondrial fusion by leucine zipper/EF-hand-containing transmembrane protein-1 plays a role in apoptosis.Cell Signal. 21(5):767-77.

14. Thoden, J.B., Holden, H.M., Zhuamg, Z., Dunaway-Mariano, D. (2002) X-ray crystallographic analysis of inhibitor and substrate complexes of wild-type and mutant 4-Hydroxybenzoyl-CoA thioesterase. J. Biol. Chem. 277, 27468-76.

15. Luo, L., Taylor, K.L., Xiang. H., Wei, Y., Zhang, W., Dunaway-Mariano, D. (2001) Role of active site binding interaction in 4-Chlorobenzoyl-Cozenzyme A dehalogenase catalysis. Biochemistry. 40, 15684-92.

16. Bunkoczi, G., Pasta, S., Joshi, A., Wu, X.Q., Kavanagh, K.L., Smith, S., Oppermann, U. (2007) Mechanism and Substrate Recognition of Human Holo ACP Synthase. Chemistry and Biology, 14, 1243-1253

17. Joshi, A.K., Zhang, L., Rangan, V.S., Smith, S. (2003) Cloning, expression, and characterization of a human 4'-phosphopantetheinyl transferase with broad substrate specificity. J. Biol. Chem. 278, 33142-149.

18. Altschul, S. F., Gish, W., Miller, W., Myers, E. W., and Lipman, D. J. (1990) Basic local alignment search tool, *J Mol Biol 215*, 403-410.

19. McCoy, A. J., Grosse-Kunstleve, R. W., Storoni, L. C., and Read, R. J. (2005) Likelihood-enhanced fast translation functions, *Acta Cryst D61*, 458-464.

20. Storoni, L. C., McCoy, A. J., and Read, R. J. (2004) Likelihood-enhanced fast rotation functions, *Acta Cryst D60*, 432-438.

21. Murshudov, G. N., Vagin, A. A., and Dodson, E. J. (1997) Refinement of macromolecular structures by the maximum-likelihood method, *Acta Cryst D 53*, 240-255.

22. Terwilliger, T. C. (2000) Maximum likelihood density modification, *Acta Cryst D 56*, 965-972.

23. Emsley, P., and Cowtan, K. (2004) Coot: model-building tools for molecular graphics, *Acta Cryst 60*, 2126-2132.

24. Smith. S. (1981) Long-Chain fatty acyl-s-4'-phosphopantetheine-fatty acid synthase thioester hydrolase from rat. Methods Enzymol. 71, 188-200.

25. Smith. S. (1981). Medium-Chain fatty acyl-s-4'-phosphopantetheine-fatty acid synthase thioester hydrolase from lactating mammary gland of rat. Methods Enzymol. 71, 181-188.

26. Naggert. J., Narasimhan. M.L., Veaux. L., Cho. H., Randhawa. Z.I., Cronan. J.E., Green. B.N., Smith. S. (1991) Cloning, sequencing and characterization of *Escherichia coli* thioesterae II. J. Biol. Chem. 266(17), 11044-50.

27. Jones. A., Davies. M., Voelker. T.A. (1995) Palmitoyl-acyl carrier protein(ACP) thioesterase and the evolutionary origin of plant acyl-ACP thioesterases. Plant Cell 7, 359-71.

28. Cao, J., Xu, H., Zhao, H., Gong, W.M., Dunaway-Mariano, D. (2009) The mechanisms of human hotdog-fold thioesterase 2 (hTHEM2) substrate recognition and catalysis illuminated by a structure and function based analysis. Biochemistry. 48(6), 1293-304.

29. Smith, R.H., Powell, G.L. (1986) The critical micelle concentration of some physiologically important fatty acyl-coenzyme A's as a function of chain length. Archives of Biochemistry and Biophysics. 244(1), 357-360.

30. Constantinides, P.P., Steim, J.M. (1985) Physical properties of fatty acyl-CoA: critical micelle concentrations and micelle size and shape. J. Bio. Chem. 260(12), 7573-80.

31. Ramachandran, G. N., Ramakrishnan, C., and Sasisekharan, V. (1963) Stereochemistry of polypeptide chain configurations, J Mol Biol 7, 95-99.

32. Laskowski, R. A., MacArthur, M. W., Moss, D. S., and Thorton, J. (1993) PROCHECK: a program to check the stereochemical quality of protein structures, J Appl Cryst 26, 283-291.

33. Benning. M.M.,Wesenberg. G., Liu. R., Taylor., K.L., Dunaway-Mariano. D., Holden. H.M. (1998) The three-dimensional structure of 4-Hydroxybenzoyl-CoA thioesterase from *Pseudomonas* sp. Strain CBS-3. J Biol Chem. 273(50), 33572-79.

34. Thoden.J.B. Zhuang. Z., Dunaway-Mariano. D., Holden., H.M. (2003) The structure of 4-hydroxybenzoyl-CoA thioesterase from *Arthrobacter* sp. Strain SU. J Biol Chem. 278(44), 43709-16.

CHAPTER THREE

INTERACTION OF HTHEM4 (CTMP) AND PROTEIN KINASE B α

(PKBα, AKT1)

3.1 Introduction

The PKB family of protein kinases play a key role in insulin signaling, and cellular survival and transformation. Therefore this family has emerged as a central player in tumorigenesis (*1*). All mammalian PKB isoforms (PKBα, PKBβ, PKBγ) share a common structure that consists of a NH_2-terminal regulatory domain with a pleckstrin homology (PH) domain (*2*), a short α-helical linker, and a carboxyl-terminal kinase domain (catalytic and regulatory domain ("RD")) that are required for the induction and maintenance of kinase activity (*3*) (Figure 3.1). Significant efforts have been made to identify potential binding partners of PKB/Akt, which may govern its biological function.

1   **100**   **411**   **480**

PH   **Catalytic**   **RD**

Figure 3.1 PKB/Akt domain structure. PH: pleckstrin homology (PH) domain, Catalytic domain: Serine/ Threonine protein kinase catalytic domain, RD: C-terminal regulatory domain, extension to Ser/Thr protein kinase.

PKBα(Akt1) is a serine-threonine protein kinase that plays a key role in cancer by stimulating cell proliferation and inhibiting apoptosis (*3*). Akt1 is recruited from the

cytoplasm to the plasma membrane via association of its PH domain with lipid-anchored phosphatidylinositol 3,4,5-trisphosphate. At the membrane Akt1 is activated by phosphorylation of Thr308 in the catalytic domain by the kinase PDK1 and phosphorylation of Ser473 in the C-terminal regulatory domain by the mTORC2 complex (*4,5*). Akt1 negative protein regulators can reduce Akt1 kinase activity by binding to Akt1 and preventing its phosphorylation at one or both sites.

hTHEM4, otherwise known as the carboxyl-terminal modulator protein CTMP, was first identified as a PKB (protein kinase B, also called Akt) inhibitor ("negative regulator") (*6*). Purportedly, hTHEM4 binds to the membrane bound PKBa/Akt1 C-terminal regulatory domain thereby blocking its activation by phosphorylation. The experimental evidence reported by Hemmings and his co-workers for the binding of hTHEM4 to the PKBa/Akt1 derived from *in vivo* studies which included (a) a yeast two-hybrid analysis with the kinase domain plus the C-terminal regulatory domain of PKBα as targets, (b) a mammalian cell two-hybrid assay, (c) an immunofluorescence analysis which demonstrated that endogenous PKB and CTMP colocalize at the plasma membrane, (d) immunoprecipitation of a complex Flag-hTHEM4 and GST-C-terminal regulatory domain of PKBa/Akt1, and (e) reduced PKBa/Akt1 PKB phosphorylation on pSer473 in *hTHEM4*-transfected HEK293 cells.

A later report challenged this original work and concluded that hTHEM4 is a positive regulator of PKBa/Akt1 (*7*). The later workers proposed that membrane bound hTHEM4 binds to cytoplasmic PKBa/Akt1, thus, recruiting the PKBa/Akt1 to the membrane where it is activated by phosphorylation. The evidence reported to support hTHEM4 interaction with PKBa/Akt1 include (1) transient hTHEM4 overexpression

enhanced PKBa/Akt1 phosphorylation and activation in COS-1, HepG2, HEK293, and Hela cells under both unstimulated and stimulated conditions, (2) PKBa/Akt1 expression induced phosphorylation of Foxo1 and GSK-3β which are substrates of PKBa/Akt1, in Hela and NIH3T3cells, (3) siRNA suppression of endogenous hTHEM4 expression led to reduced PKBa/Akt1 phosphorylation, (4) hTHEM4 enhanced membrane localization of Akt without affecting PI3-kinase activity, (5) CTMP co-expression of hTHEM4 and PKBa/Akt1 rescued Hela cells from UV-B irradiation-induced apoptosis, and (6) hTHEM4 expression in 3T3-L1 adipocytes modestly enhanced glucose uptake and glycogen synthesis.

The reason(s) for the contrasting findings from the two laboratories is not known. However, it is generally known that the outcome of *in vivo* studies of protein compartmentalization and protein-protein interaction can be dependent on the cell lines used, the level of expression of the targeted protein(s) and even the epitode tag/GFP fusion constructs of the proteins employed. Nevertheless, the common finding reported by the two laboratories is that hTHEM4 and PKBa/Akt1 associate and as a result PKBa/Akt1 activity is altered. The goal of the work reported in this chapter was to test hTHEM4 binding to PKBa/Akt1 and the impact of this binding on the PKBa/Akt1 kinase activity and activation by upstream kinases PDK1 and mTORC2.

3.2 Experimental

3.2.1 Preparation of Recombinant PKBa/Akt1 in Escherichia coli for Co-Immunoprecipitation with (fl)hTHEM4 and (Δ39)hTHEM4

The cDNA clone of the gene *AKT1* (BC000479) encoding (fl)PKBa/Akt1 was purchased from the Thermo Scientific (MHS1011-58771). The primers 5'-GCCTCGGGCCATATGAGCGACGTGGCT-3' and 5'-CAGTCCACCGGATCCTCAGGCCGTGCCGCT-3' were used to amplify the gene from the cDNA template. The gene was inserted into the Addgene plasmid 11540: pHM6g.TM1457 (to produce the His_6-MBP TEV protease cleavable construct) cut with NdeI and BamHI. The ligated plasmid containing the AKT1 gene was used to transform BL21-CodonPlus(DE3)-RIPL competent cells (Stratagene). Transformed cells were cultured at 20 °C and 180 RPM in LB media for 8 h (OD_{600} = 0.7) and then induced with 0.4 mM IPTG. After 12 h, the cells were harvested by centrifugation at 4 °C and 6500 RPM. The resulting 10 g of cell paste was suspended in 100 mL of ice-cold lysis buffer (50 mM NaH_2PO_4, 200 mM NaCl, 10 mM imidazole, pH 8.0), passed through a French press at 1200 PSIG, and then centrifuged at 48000 × g and 4 °C for 30 min. The cell lysate was first applied to a Ni-NTA column, which was pre-equilibrated with lysis buffer. The column was washed with 50 mM NaH_2PO_4/500 mM NaCl /80 mM imidazole wash buffer and then eluted with 100 mL of 50 mM NaH_2PO_4/500 mM NaCl /250 mM imidazole. His_6-TEV protease was added to the pooled fractions containing His_6-MBP-Akt1, at 1 OD_{280} of TEV protease per 20 OD_{280} of protein solution containing 50 mM NaH_2PO_4/200 mM NaCl/10 mM imidazole. Following 12 h incubation at 4°C, the protein

mixture was loaded onto a second Ni-NTA column and the His$_6$-MBP-Akt1 collected in the eluant. The Akt1 product, analyzed by using SDS-PAGE, was estimated to be *ca.* 90% pure. The yield was 5 mg/gm wet cells.

3.2.2 Preparation of Recombinant (fl)hTHEM4 and (Δ39)hTHEM4 in Escherichia coli

(fl) hTHEM4 and (Δ39) hTHEM4 used in these experiments were produced in *E. coli* by employing the procedure described in Chapter 2.

3.2.3 Co-Immunoprecipitation of Recombinant (fl)PKBa/Akt1 and (fl)hTHEM4 and (Δ39)hTHEM4.

Protein concentrations were measured by using the Bradford assay. Anti-PKBa/Akt1 antibody (Cell Signaling #9272) covalently immobilized agarose beads were prepared following the manufacturer's instructions (Thermo Scientific #26148:Pierce Direct IP Kit). Briefly, 20 µg of the PKBa/Akt1 antibody were incubated with 40 µL of the agarose bead slurry in the presence of NaCNBH$_3$ at room temperature for at least 2 h. The uncoupled antibody was removed by extensive washing and the uncoupled reactive sites in agarose beads were quenched by incubation with the primary amine and NaCNBH$_3$. Purified recombinant (fl)PKBa/Akt1 (0.1 µg/µL) and (fl)hTHEM4 (0.025 µg/µL) or (Δ39)hTHEM4 (0.05 µg/µL, 0.12 µg/µL, 0.16 µg/µL) were incubated with the PKBa/Akt1 antibody immobilized agarose beads in 600 µL of IP lysis buffer at 4°C for overnight. As a control, hTHEM4 was incubated with the PKBa/Akt1 antibody immobilized agarose beads in the absence of PKBa/Akt1. Unbound or weakly bound

protein was removed by using washing steps prior to eluting the specifically bound protein from the beads with the elution buffer (10 mM Tris with 100 mM glycine pH 7.4). The eluted protein was subjected to SDS-PAGE and the Western blot was developed using anti-THEM4 antibody (Abnova, H00117145-B01) (for details see below).

Immunoblot analysis

The antibodies used in this study were anti-Akt (Cell Signaling), anti-THEM4 (Abnova, H00117145-B01), anti-mouse HRP and anti-Rabbit HRP (Invitrogen). Protein samples were separated by using 12% SDS-PAGE before being transfered to a nitrocellulose membrane, which was then incubated for 12 h with the primary antibody at 4 °C. After extensive washing, the membrane was treated with anti-mouse (rabbit) HRP. Chemiluminescence was carried out using enhanced chemical luminescent (ECL) reagents (PerkinElmer). Finally, the image was obtained by exposing the membrane to Kodak Biomax light film (Sigma-Aldrich).

3.2.4 PDK1 Activity Assay *(as carried out by our collaborators at GSK)*

The His$_6$ tagged FL-PDK1 was produced using a Baculovirus expression system. The cells (86 g) were lysed in 50 mM Tris (pH 8.0) containing 300 mM NaCl, 10 mM imidazole, and 0.1% triton using an Avestin homogenizer (two passes at 10,000-15, 000 psi). The supernatant was loaded onto an Ni-NTA SF column and eluted with a linear gradient or 10-300 mM imidazole. The desired fractions were pooled and purified further using a Superdex 200 column with 50 mM Tris (pH 7.5) containing 150 mM NaCl and

2.5 mM DTT serving as eluant. The desired fractions were pooled and glycerol was added to make a final concentration of 20%. FL-PDK1 activity was measured using (cat)Akt1 (*8*) and ATP as substrates in the absence and in the presence of varying amounts of recombinant (fl)hTHEM4 and (Δ39)hTHEM4. Reaction buffer containing 25 mM MOPS, 0.5 mM CHAPS, 10 mM $MgCl_2$, 50 mM KCl, 1 mM DTT and 0.1 mg/mL BSA (pH 7.5) was used to prepare FL-PDK1, Akt1 and ATP solutions as well as hTHEM4 solutions. To a non-binding surface plate, 10 mL of Akt1 (0.25 mM) and ^{33}P-ATP (5 mM) mix were added along with 10 ml of hTHEM4 (0-6 mM) solution. The reaction was started by the addition of 20 mL of FL-PDK1 (10 nM) and terminated at 0, 5, 15, 30, 60, 120, 180 and 240 min by transferring 35 mL aliquots of the solution to 170 mL of ice cold 25% TCA in a Millipore MSHV filter plate. After 15 min the precipitate was washed 5-times with 100 mL of 25% TCA and the filter plate was dried at 50 ^{o}C for 30 min. Next, 50 mL of Microscint20 cocktail was added and the plate was read in TopCount using a ^{33}P protocol.

3.2.5 Full-length Akt1 and Akt1 Catalytic Domain Activity Assay *(as carried out by our collaborators at GSK)*

The catalytic activities of His$_6$ tagged (fl)Akt1 (*9*) and (cat)Akt1 were measured using GSK3a peptide (RPRAATF) and ATP as substrates in the presence or absence of hTHEM4. Reaction buffer containing 25 mM MOPS, 0.5 mM CHAPS, 10 mM $MgCl_2$, 50 mM KCl, 1 mM DTT and 0.1 mg/mL BSA (pH 7.5) were used to prepare Akt1, GSK3a and ATP solutions along with hTHEM4. To a non-binding surface plate, 10 mL

of the GSK3a (10 mM) and ^{33}P-ATP (50 mM) mix were added along with 10 mL of hTHEM4 (0-6 mM) solution. Reaction was initiated by the addition of 20 mL of Akt1 (1 nM) and terminated at 0, 5, 15, 30, 60, 120, 180 and 240 min by adding 40 mL of 1% H_3PO_4 to the plate. After 10 min, 60 mL of the quenched reaction solution was transferred to a Millipore MAPH filter plate. After 30 min the filter plate was washed 5-times with 100 mL of 1% H_3PO_4 and then the filter plate was dried at 50 ^{o}C for 30 min. Next, 50 mL of Microscint20 cocktail was added and the plate was read in TopCount using a ^{33}P protocol.

3.2.6 mTORC2 Activity Assay *(as carried out by our collaborators at GSK)*

mTORC2 was prepared as an immunoprecipitate using HEK293 MSRII (host/stable cell line: 105780) cell lysate, precleared by treatment with protein G Sepharose. To the precleared lysate 1.5 mg of Bethyl rabbit anti-Raptor or 0.4 mg of rabbit anti-Rictor is added per mg of the lysate protein and the samples were rotated for 90 min at 4 ^{o}C. Next, 26.7 mL of protein G Sepharose suspension per mg of the lysate protein was washed with lysis buffer and added to the mixture of lysate and antibody. This mixture was rotated for 90 min at 4 ^{o}C. The protein G Sepharose was then harvested by centrifugation at 3700 RPM and 4 ^{o}C. The pellet was washed with lysis buffer and then with 25 mM HEPES (pH 7.5) containing 50 mM KCl. The bead suspension was diluted with 25 mM HEPES (pH 7.5) containing 50 mM KCl to give a final volume of 100 mL per 0.46 mg of original raw lysate protein and then 25 mL aliquots were added to the wells of an Eppendorf 96 well PCR tube plate. Following centrifugation, 12.5 mL of supernatant was removed from each well without disturbing the pellets and then 3.8 mL

of 1.4 mM unactivated FL AKT and varying amounts of hHTEM4 in buffer (50 mM HEPES 7.5, 5 mM MnCl$_2$, 2 mM DTT) and 3.8 mL of 600 mM ATP, 6.67 mM magnesium acetate and 6.67 mM manganese chloride in the same buffer were added. Control wells were prequenched with 5 mL 50 mM EDTA (pH 8). The plates were sealed and shaken at 300 RPM at 30 $^{\circ}$C. After 90 min, the reactions were quenched by the addition of 5 mL 50 mM EDTA and then centrifuged for 2 min at 3700 RPM and 4 $^{\circ}$C to pellet the immunoprecipitate. To each well of a 384 well PerkinElmer white Proxiplate was added 1 mL of 5 mg/mL BSA, and then 4 mL of quenched reaction supernatant. AlphaScreen acceptor and donor bead mixes were then added to the wells following the manufacture's instructions and the plates were read using an Envision instrument.

3.3 Results and Discussion

3.3.1 Test of hTHEM4- PKBa/Akt1 Binding by Co-Immunoprecipitation

In order to test the association of PKBa/Akt1 and hTHEM4 a variant of a "pull-down" experiment was devised in which the PKBa/Akt1-hTHEM4 complex formed in a buffered solution of PKBa/Akt1 and hTHEM4 is captured by a PKBa/Akt1 antibody that was immobilized on agarose beads. The recombinant, full length PKBa/Akt1 ((fl) PKBa/Akt1, full length His$_6$-hTHEM4 (His$_6$-(fl)hTHEM4) and the MLS-removed hTHEM4 N-terminal truncate ((D39)hTHEM4-His$_6$) used in this experiment were prepared as described in the Experimental section. The SDS-PAGE gels of the purified His$_6$-MBP-(fl)PKBa/Akt1 and the (fl)PKBa/Akt1 produced by TEV cleavage are shown in Figure 3.2 and Figure 3.3, respectively, and the SDS-PAGE gel of the purified His$_6$-(fl)hTHEM4 and (Δ39)hTHEM4-His$_6$ is shown in Figure 3.4.
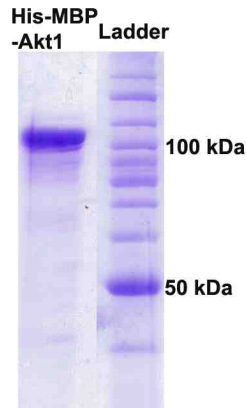
Figure 3.2 SDS-PAGE of purified His$_6$-MBP-(fl)PKBa/Akt1 (left lane). Right lane: ladder of protein molecular weight standards.
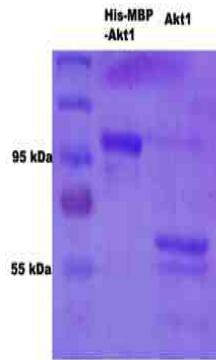
Figure 3.3 SDS-PAGE of purified His$_6$-MBP-(fl)PKBa/Akt1 (center lane) and (fl)PKBa/Akt1 derived from TEV cleavage (right lane). Left lane: ladder of protein molecular weight standards.
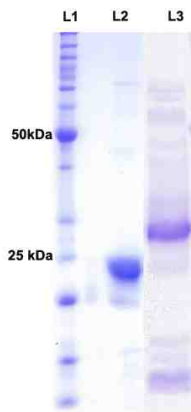
Figure 3.4 SDS-PAGE of His$_6$-(fl)hTHEM4 (lane 3) and (D39)hTHEM4-His$_6$ (lane 2). Lane 3: ladder of protein molecular weight standards.

The equilibrium mixture derived from combining His_6-MBP-(fl)PKBa/Akt1 in 2-fold molar excess to His_6-(fl)hTHEM4 was incubated with PKBa/Akt1 antibody-agarose beads, which were separated, washed and eluted. The eluate was chromatographed on a SDS-PAGE gel, which was subjected to Western blot analysis using anti-Akt antibody and anti-THEM4 antibody. The results presented in Figure 3.5 show that both His_6-MBP-(fl)PKBa/Akt1 and His_6-(fl)hTHEM4 were retained by the PKBa/Akt1 antibody-agarose beads. In order to rule out the possibility that His_6-(fl)hTHEM4 retention is due to the direct binding of PKBa/Akt1 to the antibody-agarose beads, a control experiment in which does not contain His_6-MBP-(fl)PKBa/Akt1 was carried out. The results presented in Figure 3.5 show that no His_6-(fl)hTHEM4 was present in the eluate in this case, thus, demonstrating that His_6-(fl)hTHEM4 retention is mediated by His_6-MBP-(fl)PKBa/Akt1. This finding suggests that His_6-MBP-(fl)PKBa/Akt1 and His_6-(fl)hTHEM4 bind to form a stable complex.

In parallel with studies carried out with the His_6-(fl)hTHEM4, $(\Delta39)$hTHEM4-His_6 association with (fl)PKBa/Akt1 was examined. Experiments employing concentrations of His_6-(fl)hTHEM4 (0.025 µg/µL) and (fl)PKBa/Akt1 (0.1 µg/µL) used to demonstrate association did not yield a positive result. Therefore, the experiment was repeated at a higher concentration of His_6-(fl)hTHEM4 (0.16 µg/µL). At the 6-fold higher His_6-(fl)hTHEM4 concentration, complex formation was detected (see Figure 3.6). To determine the minimal concentration needed to detect $(\Delta39)$hTHEM4-His_6 association with (fl)PKBa/Akt1, a concentration dependence study was carried out. Specifically the concentration of (fl)PKBa/Akt1 was held constant at 0.1 µg/µL and the concentration of $(\Delta39)$hTHEM4-His_6 was varied between 0.05, 0.12, 0.16 µg/µL. The results are

presented in Figure 3.7. The complex was not detected at 0.05 μg/μL (Δ39)hTHEM4-His$_6$ but it was detected at 0.12 μg/μL (Δ39)hTHEM4-His$_6$. Thus, the (Δ39)hTHEM4-His$_6$ construct binds to the (fl)PKBa/Akt1with *ca.* 5-fold lower affinity. At the current time, we do not know why the (Δ39)hTHEM4-His$_6$ construct binds less tightly. It might be a result of a difference in the position of the His$_6$-tag (C-terminal vs N-terminal) and/or the absence of the MLS sequence.
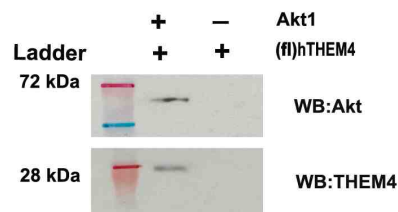
Figure 3.5 Western Blots of the protein fraction eluted from PKBa/Akt1 antibody-functionalized agarose beads incubated in a buffered solution of (fl)PKBa/Akt1 (0.1 μg/μL) and His$_6$-(fl)hTHEM4 (0.025 μg/μL) (center lane) or of His$_6$-(fl)hTHEM4 (0.025 μg/μL) (right lane) and then washed. Upper panel: Western blot developed using the anti-Akt antibody. Lower panel: Western blot developed using the anti-THEM4 antibody.
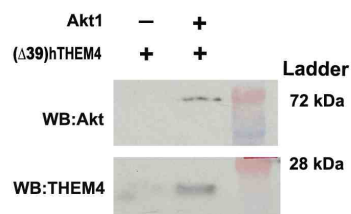
Figure 3.6 Western Blots of the protein fraction eluted from PKBa/Akt1 antibody-functionalized agarose beads incubated in a buffered solution of (fl)PKBa/Akt1 (0.1 μg/μL) and (Δ39)hTHEM4-His$_6$ (0.16 μg/μL) (center lane) or of (fl)hTHEM4-His$_6$ (0.16 μg/μL) (right lane) and then washed. Upper panel: Western blot developed using

the anti-Akt antibody. Lower panel: Western blot developed using the anti-THEM4 antibody.
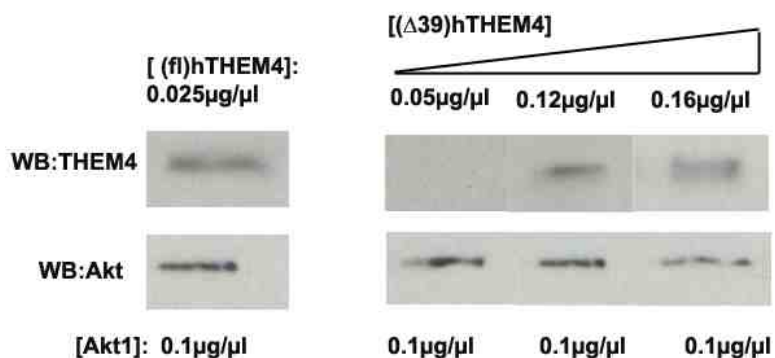
Figure 3.7 Assessment of the (Δ39)hTHEM4-His$_6$ concentration dependence of (fl)PKBa/Akt1-(Δ39)hTHEM4-His$_6$ complex formation. Left panel: Western blots of the protein fraction eluted from PKBa/Akt1 antibody-functionalized agarose beads incubated in a buffered solution of (fl)PKBa/Akt1 (0.1 µg/µL) and His$_6$-(fl)hTHEM4 (0.025 µg/µL) developed with anti-THEM4 antibody (upper panel) or anti-Akt antibody (lower panel). Right panel: Western blots of the protein fraction eluted from PKBa/Akt1 antibody-functionalized agarose beads incubated in a buffered solution of (fl)PKBa/Akt1 (0.1 µg/µL) and 0.05 µg/µL, 0.12 µg/µL or 0.16 µg/µL (lanes left to right) (Δ39)hTHEM4-His$_6$ and developed with anti-THEM4 antibody (upper panel) or anti-Akt antibody (lower panel).

3.3.2 Determination of the Effect of hTHEM4 on the Phosphorylation of Akt1 and on Akt1 Kinase Activity.

To test the effect of hTHEM4 on PKBa/Akt1 kinase activity and phosphorylation, purified recombinant His$_6$-(fl)hTHEM4 and (Δ39)hTHEM4-His$_6$ were sent to Dr. Lusong Luo at GaxoSmithKline (GSK). Dr. Luo and his co-workers had recently developed kinetic assays to evaluate PKBa/Akt1 kinase activity with peptide substrates and PDK1 and mTORC2 kinase activity towards their downstream target PKBa/Akt1.

90

Firstly, the effects of His$_6$-(fl)hTHEM4 and (Δ39)hTHEM4-His$_6$ on the kinase activities of activated (phosphorylated) full length PKBa/Akt1 ((fl)Akt1) and the PH domain truncate ((cat)Akt1) was assayed using the substrate GSK3a peptide. The titration curves depicted in Figure 3.8 show that (fl)Akt1 and (cat)Akt1 activities are reduced to 60% and 50%, respectively at 6 µM full-length hTHEM4 and 1 nM M full-length Akt1. The data were fitted (Figure 3.9) to define a K$_d$ = 0.7 ± 0.1 µM, which is likely to be within a range that is of physiological importance as defined by the cellular concentrations of hTHEM4 and Akt1 (which are not known but are assumed to be within range of the concentration used in this experiment).
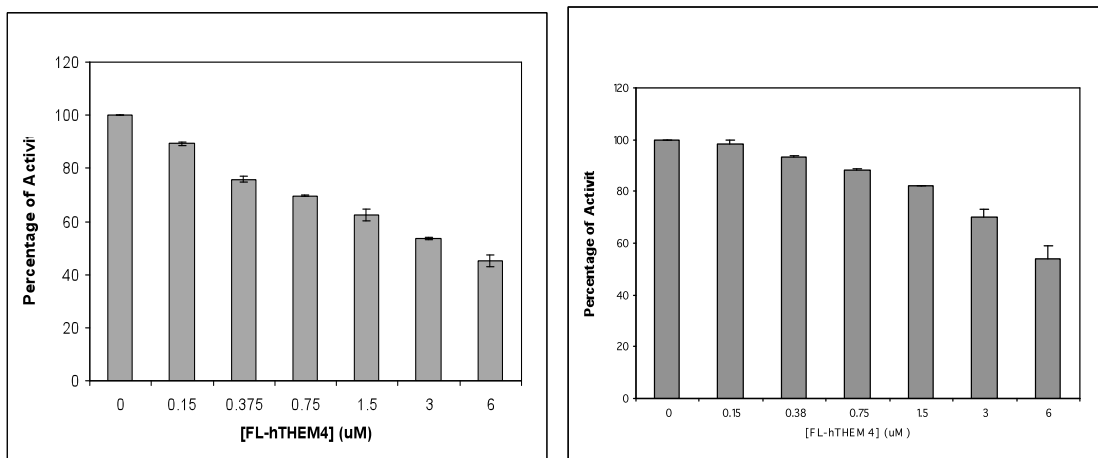
Figure 3.8 The direct effect of FL-hTHEM4 on (fl)Akt1 and truncated Akt1activity using peptide substrate. Left graph: Activity of His$_6$ tagged (fl)Akt1 was measured using GSK3a peptide (RPRAATF) and ATP as substrates in the presence different amount of FL-hTHEM4 (0,0.15,0.375,0.75,1.5,3,6 µM). Right graph: Activity of truncated Akt1-(cat)Akt1 was measured using GSK3a peptide (RPRAATF) and ATP as substrates in the presence of different amount of FL-hTHEM4

(0,0.15,0.38,0.75,1.5,3,6 µM). The activity of reaction solution without the FL-hTHEM4 is set as 100% activity.

If it is assumed that unbound (fl)Akt1 has 100% activity and (fl)Akt1+FL-hTHEM4 complex has 0 activity, conversion of the activity value of (fl)Akt1 (complex with FL-hTHEM4) into a percent activity at different concentration of FL-hTHEM4 (see Table 3.1) is possible. The binding constant Km of FL-hTHEM4 can be obtained by first plotting these data with a Y-axis corresponding to the activity of complex (Akt1+FL-hTHEM4) and the X-axis being the concentration of FL- hTHEM4, and then fitting the plot to Michaelis-Menten equation V=Vmax*[S]/Km+[S].

Table 3.1 Percentage of activity of (fl)Akt1(complex with FL-hTHEM4) at different concentration of FL-hTHEM4.

hTHEM4(nM)	Activity
0	1
150	0.89
375	0.76
750	0.7
1500	0.62
3000	0.54
6000	0.45
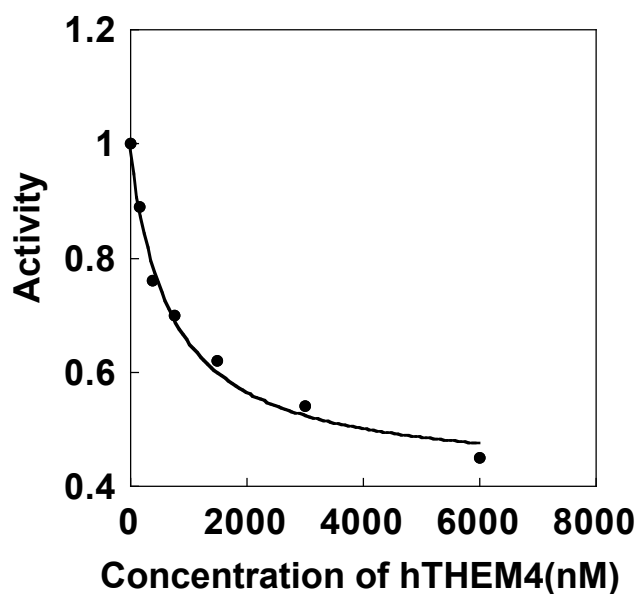
Figure 3.9 Fitting of Akt1 activity versus concentration of hTHEM4, define the binding constant (Kd) is 701.64 nM (0.7 µM). Plot data in table3.1 by inputting Y-axis with the activity of complex (Akt1+FL-hTHEM4) and X-axis with the concentration of FL- hTHEM4, taking the system as Enzyme and substrate binding reaction, fitting the plot with Michaelis-Menten equation (V=Vmax*[S]/Km+[S]) complementary function: y=m3-m1*m0/(m2+m0); FL-hTHEM4 is the substrate, m1=Vmax, m0=[S], m2=Km=Kd.

The (Δ39) hTHEM4, on the other hand, showed a less prominent effect on Akt1 activity (20 and 15% reduction, respectively) (Figure 3.10).
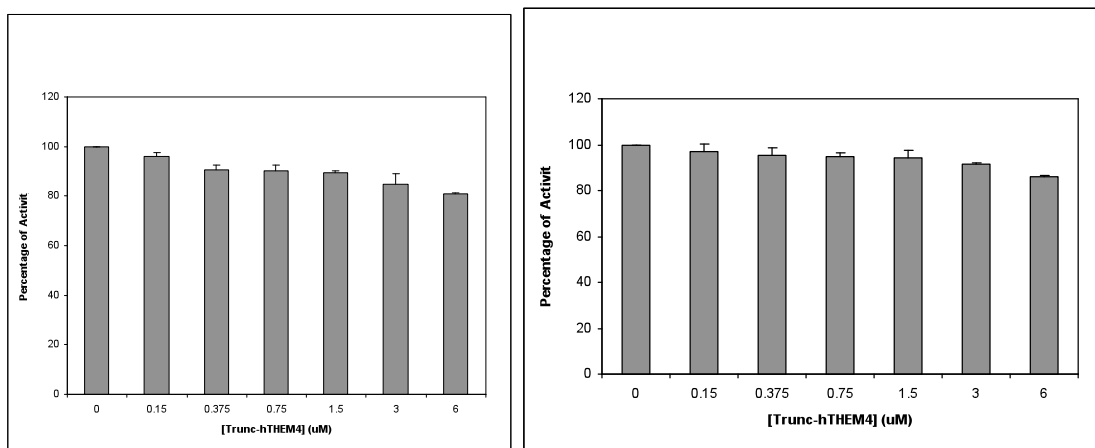
Figure 3.10 The direct effect of Trunc-hTHEM4: (Δ39) hTHEM4 on (fl) Akt1 and truncated Akt1 activity using peptide substrate. Left graph: Activity of His_6 tagged (fl)Akt1 was measured using GSK3a peptide (RPRAATF) and ATP as substrates in the presence different amount of (Δ39)hTHEM4 (0,0.15,0.375,0.75,1.5,3,6 μM). Right graph: Activity of truncated Akt1-(cat)Akt1 was measured using GSK3a peptide (RPRAATF) and ATP as substrates in the presence of different amount of (Δ39)hTHEM4 (0,0.15,0.375,0.75,1.5,3,6 μM). The activity of reaction solution without the (Δ39)hTHEM4 is set as 100% activity.

Lastly, we surveyed the effects of hTHEM4 on the activities of the Akt1 activator PDK1, which catalyzes the ATP phosphorylation of Akt1 Thr308 and the Akt1 activator mTORC2, which catalyzes the ATP phoshorylation of Akt1 Ser473. The titration curves depicted in Figure 3.11 and Figure 3.12 show that a reproducible enhancement occurs in the (unactivated) (fl) Akt1 phosphorylation rate for both PDK1 (15%) and mTORC2 (40%) at 0.2 μM FL-hTHEM4 and a decrease in phosphorylation rate for both PDK1 (40%) and mTORC2 (83%) at 6 μM FL-hTHEM4. The Trun-hTHEM4 ((Δ39) hTHEM4) produced comparatively smaller changes.

94
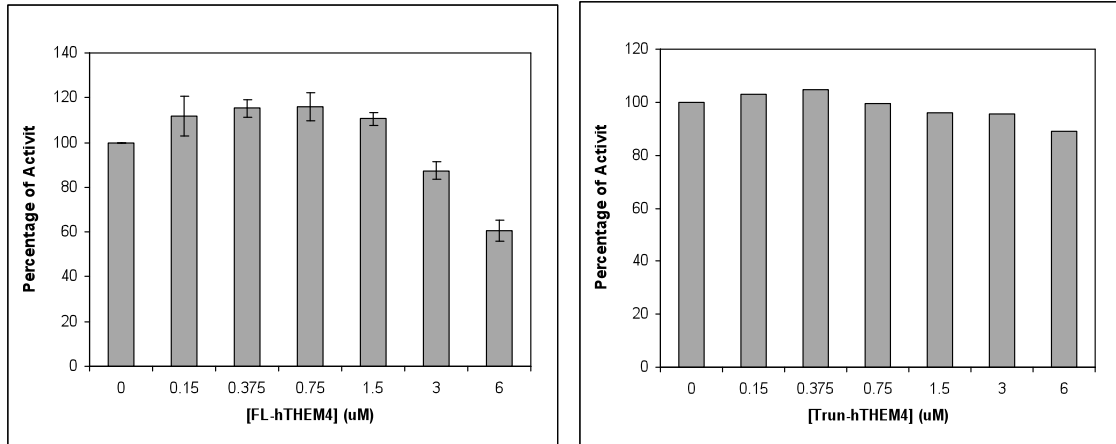
Figure 3.11 The effect of hTHEM4 on PDK1 phosphorylation of truncated Akt1 at T308. Left graph: FL-PDK1 activity was measured using (cat)Akt1 and ^{33}P-ATP as substrates in the absence and in the presence of varying amounts of FL-hTHEM4 (0, 0.15, 0.375, 0.75, 1.5, 3,6 μM). Right graph: FL-PDK1 activity was measured using (cat)Akt1 and ^{33}P-ATP as substrates in the absence and in the presence of varying amounts of Trunc-hTHEM4 (0, 0.15, 0.375, 0.75, 1.5, 3,6 μM).
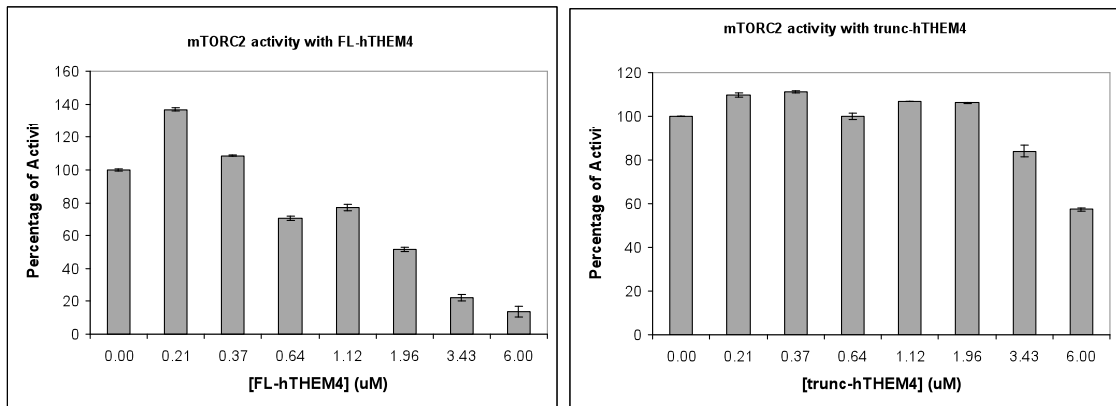
Figure 3.12 The effect of hTHEM4 on mTORC2 phosphorylation of (fl) Akt1 at S473. Left graph: FL-hTHEM4, Right graph: trunc-hTHEM4. The phosphorylation was measured by incubating immunoprecipitate purified mTORC2 with ATP and

unactivated (fl)Akt1 and varying amounts of hHTEM4 (0, 0.21, 0.37, 0.64, 1.12, 1.96, 3.43 6.0 µM) in buffer (50 mM HEPES 7.5, 5 mM MnCl$_2$, 2 mM DTT, 6.67 mM magnesium acetate and 6.67 mM manganese chloride).

3.4 Discussion

Taken together, the results of the co-immunoprecipation (hTHEM4-Akt1 pull down) experiments led to identification of physical association between hTHEM4 and Akt1, truncated form and the conclusion that (Δ39)hTHEM4 has a lower binding affinity to Akt1. The observations made in the Akt1 assay experiment show that hTHEM4 can inhibit Akt1 activity and that hTHEM4 also has an effect on the activation (phosphorylation) of Akt1 by the kinases (PDK1, mTORC2), but that the effect is concentration dependent. Fitting the assay data to a binding equation gives a K$_d$ value of *ca.* 700 nM. hTHEM4 can accelerate activation of Akt1 when present in low concentrations (< 0.5 µM, Akt1 is 1 nM) and inhibit the activation when present in higher concentrations (3-6 µM, Akt1 is 1 nM). These phenomena may explain the conflicting results arising in the earlier studies. The truncated form of protein (Δ39)hTHEM4 has much less of an effect on Akt1 compared to that of FL-hTHEM4 in the Akt1 activity assay experiment, which is consist with the co-immunoprecipitation result. The reason(s) for the different binding affinities is not clear yet. In addition, the molecular mechanism for the interaction between hTHEM4 and Akt1 requires further investigation.

References

1. Testa, J. R., and Bellacosa, A. (2001) AKT plays a central role in tumorigenesis, *Proc Natl Acad Sci U S A 98*, 10983-10985.

2. Milburn, C. C., Deak, M., Kelly, S. M., Price, N. C., Alessi, D. R., and Van Aalten, D. M. (2003) Binding of phosphatidylinositol 3,4,5-trisphosphate to the pleckstrin homology domain of protein kinase B induces a conformational change, *Biochem J 375*, 531-538.

3. Chan, T. O., Rittenhouse, S. E., and Tsichlis, P. N. (1999) AKT/PKB and other D3 phosphoinositide-regulated kinases: kinase activation by phosphoinositide-dependent phosphorylation, *Annu Rev Biochem 68*, 965-1014.

4. Cross, D.A., Alessi, D.R., Cohen, P., Andjelkovic, M., Hemmings, B.A. (1995) Inhibition of glycogen synthase kinase-3 by insulin mediated by protein kinase B. Nature 378, 785-9.

5. Andjelkovic , M., Jakubowicz, T., Cron, P., Ming, X.F., Han, J.W., Hemmings, B.A. (1996) Activation and phosphorylation of a pleckstrin homology domain containing protein kinase (RAC-PK/PKB) promoted by serum and protein phosphatse inhibitors *Proc. Natl. Acad. Sci. U.S.A.* **93**, 5699-5704.

6. Maira, S. M., Galetic, I., Brazil, D. P., Kaech, S., Ingley, E., Thelen, M., and Hemmings, B. A. (2001) Carboxyl-terminal modulator protein (CTMP), a negative regulator of PKB/Akt and v-Akt at the plasma membrane, *Science 294*, 374-380.

7.Ono, H., Sakoda, H., Fujishiro, M., Anai, M., Kushiyama, A., Fukushima, Y., Katagiri, H., Ogihara, T., Oka, Y., Kamata, H., Horike, N., Uchijima, Y., Kurihara, H., and Asano, T. (2007) Carboxy-terminal modulator protein induces Akt phosphorylation and

activation, thereby enhancing antiapoptotic, glycogen synthetic, and glucose uptake pathways, *Am J Physiol Cell Physiol 293*, C1576-1585.

8. Klein. S., Geiger. T., Linchevski. I., Lebendiker. M., Itkin. A., Assayag. K., Levitzki. A. (2005) Expression and purification of active PKB kinase from *Escherichia coli*. Protein Expression & Purification. 41,162-69.

9.Lin. H.J., Zou. T., Lin. C.H., Kuo. C.T., Liyanarachchi. S., Sun. S. Shen. R., Deatherage. D.E. Potter. D., Asamoto. L., Lin. S., Yan. P.S., Cheng. A.L., Ostrowski. M.C. Huang. T. (2008) Breast cancer-associated fibroblasts confer Akt1-mediated epigenetic silencing of cystatin M in epithelial cells. Cancer Res, 68(24), 10257-66.

CHAPTER FOUR

HUMAN THIOESTERASE SUPERFAMILY MEMBER 5 (HTHEM5)

4.1 Introduction

The human thioesterase superfamily member 5 (hTHEM5), NP_872384, consists of 247 amino acids, locates at the chromosome: 1q21.3, it is the paralog of hTHEM4 whose encoding gene is neighbor on the human chromosome. The C-terminal region of 140-237 amino acids is shown to be the hotdog fold, while function and fold of the N-terminal is unknown. hTHEM5 and hTHEM4 share 35% sequence identity, which suggests that they may show similar catalytic activity. In addition MitoProtII predicts that hTHEM5 also has a ~32 amino acids at the beginning of the N-terminal region which is a mitochondria localization sequence (MLS).

There are another two human THEM5s in the NCBI: CAI12160 (249 amino acids), EAW53404 (364 amino acids). Here label them as hTHEM5-other (249 amino acids) and hTHEM5-like (364 amino acids). The gene coding these three proteins locate at same position in chromosome: 1 q 23.1, so they are believed to be the different products of gene splicing, currently only clone cDNA for the 247 amino acids protein is available. The sequence alignment among these three THEM5 proteins (h5/h5-like/h5-other) is shown in Figure 4.1: hTHEM5-other does not have the first 54 amino acids as the other two, these sequences are thought to be the mitochondria signal sequence, so the hTHEM5-other might localize at different cellular compartment. hTHEM5-like has an extending C-terminal domain with more than 100 amino acids, the fold or function of this domain is still not clear. hTHEM5-other also has a short extending C-terminal compared to the hTHEM5, which is about 60 amino acids long.

```
h5         MIRRCFQVAARLGHHRGLLEAPRILPRLNPASAFGSSTDSMFSRFLPEKTDLKDYALPNA
h5_like    MIRRCFQVAARLGHHRGLLEAPRILPRLNPASAFGSSTDSMFSRFLPEKTDLKDYALPNA
h5_other   ------------------------------------------------------YALPNA
                                                                 ******


h5         SWCSDMLSLYQEFLEKTKSSGWIKLPSFKSNRDHIRGLKLPSGLAVSSDKGDCRIFTRCI
h5_like    SWCSDMLSLYQEFLEKTKSSGWIKLPSFKSNRDHIRGLKLPSGLAVSSDKGDCRIFTRCI
h5_other   SWCSDMLSLYQEFLEKTKSSGWIKLPSFKSNRDHIRGLKLPSGLAVSSDKGDCRIFTRCI
           ************************************************************


h5         QVEGQGFEYVIFFQPTQKKSVCLFQPGSYLEGPPGFAHGGSLAAMMDETFSKTAFLAGEG
h5_like    QVEGQGFEYVIFFQPTQKKSVCLFQPGSYLEGPPGFAHGGSLAAMMDETFSKTAFLAGEG
h5_other   QVEGQGFEYVIFFQPTQKKSVCLFQPGSYLEGPPGFAHGGSLAAMMDETFSKTAFLAGEG
           ************************************************************


h5         LFTLSLNIRFKNLIPVDSLVVMDVEVDKIEDQKLYMSCIAHSRDQQTVYAKSSGVF----
h5_like    LFTLSLNIRFKNLIPVDSLVVMDVELDKIEDQKLYMSCIAHSRDQQTVYAKSSECFNFLN
h5_other   LFTLSLNIRFKNLIPVDSLVVMDVELDKIEDQKLYMSCIAHSSWKKSLPSNSHCACR---
           *************************:****************  ::::  ::*


h5         -----------------------------------------LQLQLEEESPQ--------
h5_like    EMEGKAISGERGLEEGGWFGKTAVGIRKTGTRYMCDQDILSAQLLVENSPPPPLSSPASA
h5_other   ---------------------------------RATASPACLLPPASPACLLPPASP
                                                    :       .*


h5         ------------------------------------------------------------
h5_like    EEAWAQEWIVARNLASAGGSQKTGLMAAQTELCLSRKRGVRAPSGSGDRGAVADRPVYAS
h5_other   ACLLP-------------PLPASCLLPPLPASCLLPPLPAWDPSKSREGSSSSNW-----


h5         ----
h5_like    ITHL
h5_other   ----
```

Figure 4.1 Sequence alignment of hTHEM5s: h5(247 amino acids), h5-like(364 amino acids), h5-other(249 amino acids).

100

The initial objectives of my work here are (1) to determine if hTHEM5 catalyzes acyl-CoA hydrolysis by isolating the enzyme and testing it against a panel of potential thioester substrates (2) to find out the cellular location of hTHEM5 (3) to determine the mechanism by which hTHEM5 catalyzes thioester hydrolysis and to determine the structure of hTHEM5. (4) to find out the difference between hTHEM4 and hTHEM5, to further explore the reason that two very like proteins are coding in the neighbor positions of the same chromosome in human cell.

4.2 Experimental

4.2.1 Cloning, expression and purification in *E. coli* system

To Prepare recombinant full-length hTHEM5 from *E. coli*, the gene encoding hTHEM5 in human (GI: 32698978) was amplified by PCR from cDNA clone MGC126659 (ATCC, GenBank accession number: BC101610), this was achieved by using primers 5'-GGATCCTTGCACTTGCATATGATAAGGAGA-3' and 5'-CAGGCACAGTGACTCGAGCTGGGGAGACTC-3', which incorporate an NdeI site and a XhoI site. The resulting PCR fragment was digested and inserted into the respective sites in pET-23b vector (Novagen), the C-terminal 6x Histidine tags construct was obtained and then transformed into Bl21 codon plus RIPL competent cells. The sequence was confirmed by DNA sequencing in the Health Sciences Center of the University of New Mexico. The cells were cultured at 20 °C and 180 RPM in LB Broth medium for 8 h, induced with 0.4 mM IPTG when OD at 600 nm is 0.7. After 12 h, the cells were harvested by centrifugation at 4°C and 6500 RPM. The 10 g of cell paste was suspended

in 100 ml of ice-cold lysis buffer (50 mM NaH_2PO_4, 200 mM NaCl, 10 mM imidazole, 0.5 ml protease inhibitor Cocktail solution, pH 8.5), passed through a French press at 1200 PSIG, and then centrifuged at 48000 × g and 4 °C for 30 mins. The supernatant was loaded onto a Ni-NTA Agarose column (QIAGEN, 15 ml) pre-equilibrated with the lysis buffer. The column was washed with 300 mL buffer of 50 mM NaH_2PO_4/200 mM NaCl /70 mM imidazole (pH 8.5) and then the column was eluted with 100 mL of 50 mM NaH_2PO_4/200 mM NaCl /250 mM imidazole (pH 8.5). The fractions were analyzed by SDS-PAGE and then selectively pooled and concentrated using Centricon (10 kDa, Pall Filtron) at 4 $^\circ$C, then dialyzed into buffer containing 50 mM Tris /200 mM NaCl (pH 8.0) and stored in -80°C.

A truncated form of hTHEM5 by removing the first 40 amino acids, termed as hTEHM4 (Δ40), was also prepared. The truncated gene was prepared using a PCR based strategy, with the full-length gene serving as template and using primers: 5'-GAGGTCATTTTCTTCATATGGAAGTCATTC-3' and 5'-CACCAGCAGCTCTCGAGTGTCAGACTTTTAGC-3', which contains NdeI and XhoI sites. The PCR fragment was ligated into the pET-23a vector, which introduces a C-terminal His_6 tag. The plasmid was transformed into BL21-codon plus (DE3) RIL competent cells for overexpression. The cells incubated at 20 °C and 200 RPM for 8 h, then induced with 0.4 mM IPTG. After 12 h, the cells were harvested by centrifugation at 4°C and 6500 RPM. The suspended cells were lysed by French press, and following centrifugation of the lysate, the supernatent was loaded onto the Ni-NTA Agarose column pre-equilibrated with the lysis buffer. The column was washed with 300 mL of 50 mM NaH_2PO_4/500 mM NaCl /70 mM imidazole (pH 8.0) and then the column was

eluted with 100 mL of 50 mM NaH₂PO₄/500 mM NaCl /250 mM imidazole (pH 8.0).

The desired fractions were combined and concentrated before loading onto a 2 x 180cm

Sephacryl 100 size exclusive column, the column was eluted with 50 mM NaH₂PO₄/50

mM NaCl /10 mM imidazole buffer (pH 8.0) at 4 °C, The fractions were analyzed by

SDS-PAGE, and then the final desired fractions were combined and concentrated using

Centricon (10 kDa, Pall Filtron) at 4 °C, then dialyzed into buffer containing 50 mM Tris

/200 mM NaCl (pH 8.0) and stored in -80°C. Yield is about 10 mg protein/ gm wet cell.

4.2.2 Cloning, expression and purification in HEK293T cell line system

pcDNA 3.1/- hTHEM5- myc-His construction

To express hTHEM5 protein in HEK 293 cell line for physiological properties

determination, the gene encoding hTHEM5 was cloned into the pcDNA 3.1/myc-HisA

vector by using the cloning sites: EcoRI and AgeI, giving the C-terminal tag. The

sequence was confirmed by DNA sequencing in the Facility of the Health Sciences center

in the University of New Mexico, and transfections were performed using the

Lipofectamine 2000 reagent (Invitrogen), for a standard 24-well cell culture plate (2cm²

surface area per well), 1 μg of plasmid DNA was added to 50 μl of Opti-MEM I Reduced

Serum Medium (Invitrogen) and mixing was followed by the addition of solution

containing 2 μl of Lipofectamine 2000 and 50 μl of Opti-MEM I Reduced Serum

Medium. The solution was incubated for 20 min at room temperature before adding it

into the well. The cells were incubated at 37°C in a 5% CO₂ incubator for 48 h prior to

testing for transgene expression. The protein expression was monitored by doing Western

Blot of the whole cell extract, which using commercial anti-C-terminal His-tag antibody (Invitrogen, 46-0693) or anti-hTHEM5 antibody (Abcam, ab69384).

pcDNA 4/HisMax TOPO construction

hTHEM5 was also cloned by pcDNA4/HisMax TOPO TA Expression Kit (Invitrogen K864-20).The Feature of this vector is that human cytomegalovirus (CMV) promoter in pcDNA4 allows high-level expression of PCR product, and the recombinant protein expression is further enhanced by the presence of the QBI SP163 translational enhancer. The PCR product will be expressed as a fusion to the N-terminal Xpress epitope and a polyhistidine (6xHis) tag for detection and purification. For hTHEM5/pcDNA4 HisMAX stably transfected cell lines, selections were carried out in culture medium with 500 μg/mL Zeocin.

Immunoprecipitation (IP) purification

Anti-Xpress antibody covalently immobilized agarose beads were prepared following the manufacturer's instruction. In brief, 10-50 μg of primary antibody was incubated with 20-100 μL agarose bead slurry in the presence of $NaCNBH_3$ at room temperature for at least 2 hour. Uncoupled antibody was removed by extensive washing and uncoupled reactive sites in agarose beads were quenched by incubation in solution with primary amine and $NaCNBH_3$. Lysate of hTHEM5/pcDNA4 HisMAX stably transfected HEK cell was incubated with antibody immobilized agarose beads at 4°C overnight. Unbound proteins were removed in washing steps. Finally, the antigen

hTHEM5, was eluted by applying elution buffer (10 mM Tris with 100 mM glycine pH 7.4) to beads.

4.2.3 Native Molecular Weight determination

The native molecular weight of hTHEM5 was done by the Biophysics Resource of Keck Facility at Yale University. HPLC (High Performance Liquid Chromotography) SEC (Size Exclusive Chromotography) Light Scattering technique was used to determine the native molecular weights and sizes of protein. The MW determination depends only upon the downstream light scattering (LS) and refractive index (RI) detectors.

4.2.4 Steady-state kinetic test for substrate screening

DTNB assay: Reactions were monitored at 25 °C and pH 7.5 by measuring the 412 nm absorbance of 5-thio-2-nitrobenzoate formed by the reaction of DTNB with the CoA anion liberated from the acyl-CoA substrates (short, medium and long chain, saturated and unsaturated aliphatic acyl-CoAs and aromatic acyl-CoAs). Reactions were initiated by adding hTHEM4 to assay solutions composed of substrate (at varying concentration: 1-10 fold K_m), DTNB (2 mM), KCl (0.2 M) and 50 mM K^+Hepes (pH 7.5) contained in quartz cuvettes (1 cm light path). The kinetic parameters V_{max} and K_m were determined from initial velocity data, measured as a function of substrate concentration, by using equation (1) and KinetAsyst (IntelliKinetics, PA).

$$V = V_{max} [A] / ([A] + K_m) \qquad (1)$$

Where [A] is the substrate concentration, V is the initial velocity, V_{max} is the maximum velocity and K_m is the Michaelis constant. The reported error was computed for the data

fitting. The k_{cat} was calculated from the ratio of V_{max} and the total enzyme concentration. The enzyme concentration was determined using the Bradford method.

232nm direct assay: the long chain acyl-CoA compounds hydrolysis reaction could be monitored by the decrease in absorbance at 232 nm due to the cleavage of the thioester bond. The standard reaction mixture contained 1 to 10 μM palmitoyl-CoA, 100 mM sodium phosphate (pH7.4) and the enzyme in a final volume of 500μl. After an incubation at 25 °C for 120 sec, the reaction was started by adding the substrate, and the absorbance was monitored at 232nm. The molar absorption coefficient ε_{232}=4250 M^{-1}cm^{-1} was used to calculate cleavage of the thioester bond (*1,2*).

4.2.5 Substrates and assays for determination of acyl-ACP hydrolysis activity

Preparation of Myristoyl-ACP (Palmitoyl-ACP).

Myristoyl-holo-acyl carrier protein (ACP) was synthesized by reacting the *apo* human cytosolic ACP with myristoyl-CoA catalyzed by the human phosphopantetheinyl transferase (PPTase). Human cytosolic ACP fragment and PPTase plasmids were a kind gift from Dr. Stuart Smith, Children's Hospital Oakland Research Institute, Oakland, CA. The two apoproteins were purified as described earlier (*3,4*). The reaction mixture contained 60 μM apo-ACP, 150 μM acyl-CoA and 2 μM PPTase in 20 ml of 20 mM Tris/1mM MgCl$_2$ (pH 7.0; 25 °C) for 3 h. The concentrated acyl-ACP was prepared using a PALL 10K centrifuge device, the product was verified by TOF MS ES+. Apo-ACP (MW in Da) calculated: 13067, observed: 13066 and 13143 (posttranslational modified form); Myristoyl-holoACP calculated: 13618, observed: 13617 and 13694

106

(posttranslational modified form); Palmitoyl-holoACP calculated: 13646, observed: 13643 and 13720 (posttranslational modified form).

Hydrolysis reaction of myristoyl-ACP catalyzed by hTHEM5(Δ40).

The hTHEM5(Δ40) catalyzed hydrolysis reaction was monitored by HR-MS. The 200 μL reaction solution containing 44 μM myristoyl-CoA, 10 μM hTHEM5(Δ40), 50 mM HEPES and 100 mM NaCl at pH 7.5 was incubated at room temperature for 15 mins. The control reaction lacked the hTHEM5(Δ40).

4.2.6 Determination of the inhibition constants for hTHEM5

The competitive inhibition constant K_i for undeca-2-one-CoA (and other product inhibitors) was determined by measuring the initial velocity of hTHEM5 catalyzed substrate hydrolysis as a function of substrate concentration (K_m to $10K_m$) and inhibitor concentration (0, $1K_i$ and $2K_i$ μM). The initial velocity data were fitted to equation (2) using KinetAsyst (IntelliKinetics, PA),

$$V = V_{max} [A] / ([A] + K_m (1 + [I]/K_i)) \qquad (2)$$

Where [A] is the substrate concentration, V is the initial velocity, V_{max} is the maximum velocity, K_m is the Michaelis constant, K_i is the competitive inhibition constant and [I] is the inhibitor concentration.

The palmitoyl-CoA substrate inhibition constant was determined by measuring the initial velocity of hTHEM5(Δ40) catalyzed palmitoyl-CoA hydrolysis in triplicate for

solutions initially containing hTHEM5(Δ40) (0.248 µM), palmitoyl-CoA (3 - 80 µM), DTNB (2 mM), KCl (0.2 M) and 50 mM K$^+$HEPES (pH 7.5, 25 ^{o}C). The initial velocity data were fitted to equation (3) using y= m1*m0/(m2+m0*(1+m0/m3)).

$$V=V_{max} [S]/(K_m+ [S](1+[S]/K_I)) \qquad (3)$$

Where [S] is the substrate concentration, V is the initial velocity, V_{max} is the maximum velocity, K_m is the Michaelis constant, K_i is the substrate inhibition constant. Fitting kinetic data into equation: m1*m0/(m2+m0*(1+m0/m3)). m1=V_{max}; m2=K_m; m3=K_I.

Preparation of solution of lauric acid and octanoic acid for carboxylate compound inhibition test Due to the poor water solubility, lauric acid was dissolved in H$_2$O: CH$_3$CH$_2$OH=1:3 mixed solvent, the final concentration is 25 mM. Octanoic acid water solubility is a little better, H$_2$O: CH$_3$CH$_2$OH =1:1 mixed solvent was used and final concentration is 50mM.

4.2.7 Structure-Function study

Crystals of hTHEM5 (Δ40) were obtained by Dr. Osnat Herzberg's lab at University of Maryland.

The corresponding substitution of each putative catalytic residue was investigated through the site-directed mutagenesis. The contribution to the catalytic activity of each residue was determined, through comparing and analyzing kinetic constants among each mutant. Site directed mutagenesis was carried out using a PCR-based strategy with the

WT-hTHEM5 (Δ40)/ pET-23a (+) plasmid as template, commercial primers and dNTP (Invitrogen), P*fu Turbo* DNA polymerase, and the Techgene thermal cycler manufactured by TECHNE (Princeton, NJ). The PCR products were treated with DpnI to remove the wild type plasmid before transformation into competent *Escherichia coli* cells (BL21 Star™ (DE3) One Shot). The sequence of the mutated gene was confirmed by DNA sequencing carried out by the DNA Sequencing Facility of the Health Sciences center in the University of New Mexico, the plasmid was prepared using a QIAprep Spin Miniprep Kit (Qiagen). The hTHEM5 mutants were purified to homogeneity (monitored by SDS-PAGE) by the same procedure used to purify the wild-type enzyme.

4.2.8 Cellular location investigation

hTHEM5/pcDNA3.1 CT-GFP and *hTHEM5(Δ32)/pcDNA3.1 CT-GFP fusion protein cloning, transfection, growing and imaging*

To obtain a fluorescence fusion protein for imaging, the gene encoding hTHEM5 or hTHEM5(Δ32) was cloned into pcDNA3.1 CT-GFP vector. Transfections were performed using the Lipofectamine 2000 reagent (Invitrogen), HEK293T/17 cells were cultured on the coverslip, for a standard 24-well cell culture plate ($2cm^2$ surface area per well), 1 µg of plasmid DNA was added to 50 µl of Opti-MEM I Reduced Serum Medium (Invitrogen) and mixing was followed by the addition of solution containing 2 µl of Lipofectamine 2000 and 50 µl of Opti-MEM I Reduced Serum Medium. The solution was incubated for 20 min at room temperature before adding it into the well. After 12-24 hours post-transfection, cells were fixed using 4% PFA in PBS buffer at 37 °C for 15 mins. Subsequently, fixed cells on coverslip were incubated with 1 μM Hoechst 33342,

109

and either 50 μM Mitotracker Red CMXRox or 5 μg/mL WGA/Alexa Fluor 594 conjugate at room temperature for 20 mins. Finally, coverslip was rinsed with PBS, mounted onto slides, and subject to confocal microscope analysis (Cancer Center Fluorescence Microscopy Facility, University of New Mexico School of Medicine).

Mitochondria isolation

Mitochondria isolation was performed following the manufacturer' instructions (Pierce 89874, Mitochondria isolation kit for cultured cells). In brief, ~$2\text{x}10^7$ of stably transfected cells were pellet by centrifuge and resuspended in mitochondria isolation reagent A. Cells were lysed by Dounce Tissue Grinder. Mitochondria isolation reagent C was added to cell lysate. Cytosolic and mitochondrial fractions were separated by centrifuge. Mitochondria pellet was washed once by reagent C and resuspended in suitable buffer for down stream processing.

4.3 Results and Discussion

4.3.1 Purification of hTHEM5 expressed in *E.coli*

The SDS-PAGE analysis of full-length hTHEM5 suggests that product is splitting into two major bands, one is at around 29kDa, the other is at 23 kDa. The sample was submitted for Mass Spectroscopy, the final MW peak is only 23821.1 Da, which corresponding to the small band on the gel. While calculated theoretical MW of hTHEM5-His is 28727 Da, the splitting behavior is exactly same as what we saw in the full-length hTHEM4 purification. So it is also possible that the N-terminal signal

sequence of hTHEM5 is cleaved. The Commassie blue stained SDS-PAGE gels are showed in Figure 4.2.
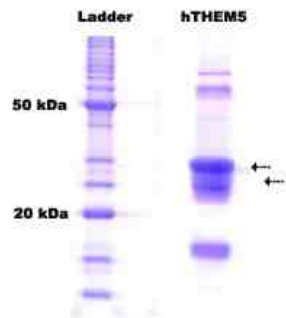
Figure 4.2 SDS-PAGE of full-length hTHEM5 (C-terminal His tagged) expressed in *E. coli*

Truncated construction was over-expressed in *E. coli* system, see Figure 4.3.
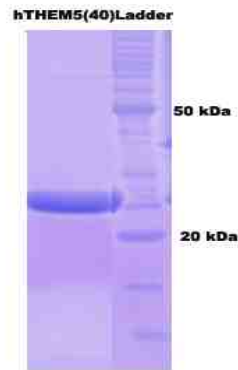
Figure 4.3 SDS-PAGE of truncated hTHEM5(Δ40) (C-terminal His tagged) expressed in *E. coli*

4.3.2 Expression in HEK293T cell and purification

Interestingly, western blot of the overexpressed Xpress-hTHEM5 revealed one single signal (~ 30 kDa) when using anti-Xpress antibody and a dual mobility pattern when using anti-hTHEM5 (~30kDa and ~25kDa), suggests that posttranslational modification (cleavage) of hTHEM5 in the cell.
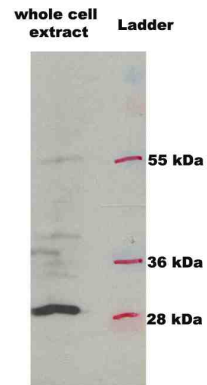
Figure 4.4 Western Blot (anti-Xpress antibody) of whole cell extract, HEK293T cells were transfected by Xpress-hTHEM5 (pcDNA4.0 vector).
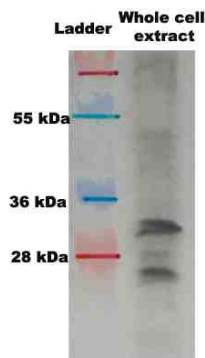
Figure 4.5 Western Blot (anti-hTHEM5 antibody) of whole cell extract, HEK293T cells were transfected by Xpress-hTHEM5 (pcDNA4.0 vector).

hTHEM5 was purified by applying anti-Xpress antibody (Invitrogen) through Thermo Scientific Pierece Direct IP Kit for Immunoprecipitation (IP) .

Figure 4.6   Western Blot (anti-Xpress antibody) of eluted fraction solution after the IP, showing the purified Xpress-hTHEM5 (~29 kDa) in the Left lane, standard protein ladder in Right lane.

4.3.3 Native molecular weight

The native molecular weight was determined by HPLC SEC Laser Light Scattering in the Keck Biotechnology Resource Laboratory at Yale University. Samples submitted are 3.5 mg/ml of full length THEM5 (purified from *E coli*) in buffer of 50mM Tris, 200mM NaCl, pH 8.0, and 20mg/ml of THEM5 (Δ40) (purified from *E coli*) in buffer of 50mM Hepes, 200 mM NaCl, pH 7.5. Both full length and truncated protein tend to be a dimer in the solution. The final result is shown in Figure 4.7, 4.8 and Table 4.1.
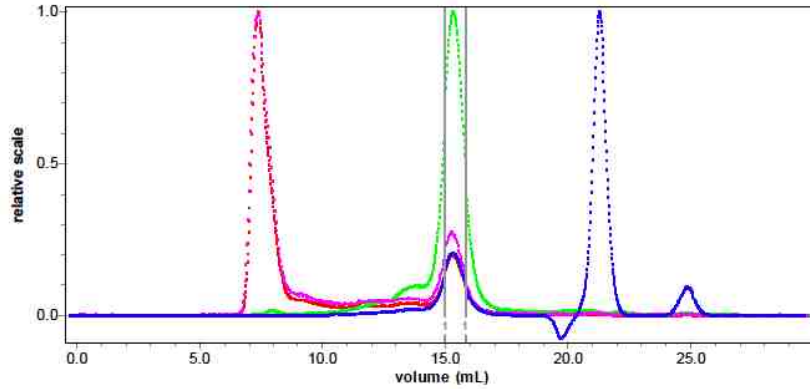
Figure 4.7 Peak ID plot of the full length THEM5, major peak is at elution 15.31ml, other peaks are noise from the protein sample. Green: UV signal (absorbance at 280 nm). Blue: RI signal (refractive index change) .Red: 90° Detector (LS trace recorded for the detector at 90 degree angle). Note: the RI and UV signals are scaled to LS signal
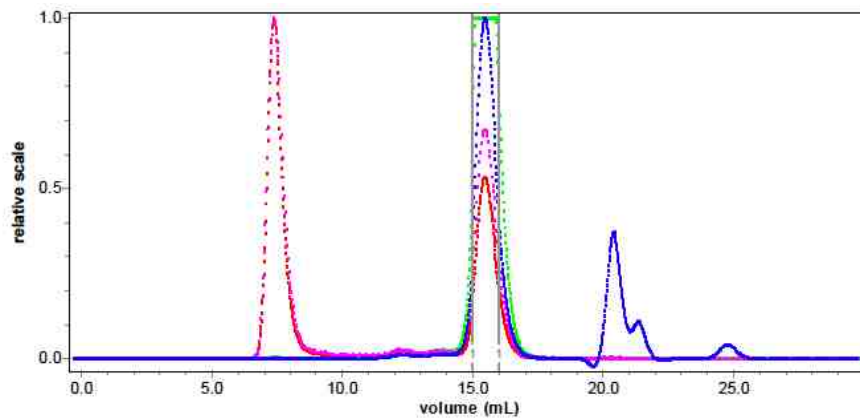
Figure 4.8 Peak ID plot of the THEM5 (Δ40), major peak is at elution 15.45 ml, other peaks are noise from protein sample. Green: UV signal (absorbance at 280 nm). Blue: RI signal (refractive index change). Red: 90° Detector (LS trace recorded for the detector at 90 degree angle). Note: the RI and UV signals are scaled to LS signal

Table 4.1 Results of SEC-LS/RI/UV analysis from ASTRA (reports for major peaks of selected analyses)

RUN	PEAK Elution at UV trace (mL)	MW (kDa) Calculated by ASTRA Average for the major peak (Mw)	MW (kDa) Calculated by ASTRA range of Mw observed	Sequence Predicated MW for monomer (kDa)	Oligomeric association
Full length THEM5	15.31	53.2	53-55	29	Dimer
THEM5 (Δ40)	15.45	50.5	48-51	24	Dimer

4.3.4 Catalytic activity and substrate specificity

The activity of hTHEM5 (Δ40) catalyzing the hydrolysis of different acyl-CoAs was tested by DTNB assay or 232nm direct assay. In general, hTHEM5 shows only moderate activity towards the acyl-CoAs, k_{cat}/K_m is at the rage of 10^3 to 10^5 $M^{-1}s^{-1}$. The best substrate is long-chain palmitoyl-CoA, while the k_{cat} value is 0.15 s^{-1}, and it is tight binding (K_m=1.05 μM), final k_{cat}/K_m is 10^5 $M^{-1}s^{-1}$. The hTHEM5 shows activity in a relative narrow range of substrates, it does not have significant activity to the short-chain acyl-CoAs (C_2-C_8) and those has longer chain than the palmitoyl-CoA, also not active on the short polar and aromatic acyl-CoAs.

Table 4.2 Steady-State Constants for hTHEM5 (Δ40) Catalyzed Hydrolysis of acyl- CoAs, monitored by DTNB assay in 50 mM K$^+$HEPES (pH 7.5 and 25 °C) and 2mM DTNB.

Substrate	k_{cat} (s^{-1})	K_m (μM)	k_{cat} / K_m (M^{-1}s^{-1})
Acetyl-CoA	<0.00001		
Butyryl-CoA	<0.00001		
Octanoyl-CoA	$k_{observe}$=0.003		
Decanoyl-CoA	0.033 ±0.001	9.1±0.6	3.6×10^3
Lauroyl-CoA	0.029±0.001	2.3±0.2	1.2×10^4
Myristoyl-CoA	0.080±0.003	1.0±0.2	7.7×10^4
Palmitoyl- CoA	**0.15 ±0.004**	**1.1±0.1**	**1.4×10^5**
Stearoyl-CoA	<0.00001		
Arachidonyl-CoA	<0.00001		
Succinyl-CoA	<0.00001		
3-HPA-CoA	<0.00001		
4-HBA-CoA	<0.00001		

Acyl-holoACP is also the substrate of hTHEM5. In order to test the activity of hTHEM5 (Δ40) towards the engineered cytosolic myristoyl-ACP (prepared as described in the Experimental) we used ES-MS to monitor the reaction. As shown in Figure 4.9, the mass spectrum of the reaction solution (44 μM myristoyl-holoACP in 50mM HEPES

and 100mM NaCl buffer @ pH 7.5 and room temperature) prior to the addition of hTHEM5 (Δ40) is characterized by two peaks: 13617 Da (myristoyl-holoACP; calculated 13618 Da) and 13693 Da (the posttranslational modified counterpart of myristoyl-holoACP). The control experiment was run by incubating the reaction solution without any hTHEM5(Δ40) (lane A): there is no any changes in the spectrum compared to the original myristoyl-holoACP sample. Following 15 mins incubation with 10 μM hTHEM5(Δ40) spectroscopy(lane B): holo-ACP calculated: 13408, observed: 13406 and 13483 (modified form) was found as the MW peak. The molecular weight difference is 210 Da, which shows that enzyme hydrolyzes the myristoyl-holo-ACP into holo form completely after incubation.
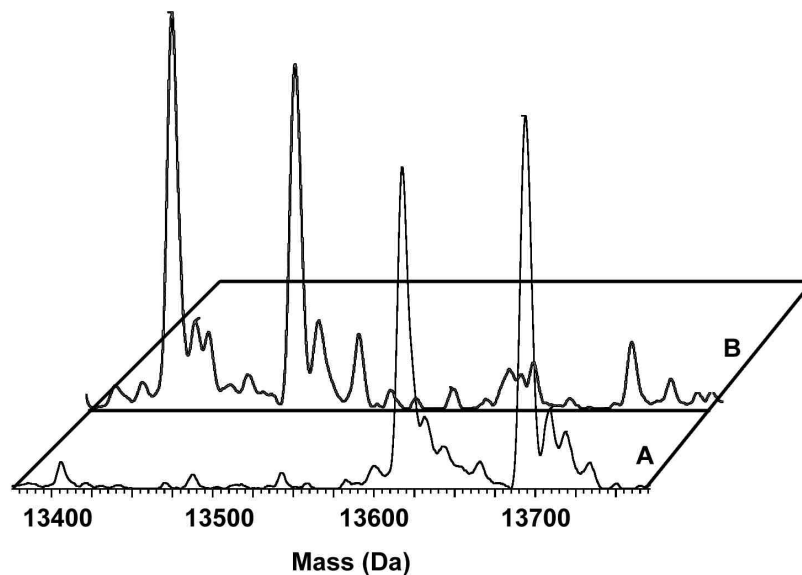
Figure 4.9 Mass spectra diagram of hydrolysis of Myristoyl-holoACP catalyzed by hTHEM5 (Δ40). Lane A, Control reaction: without hTHEM5(Δ40), incubated at RT for 15 min (no change: MW peak @ 13617 and 13693 Da); Lane B, Reaction run with hTHEM5(Δ40), incubated at RT for 15 min, product is holo-ACP (MW peak @13405.5, 13483 Da).

4.3.5 Determination of the Inhibition Constants

a. Evaluation of Inert Substrate Analogue Inhibitors

To access the importance of the thioester C=O in substrate binding, the competitive inhibition of the decanoyl-CoA analog undecan-2-one-CoA (thioester C=O is replaced by CH_2) was tested, the plot (Figure 4.10) defines $K_i = 6.0\pm0.7$ μM, which is relatively same binding compared to the analogue substrate decanoyl-CoA: $K_m=9$ μM, suggests that the substrate thioester C=O may not have significant contribution to the substrate binding energy. Also the binding is about 10 times less compared to that between inhibitor undecan-2-one-CoA and hTHEM4 ($K_i= 0.8\mu$M), suggests that hTHEM5 has less binding capability with acyl-CoA compounds.

Figure 4.10 Double reciprocal plot of the initial reaction velocity (V) vs the concentration of the myristoyl-CoA substrate. Reaction solutions initially contained 3 to 18μM myristoyl-CoA, 0.5μM (Δ39) hTHEM5(Δ40), 2mM DTNB (pH 7.5, 25 $^{\circ}$C) and 0(O), 10 (●)and 20(■) μM undeca-2-one-CoA. Data fitting defines $K_i = 6.0\pm0.7$ μM.

b. Product inhibition

To look for if there is some form of self-regulation of catalytic activity in hTHEM5, CoASH and carboxylate product formed in the hTHEM5 catalyzing hydrolysis of the acyl-CoA substrates were tested as feedback inhibitors.

Inhibition of Lauric acid and Octanoic acid

The palmitoyl-CoA was used as substrate in the DTNB assay, the concentration of substrate is from 0.8 μM to 4 μM (K_m is about 1 μM), the concentration of the inhibitor is from 0μM to 500 μM. Results show that the K_i of Lauric acid is about 290μM (Figure 4.11) and The K_i of Octanoic acid is larger than 1mM. Interestingly the lauric acid has significant inhibition on hTHEM5 when concentration is lower than 500 μM, which is not normal for many other hot-dog thioesterases, suggests that the acyl arm may contribute a little differently in hTHEM5 substrate binding.
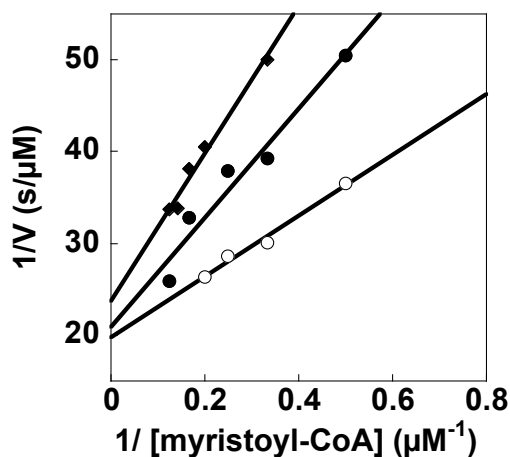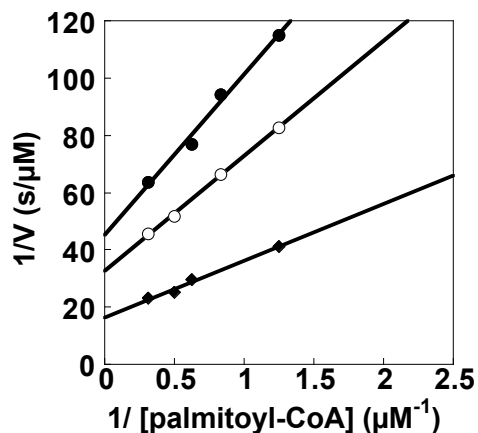

Figure 4.11 Double reciprocal plot of the initial reaction velocity (V) vs the concentration of the palmitoyl-CoA substrate. Reaction solutions initially contained 0.8 to 5 μM palmitoyl-CoA, 0.2 μM hTHEM5(Δ40), (pH 7.5, 25 ^oC) and 0($\blacklozenge$), 250(O), and 500($\bullet$) μM Lauric acid.

119

CoASH inhibition

To test if CoASH serves as a feedback inhibitor to hTHEM5, the 232nm direct assay was applied in the kinetic test. But one problem here is that the whole absorbance will be at around 1.5 when CoASH concentration is at 500 μM, which is too high to get stable trend line monitoring reaction. No significant inhibition effect was observed when using CoASH @ 150µM and 250µM, which indicate that the binding constant of CoASH might be larger than 500 µM. Again the result suggests both pantetheneine and nucleotide moity of CoA do not contribute to substrate binding of hTHEM5, which is not usual for many acyl-CoA thioesterase enzymes.

c. Substrate inhibition

hTHEM5 is inhibited by palmitoyl-CoA at concentrations above 9 µM, 3.5-fold lower than the critical micelle concentration (CMC) of the palmitoyl-CoA: 42 µM (*5,6*). Fitting the kinetic data in table 4.3 into equation 3 (for details see the Experimental section) to define $K_I = 11$ µM, which indicates a strong substrate inhibition. The substrate inhibition can also be explained based on the X-ray structure, like the situation for hTHEM4 in Chapter2. Because, similar to hTHEM4, a nonproductively (backwards) binding acyl arm was seen in the hTHEM5 X-ray structure.

Table 4.3 The initial velocities determined for (0.248 µM) hTHEM5(Δ40) catalyzed hydrolysis of palmitoyl-CoA measured over a large range of palmitoyl-CoA concentrations (3-80 mM) at pH 7.5 and 25 °C using the DTNB assay. The velocities wee measured in triplicate and the average of the three values are reported.

[Substrate] µM	3.0000	6.0000	9.0000	15.000	18.000
Velocity µM/s	0.038800	0.042400	0.043800	0.040200	0.037800
[Substrate] µM	21.000	27.000	40.000	60.000	80.000
Velocity µM/s	0.028500	0.025200	0.022000	0.013600	0.013400
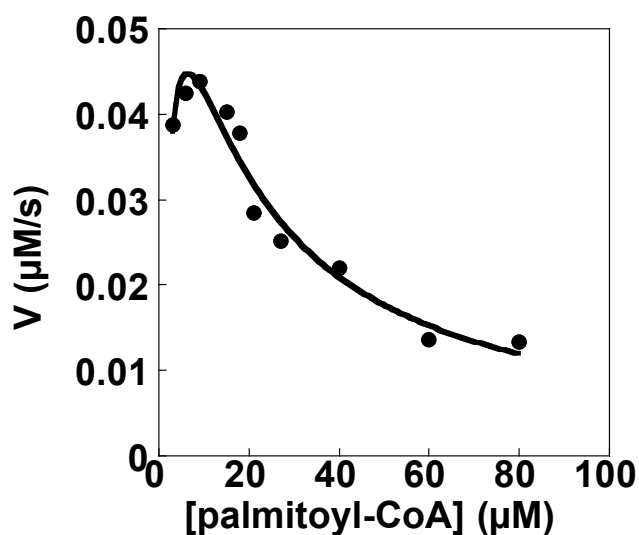
Figure 4.12 A plot of the data reported in Table 4.3. The curve represents fit to equation 3 (see Experimental). The result is m1 (Vmax)=0.098; m2 (Km) =3.9627; m3 (K_I) =11.146.

4.3.6 Crystal structure determination of hTHEM5 (Δ40)

Overall structure

The structure of the truncated form of hTHEM5 (residues 41-247) containing C-terminal His_6-tag (a LEHHHHHH sequence) was successful. This construct contains a region (residues 122-237) homologous to acyl-CoA thioesterase that adopt the hotdog fold whereas residues 41-120 show no significant homology to proteins with known structures. Accordingly, the Molecular Replacement solution yielded a dimeric protein, consistent with the oligometric state of the hTHEM5 in solution.

In the dimer structure, subunits are termed A and B. The model of subunit A and B contains amino acid residues 47-103 and 107-233 whereas residues 104, 105 and 106 are structurally disordered.

The N-terminal residues 47-122 form a similar fold as that of hTHEM4, two major α- helices (α1 and α2) and largely loop-like fold. Residues 47-59, 75-85, 93-103 and 107-122 are all loops, the big α- helix (α1) contains residues 60-74, the smaller helix (α2) is 86-92. (Figure 4.13 Figure 4.14)
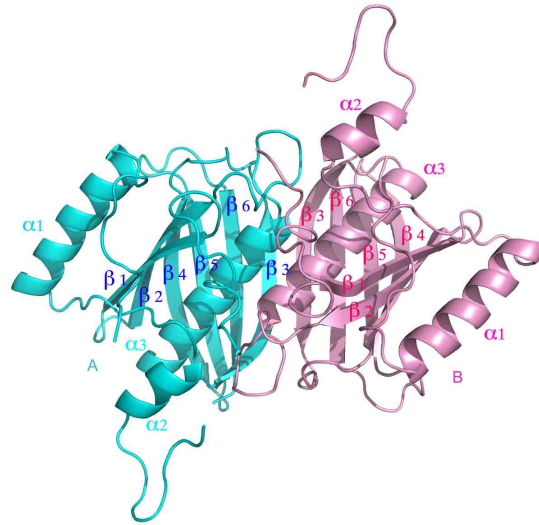
Figure 4.13 Overall structure of hTHEM5(Δ40). The subunit A is colored in pale green and subunit B is in pink.
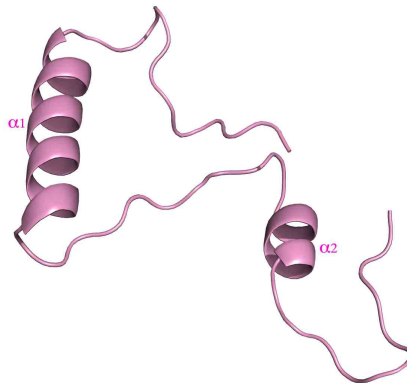
Figure 4.14 N-terminal folding of hTHEM5, two major α-helices:α1 and α2.

The hotdog-fold consists of a central α-helix (α3) and six β-strands (β1-β6). The two central α-helices are positioned anti-parallel to one another. The dimer surface is thus formed by the continuous interaction of the β-sheet and two α3 helices. In addition,

123

the residues 107-120 pack above the α3 helix, which extends the pocket formed by the dimer interface.

The hypothesis of the active sites by overlap the hTHEM5 structure with the hTHEM4 structure and Mutagenesis study

There is 35% sequence identity between hTHEM5 and hTHEM4, the inert substrate analogue liganded hTHEM4 structure is available, the active sites model of hTHEM5 could be obtained by overlapping the two structures, see Figure 4.15 and Figure 4.16. Residues bind close to the reaction center (S-CH$_2$-C=O) are Asp167, Glu168, Ser171, His158 and Thr183.
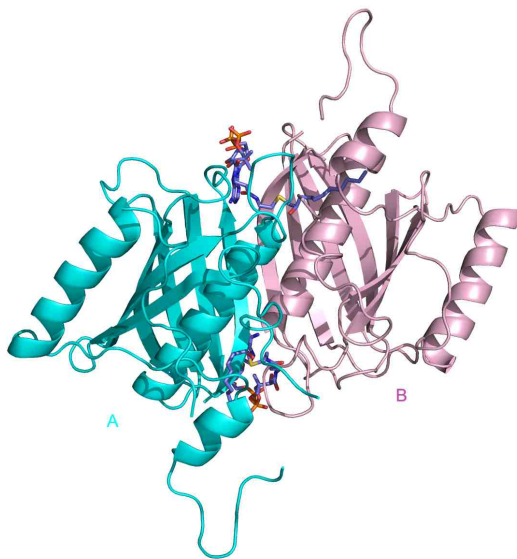
Figure 4.15 Liganded model structure, obtained by overlapping the hTHEM5 apo-structure with hTHEM4 liganded structure.
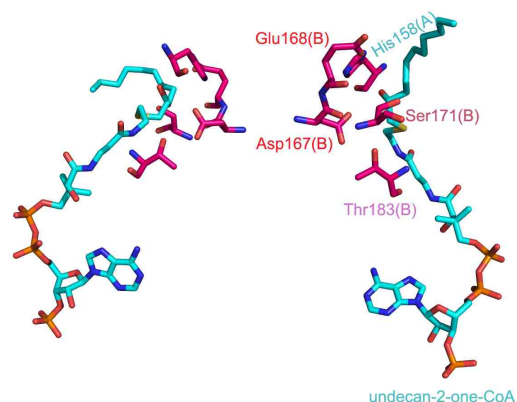
Figure 4.16 hTHEM5 active sites binding model, ligand (undecan-2-one-CoA, blue) binding in hTHEM4 structure was modeled into hTHEM5 apo structure by overlapping two structures. The putative active sites (purple) binding around one ligand unit (blue) are His158 from subunit A, and Glu168, Asp167, Ser171, Thr183 from subunit B.

The corresponding substitution of each residue was made by the single-site mutagenesis. The activity of mutants towards the hydrolysis of palmitoyl-CoA is determined by 232nm assay, which monitors the cleavage of the thioester bond. The kinetic data showed that each substitution results in at least 150-fold decrease in the k_{cat} value, which suggests that the original catalytic efficiency of hydrolysis of palmitoyl-CoA might be low (decrease by 100 has already exceeded the measurable data), or palmitoyl-CoA is not the best substrate for hTHEM5, or each single mutant could disrupt the active sites arrangement.

Table 4.4 Kinetics test of hTHEM5 (40) mutants, taking the Palmitoyl-CoA as the substrate, 232nm assay, in PBS buffer, pH7.4, 25 °C.

Enzyme	k_{cat} (s^{-1})	$K_m(\mu M)$	k_{cat} / K_m $(M^{-1}s^{-1})$
WT	0.15 ± 0.004	1.05 ± 0.13	1.4×10^5
D167A	<0.001		
D167E	$k_{obs}=0.00304$		
D167N	<0.001		
E168A	<0.001		
T183A	<0.001		
S171A	<0.001		
H158A	<0.001		

(*Note, it is not proper to continue using the DTNB assay here, because of the large background of enzyme reacting with DTNB when using high concentration ([E]>1 μM). The 232nm assay works well for wild type hTHEM5, get a consisted result compared to DTNB assay, so it is proper to use it for mutant kinetic test).*

4.3.7 Subcellular location determination

Confocal microscope cell imaging showed specific mitochondrial location of hTHEM5-GFP and a relative distributive location of the (Δ32)-hTHEM5-GFP, which suggests that hTHEM5 localizes at the mitochondria because of its leading MLS. While the exact sub-mitochondria location still need further investigation.

| Nuclei | Mitochondria | GFP | Merge |
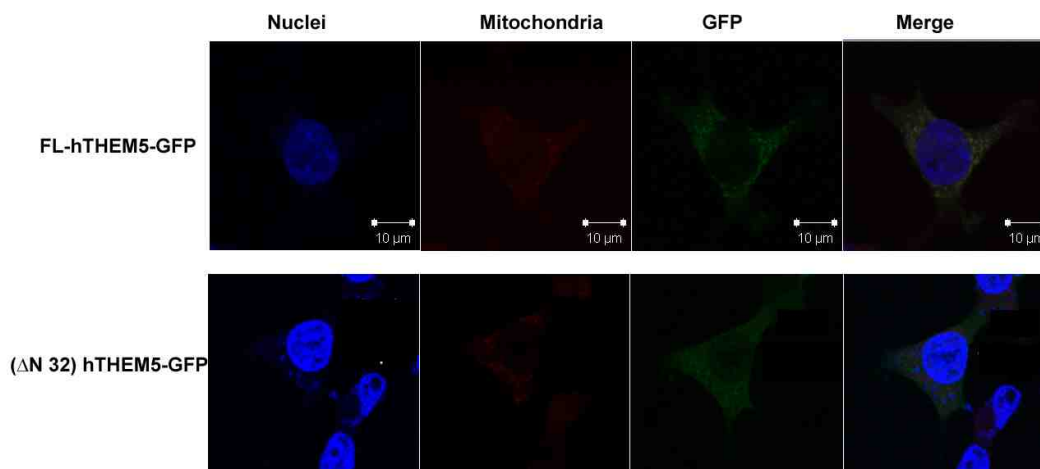
Figure 4.17 hTHEM5 Mitochondria localization imaging: top panel is HEK293T cell transfected by FL-hTHEM5-GFP, lower panel is HEK293T cells transfected by N-terminal truncate: (Δ32)hTHEM5-GFP.

Mitochondria isolation experiment also showed that hTHEM5 mostly is in the mitochondria fraction.
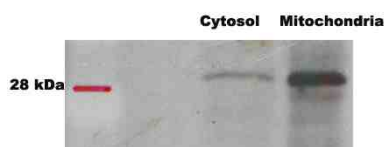
Figure 4.18 Western blot (anti-Xpress) of cell lysate after mitochondria isolation experiment: left lane: cytosol fraction, right lane: mitochondria fraction. hTHEM5 was seen mostly in the mitochondria fraction.

4.4 Discussion and Future Work

The full-length hTHEM5 was expressed in HEK 293T cells at a high level compared to that observed for the hTHEM4. The N-terminal truncate hTHEM5 (Δ40) was constructed and successfully expressed in *E. coli* for protein production, which

127

allowed structure-activity analysis. The hTHEM5 (Δ40) X-ray structure depicts essentially the same active site observed for hTHEM4, and no features that we recognize which might explain the difference in expression level in transfected HEK 293T cells. Interestingly, the in vitro kinetic studies carried out with hTHEM5 (Δ40) showed a similar substrate specificity profile, yet a 100-fold drop in k_{cat}. The experiment to determine the cellular location of hTHEM5 in transfected HEK 293T cells indicates the specific mitochondrial location of hTHEM5-GFP.

The research on the mitochondrial thioesterase hTHEM5 (247 amino acid) has not been completed yet, the understanding of the biological function of it is still not clear. There is many tasks need to work on in future: 1. Determination of the sub-mitochondria location by using digitonin permeabilization process, 2. Continue looking for the biological substrate for hTHEM5, mitochondria Acyl Carrier Protein may be one target, and 3. Identify if there is post-translational modification.

Reference

1. Miyazawa, S.,Furuta, S.,Hashimoto, T.(1981) Induction of a novel long-chain acyl-CoA hydrolase in rat liver by administration of peroxisome proliferators. Eur J Biochem. 117, 425-30.

2. Yamada, J., Matsumoto, I., Furihata, T., Sakuma, M., Suga, T. (1994) Purification and properties of long-chain acyl-CoA hydrolases from the liver cytosol of rats treated with peroxisome proliferator. Arch. Biochem. Biophys. 308(1), 118-25.

3. Bunkoczi, G., Pasta, S., Joshi, A., Wu, X.Q., Kavanagh, K.L., Smith, S., Oppermann, U. (2007) Mechanism and Substrate Recognition of Human Holo ACP Synthase. Chemistry and Biology, 14, 1243-1253

4. Joshi, A.K., Zhang, L., Rangan, V.S., Smith, S. (2003) Cloning, expression, and characterization of a human 4'-phosphopantetheinyl transferase with broad substrate specificity. J. Biol. Chem. 278, 33142-149.

5. Smith, R.H., Powell, G.L. (1986) The critical micelle concentration of some physiologically important fatty acyl-coenzyme A's as a function of chain length. Archives of Biochemistry and Biophysics. 244(1), 357-360.

6. Constantinides, P.P., Steim, J.M. (1985) Physical properties of fatty acyl-CoA: critical micelle concentrations and micelle size and shape. J. Bio. Chem. 260(12), 7573-80.

CHAPTER FIVE

THE *E. COLI.* HOTDOG-FOLD THIOESTERASE YCIA

This chapter is adapted from the published paper: Divergence of Function in the Hotdog Fold Enzyme Superfamily: The Bacterial Thioesterase YciA. Zhuang Z, Song F, Zhao H, Li L, Cao J, Eisenstein E, Herzberg O, Dunaway-Mariano D. *Biochemistry* 2008, 47(9), 2789-2796. The author did the experiment of EcYciA.

5.1 Introduction

Thioesters play a central role in the cells where they participate in metabolism, membrane synthesis, signal transduction and gene regulation (*1*). The carboxylic acid components of biological thioesters are metabolites of varied size, shape and polarity. They are converted to thioesters by ligases for the purpose of solubility, transport, signaling, or activation for reaction in biosynthetic or biodegradation pathways. The naturally occurring thiols include coenzyme A (CoA), glutathione, the pantetheine unit of the holoacyl carrier protein (ACP), or the cysteine residue of a protein. Thioesters are reverted to the thiol and carboxylic acid components by hydrolysis catalyzed by thioesterases. Thioesterases have primarily evolved within the α/β-fold hydrolase enzyme superfamily (*2*) and the hotdog fold enzyme superfamily (*3*). The conserved fold of the hotdog-fold superfamily proteins consists of a five-stranded anti-parallel β-sheet wrapped around an elongated α-helix. This topology is reminiscent of a hotdog "bun" wrapping around a "sausage", hence the name hotdog-fold (*4*).

Following the discovery of the first hotdog-fold thioesterase (viz. the 4-

hydroxybenzoyl-CoA thioesterase from *Pseudomonas* sp. strain CBS3) (*5*) we embarked on a long-term study of the diversification of function within the hotdog-fold thioesterase family (*6-14*). During the course of this work we have discovered that: (i) the hotdog-fold is conserved despite the low amino acid sequence conservation within the family, (ii) divergent evolution within this family is based on two rather than one catalytic scaffold (*6*), (iii) there is no conservation of a set of core catalytic residues and instead, one carboxylate residue (Asp or Glu located at either of two positions of the catalytic scaffold (*6, 12*) operates within a variety of sequence contexts, and (iv) the absence of well defined, desolvated substrate binding pockets is responsible for low substrate specificity (*13*). These family features combine in such a way to severely impede a sequence based, and even a three-dimensional structure based, approach to function assignment. It is for this reason that we have focused our attention on a set of hotdog thioesterases that are produced by the well-characterized organism, *Escherichia coli* so that we may use gene context, as well as the knowledge of metabolic pathways and known protein components of cellular processes to guide the discovery of thioesterase biochemical and biological function.

There are seven different hotdog thioesterases encoded by the *E.coli* genome and each has a known X-ray structure. However, only one of these thioesterases has been assigned a biological function. It is PaaI (PDB entry code 2fs2; Swiss-Prot P76084), which we discovered to participate in the phenylacetate degradation pathway to free CoA from the product of the first pathway reaction, phenylacetyl-CoA in the event that downstream pathway enzymes are not present (*12*). The other six hotdog thioesterases are YciA (Swiss-prot P0A8Y8) (PDB 1yli of the *Haemophilus influenzae* homolog HI0827;

Swiss-prot P44886) YbgC (PDB 1s5u; Swiss-prot P0A8Z3), YbaW (PDB 1njk; Swiss-prot P77712), YbdB (PDB 1vh9; Swiss-prot P0A8Y8), YdiI (PDB 1vi8; Swiss-prot P77781) and the double domain hotdog thioesterase TEII (PDB 1c8u; Swiss-prot P0AGG2).

Here, we report data that define the substrate range and CoA-directed regulation of YciA activity in *E. coli*. Also, we present the results from a bioinformatics study of the phylogenic distribution of YciA and the variation in *yciA* genetic context. We conclude that YciA is responsible for the efficient, "seemingly" indiscriminant hydrolysis of cellular acyl-CoA thioesters in a wide range of bacteria, and hypothesize that this activity may support membrane biogenesis. We describe the three dimensional structures of wild type and mutant *H. influenzae* YciA (HI0827), and identify the structural basis for substrate binding, catalytic turnover, and CoA-directed regulation in another biochemistry paper (*15*).

5.2 Experimental

5.2.1 Materials

All oligonucleotide primers and restriction enzymes, and the T4 DNA ligase were purchased from Invitrogen. DNA sequencing was performed by the DNA Sequencing Facility of the University of New Mexico. All biochemicals, including a majority of the acyl-CoAs, were purchased from Sigma. The 4-hydroxybenzoyl-CoA, 4-hydroxyphenylacetyl-CoA and 3- hydroxyphenylacetyl-CoA were prepared as previously described (*12*).

5.2.2 Preparation of Recombinant EcYciA

The gene encoding YciA from *E. coli* (Swiss-Prot entry P0A8Z0) was amplified by PCR using the clone 10798D-5 obtained from ATCC (Manassas, VA) and *PfuTurbo* DNA polymerase (Stratagene). Primers containing restriction endonuclease cleavage sites *Nde* I and *Xho* I were used. The amplification protocol employed 30 cycles of denaturation at 95 °C, annealing at 55 °C, and elongation at 72 °C. The pET-23b vector (Novagen), which was cut with the restriction enzymes 5'-*Nde* I and 3'-*Xho* I (C-terminal His tag), was ligated to the isolated gene. The ligation product was used to transform *E.coli* JM109 competent cells (Stratagene). Plasmid was prepared using a QIAprep Spin Miniprep Kit (Qiagen). The gene sequence was confirmed by DNA sequencing. The recombinant plasmid was used to transform BL21 (DE3) competent cells (Novagen). The transformed cells were grown at 32 °C in 1.5 L Luria broth (LB) containing 50 μg/ml carbenicillin to an $OD_{600nm} \sim 0.8$ and then induced using 0.4 mM IPTG until an OD_{600nm} ~2.0 was reached. The cells were harvested by centrifugation and the 10 gm cell pellet was suspended in100 mL ice-cold lysis buffer (50 mM NaH_2PO_4, 300 mM NaCl, pH 8.0, 10 mM imidazole, 1 mM DTT) containing 10 μL 0.1 mM of the protease inhibitor PMSF, passed through a French press at 1200 PSIG and then centrifuged at 48000 × g and 4 °C for 30 min. The supernatant was loaded onto a Ni-NTA Agarose column (QIAGEN, 25 mL) pre-equilibrated with the lysis buffer. The column was washed with 500 mL of 50 mM NaH_2PO_4/300 mM NaCl /50 mM imidazole/1 mM DTT (pH 8.0) and then the YciA was eluted with 200 mL of 50 mM NaH_2PO_4/300 mM NaCl /250 mM imidazole/1 mM DTT (pH 8.0). The fractions were analyzed by SDS-PAGE and then selectively pooled and concentrated using Centricon (10 kDa, Pall Filtron) at 4 ^{o}C before

loading onto a 2 x 180cm Sephacryl 100 size exclusive column equilibrated with 50 mM

NaH$_2$PO$_4$/50 mM NaCl /10 mM imidazole/1 mM DTT (pH 8.0). The column was eluted

with 50 mM NaH$_2$PO$_4$/50 mM NaCl /10 mM imidazole/1 mM DTT (pH 8.0) at 4 ^{o}C. The

desired fractions were combined and concentrated the yield homogenous EcYciA at 25

mg protein/ gm wet cell.

5.2.3 Determination of the Steady-State Kinetic Constants for YciA Catalyzed Acyl-CoA Thioester Hydrolysis.

Reactions were monitored at 25 °C by measuring the 412 nm absorbance of 5-thio-2-nitrobenzoate formed by reaction of DTNB with the CoA, pantetheinephosphate or Nacetylcysteine liberated from the acyl-CoA, acyl-pantetheinephosphate or acyl-(Nacetyl) cysteine substrate, respectively. Reactions were initiated by adding YciA to assay solutions composed of substrate, DTNB (1 mM), KCl (0.2 M) and 50 mM K+Hepes (pH 7.5) and contained in quartz cuvettes (1 cm light path). The kinetic parameters of Vmax and Km were determined from initial velocity data, measured as a function of substrate concentration, by using equation (1) and KinetAsyst (IntelliKinetics, PA).

$$V = Vmax [A] / ([A] + Km) \text{ eq. (1)}$$

where [A] is the substrate concentration, V is the initial velocity, Vmax is the maximum velocity and Km is Michaelis constant. The reported error was computed for the data fitting. The kcat was calculated from the ratio of Vmax and the total enzyme concentration. The enzyme concentration was determined using the Bradford method.

5.2.4 Determination of Inhibition Constants.

The inhibition constants were determined for YciA inhibitors at pH 7.5 and 25 °C by measuring the initial velocity of YciA catalyzed acyl-CoA thioester hydrolysis as a function of substrate (0.5 to 5 Km) and inhibitor (1 to 3 Kis) concentration. The initial velocity data were analyzed using equation (2) for competitive inhibition or equation 3 for mixed-type inhibition and the computer program KinetAsyst (IntelliKinetics, PA).

$$V = Vmax \ [S] \ / \ [Km \ (1+[I]/Ki) + [S] \ ] \ (2)$$

$$V = Vmax \ [S] \ / \ [Km \ (1+[I]/Kis) + [S] \ (1+[I]/Kii)] \ (3)$$

where V = initial velocity, Vmax = maximum velocity, [S] = substrate concentration, Km=Michaelis constant, [I] = inhibitor concentration and Kis and Kii are the slope and intercept inhibition constants, respectively.

5.2.5 Determination of E. coli Growth Curves

E.coli K-12 strain (BW25113) and the corresponding *yciA*-knock out strain (JW1245) were obtained from the *E. coli* Genetic Stock Center of Yale University. JW1245 cells were grown aerobically at 37 °C in 2 L of LB media containing 15μg/ml kanamycin. BW25113 cells were cultured under the same conditions but without the kanamycin. The optical density of the culture at 600 nm was monitored.

5.3 Results and Discussion

5.3.1 EcYciA Physical Properties

Homogeneous His$_6$-tagged EcYciA was prepared, the SDS-PAGE gel is seen in Figure 5.1. The predicated molecular mass of the His6-tagged EcYciA is 15166 Da, the

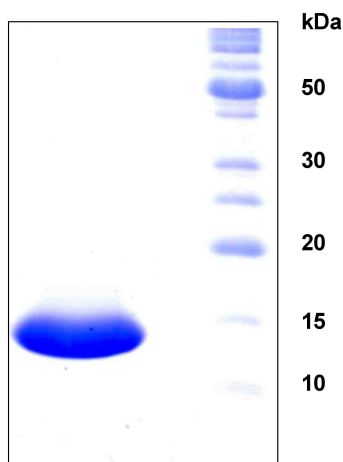mass determined by electronspray ionization mass spectroscopy is 15163 Da.

Figure 5.1 SDS-PAGE of EcYciA

5.3.2 Substrate Specificity

YciA thioesterase activity towards acyl-CoA substrates was determined using steady-state kinetic methods. The kcat and kcat/Km values reported in Table 5.1 reveal a striking combination of high catalytic efficiency and low substrate specificity. Almost all of the kcat/Km values measured are within what might be considered to be a "physiologically relevant" range (*viz*. kcat/Km > 10^4 M^{-1} s^{-1}), displaying for its best substrates kcat/Km values between 1 x 10^5 and 1 x 10^6 M^{-1} s^{-1}, and kcat values between 9 and 16 s-^{1}. The long, medium chain fatty acyl-CoAs are very good substrates.

Table 5.1 Summary of Kinetic test for EcYciA hydrolyzing acyl-CoA at pH 7.5 and 25℃ determined by using DTNB assay

Substrate	$k_{cat}(s^{-1})$	K_m (µM)	k_{cat}/K_m ($M^{-1}s^{-1}$)
Acetyl-CoA	$(5.5\pm0.1)\times10^{-1}$	$(16.7\pm0.4)\times10$	3.29×10^3
n-Butyryl-CoA	6.7 ± 0.4	67.5 ± 1.0	9.9×10^4
n-Decanoyl-CoA	16.4 ± 1.7	12.9 ± 2.9	1.3×10^6
Lauroyl-CoA	9.6 ± 0.6	19.5 ± 2.6	4.9×10^5
Oleoyl-CoA	13.0 ± 0.5	10.9 ± 1.3	1.2×10^6
Isobutyryl-CoA	9.5 ± 0.7	14.9 ± 2.2	6.3×10^5
β-Methylcrotonyl-CoA	$(1.0\pm0.1)\times10^{-1}$	$(28.6\pm4.9)\times10$	3.66×10^2
4-HBA-CoA	$(6.2\pm0.2)\times10^{-2}$	24.7 ± 1.9	2.4×10^3
Phenylacetyl-CoA	9.4 ± 0.7	15.6 ± 3.1	6.0×10^5

5.3.3 Product Inhibition

The high catalytic efficiency of YciA towards most cellular acyl-CoA metabolites presents a potential danger to the cell. We therefore looked for known cell export sequence motifs within the YciA gene but found none. Likewise, no evidence that YciA is localized at the cell membrane by a transmembrane helix or a palmitoyl appendage was found. Assuming that YciA is a cytoplasmic enzyme, it follows that there must exist some form of cellular regulation to prevent YciA from hydrolyzing all of the acyl-CoA metabolites present in the cytoplasm. CoA product inhibition was suggested by the

observation that YciA is purified from the cell with CoA bound. The effectiveness at which CoA serves as a feedback inhibitor was evaluated. The time course for the catalyzed hydrolysis of 4-hydroxybenzoyl-CoA measured in the presence of DTNB reflects a higher rate and product yield than that measured in the absence of DTNB (Figure 5.2).
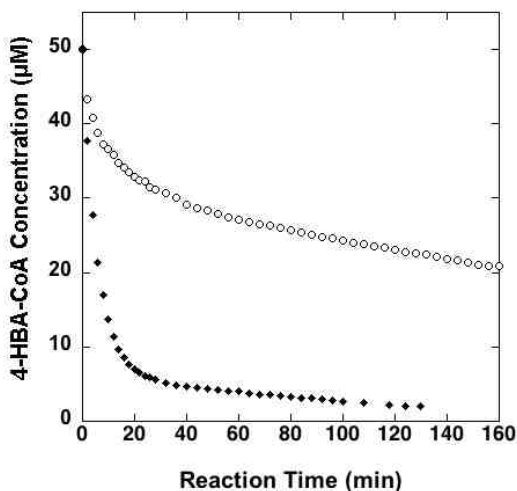

Figure 5.2 Time course of hydrolysis of 4-HBA-CoA by YciA at pH 7.5 and 25 °C. Direct assay (○), DTNB continuous assay (◆).

5.3.4 YciA and E. coli Cell Survival under Optimal Aerobic Growth Conditions.

To determine whether YciA is required for *E. coli* survival we measured the growth curves for wild-type *E. coli* K-12 and for the corresponding *yciA*-knock out mutant strain. The growth curves (Figure 5.3) are identical. Thus, under optimal growth conditions the absence of YciA does not appear to impede the rate of cell multiplication. This result is consistent with a previous study (*16*), which showed that a *Shigella flexneri* mutant strain lacking a functional septation protein gene displayed the abnormal growth

phenotype (filament formation) only under *in vivo* conditions (i.e., inside cultured mammalian host cells) or under oxidative-stress inducing (*in vivo*-like) *in vitro* conditions.
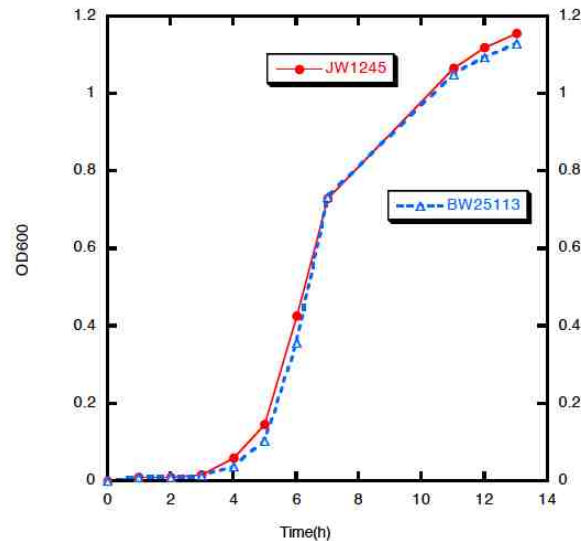

Figure 5.3 A plot of the culture optical density at 600nm vs the cultivation time (h) measured for the aerobic growth of the wild-type *E. coli* K-12 strain (BW25113)(blue) and the *E. coli* yciA-knockout strain JW1245 (red) in LB media at 37 °C.

5.3.5 EcYciA Phylogenic Distribution and Gene Context Analysis

In *E. coli,* the genes *yciA, yciB, yciC and yciI* are juxtaposed, they are not located adjacent to the peptidoglycan remodeling genes (Figure 5.4). Instead, the gene that encodes cardiolipin synthase is in the neighborhood. Cardiolipin synthase functions to increase the level of cardiolipin in the cell membrane, which in turn results in increased membrane fluidity. Membrane fluidity affects the function of integral membrane proteins (*17*). Cardiolipin also functions to organize the membrane protein partners, such as the proteins of a membrane transporter, into a functional complex (*18*) and to recruit proteins

to the poles and septa of the inner membrane (*19*). Notably, among these recruited proteins are the cell cycle and septation peripheral proteins DnaA and MinD. The *E. coli* cluster of *yciA, yciB, yciC and yciI* genes is in register with genes on the opposing DNA strand which encode the oppA-F protein transporter, tonB the periplasmic membrane linker protein, and the outer membrane protein yciD. Together, this cluster encodes a protein export system that is used for protein secretion.

YciI is a small cytoplasmic protein that has a structure suggestive of an enzyme, however we have not yet been successful in identifying it physiological substrate (*20*). The gene *yciI* is frequently coupled with *yciB* with or without the inclusion of *yciA*. YciI is observed as a fusion protein with BolA in *Coxiella burnetii*. BolA is required for normal cell morphology under conditions of stress and it has been suggested that it is a regulator of cell wall biosynthesis and that is a disulfide reductase (*21-23*).

In summary, YciA occurs in a variety of gene contexts, the emerging common theme is suggestive of YciA involvement in the biogenesis of the inner membrane for division or insertion of transport proteins.
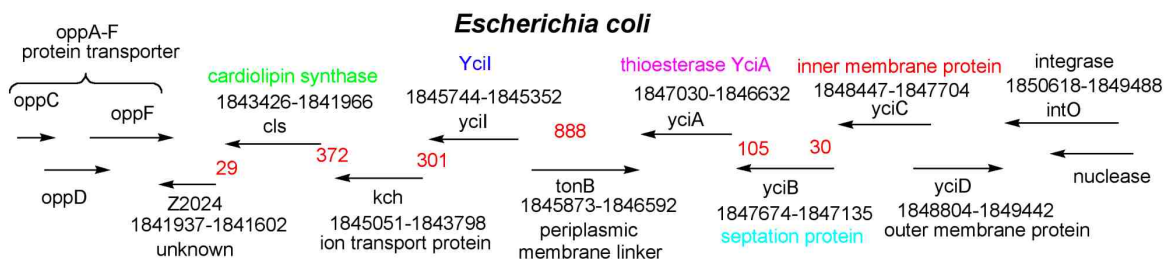

Figure 5.4 Gene context of EcYciA

5.3.6 Divergence of Function among E. coli Hotdog Thioesterases.

The *E.coli* cell produces seven hotdog thioesterases. In what way(s) does YciA

140

distinguish itself from the other six thioesterases? Considering the gene context, *ybdB* is a member of the enterobactin based iron acquisition gene locus, *ydiI* is a member of the cysteine sulfur recruitment/iron-sulfur cage synthesis gene cluster (*viz,* the suf operon), *ybgC* is a member of the Pal-tol septation ring gene locus, *ybaW* is a member of a peptide generation/export gene locus, *tesB* (encodes TE-II) is not located in a recognizable function gene locus, and *paaI* is a member of the phenylacetate degradation operon.

The substrate ranges of the *E. coli* hotdog-fold thioesterases also differ. YbgC and YbdB have low hydrolytic activity with acyl-CoAs (*7, 24*) and protein-protein binding partner analyses (*24-25*) suggest that the physiological substrates are acylated-pantetheine-modified proteins. PaaI hydrolyzes phenylacetyl-CoA and its mono and dihydroxy ring analogs, but not alphatic acyl-CoAs (*12*). The substrate range of YbaW and YdiI have not, to our knowledge, been reported. The substrate range of TE-II is, like that of YciA, reported to be broad with regard to acyl-CoA thioester metabolites, but unlike YciA includes acylated ACPs (*26*). It is clear that each of the seven *E. coli* hotdog-fold thioesterases performs a unique biological function. Our goal is to determine the biological functions of these thioesterases and to identify the elements in their structures that support these functions.

References

1. Hunt, M. C., and Alexson, S. E. (2002) The role Acyl-CoA thioesterases play in mediating intracellular lipid metabolism. *Prog Lipid Res* 41, 99-130.

2. Nardini, M., and Dijkstra, B. W. (1999) Alpha/beta hydrolase fold enzymes: the family keeps growing. *Curr Opin Struct Biol* 9, 732-7.

3. Dillon, S. C., and Bateman, A. (2004) The Hotdog fold: wrapping up a superfamily of thioesterases and dehydratases. *BMC Bioinformatics* 5, 109.

4. Leesong, M., Henderson, B. S., Gillig, J. R., Schwab, J. M., and Smith, J. L. (1996) Structure of a dehydratase-isomerase from the bacterial pathway for biosynthesis of unsaturated fatty acids: two catalytic activities in one active site. *Structure* 4, 253-64.

5. Benning, M. M., Wesenberg, G., Liu, R., Taylor, K. L., Dunaway-Mariano, D., and Holden, H. M. (1998) The three-dimensional structure of 4-hydroxybenzoyl-CoA thioesterase from *Pseudomonas* sp. strain CBS-3. *J Biol Chem* 273, 33572-9.

6. Thoden, J. B., Zhuang, Z., Dunaway-Mariano, D., and Holden, H. M. (2003) The structure of 4-hydroxybenzoyl-CoA thioesterase from *Arthrobacter* sp. strain SU. *J Biol Chem* 278, 43709-16.

7. Zhuang, Z., Song, F., Martin, B. M., Dunaway-Mariano, D. (2002) The YbgC protein encoded by the ybgC gene of the tol-pal gene cluster of *Haemophilus influenzae* catalyzes acyl-coenzyme A thioester hydrolysis. *FEBS Lett.* 516, 161-3.

8. Thoden, J.B., Holden, H.M., Zhuang, Z., Dunaway-Mariano, D (2002) X-ray crystallographic analyses of inhibitor and substrate complexes of wild-type and mutant 4-hydroxybenzoyl-CoA thioesterase. *J Biol Chem*. 277, 27468-76.

9. Zhuang, Z., Song, F., Zhang, W., Taylor, K., Archambault, A., Dunaway-Mariano, D.,

Dong, J., Carey, P.R. (2002) Kinetic, Raman, NMR, and site-directed mutagenesis studies of the *Pseudomonas* sp. strain CBS3 4-hydroxybenzoyl-CoA thioesterase active site. *Biochemistry* 41, 11152-60.

10. SU Zhuang, Z., Gartemann, K. H., Eichenlaub, R., Dunaway-Mariano, D (2003) Characterization of the 4-hydroxybenzoyl-coenzyme A thioesterase from *Arthrobacter* sp. strain. *Appl. Environ. Microbiol.* 69, 2707-11.

11. Zhuang, Z., Song, F., Takami, H., and Dunaway-Mariano, D. (2004) The BH1999 Protein of Bacillus halodurans C-125 Is Gentisyl-Coenzyme A Thioesterase. *J. Bacteriol.* 186, 393-399.

12. Song, F., Zhuang, Z., Finci, L., Dunaway-Mariano, D., Kniewel, R., Buglino, J.A., Solorzano, V., Wu, J., Lima, C.D (2006) Structure, function, and mechanism of the phenylacetate pathway hot dog-fold thioesterase PaaI. *J. Biol. Chem.* 281,11028-38.

13. Cheng, Z., Song, F., Shan, X., Wei, Z., Wang, Y., Dunaway-Mariano, D., Gong, W (2006) Crystal structure of human thioesterase superfamily member 2. *Biochem. and Biophys. Res.Comm.* 349, 172-177.

14. Song, F., Zhuang, Z., Dunaway-Mariano, D. (2007) Structure-activity analysis of base and enzyme-catalyzed 4-hydroxybenzoyl coenzyme A hydrolysis. *Bioorg. Chem.* 35, 1-10.

15.Willis, M.A., Zhuang, Z., Song, F., Howard, A., Dunaway-Mariano,D. Herzberg, O. (2008) Structure of YciA from *Haemophilus influenzae* (HI0827), a hexameric broad specificity acyl-CoA thioesterase. Biochemistry. 47(9), 2797-805.

16. Mac Siomoin, R. A., Nalata, N, Murai, T, Yoshikawa, M, Tsuji, H, Sasakawa, C. (1996) Identification and characterization of ispA, a *Shigella flexneri* chromosomal gene

essential for normal in vivo cell division and intercellular spreading. *Molecular Microbiology* 19, 599-09.

17. Bernal, P., Segura, A. and Ramos, J-L (2007) Compensatory role of the cis-trans-isomerase and cardiolipin synthase in the membrane fluidity of *Pseudomonas putida* DOT-T1E *Environmental Microbiology* 9, 1658-1664

18. Mileykovskaya, E. (2007) Subcellular localization of Escherichia coli osmosensory transporter ProP: focus on cardiolipin membrane domains. *Molecular Microbiology* 64, 1419-1422

19. Romantsov T, Helbig S, Culham DE, Gill C, Stalker L, Wood JM. (2007) Cardiolipin promotes polar localization of osmosensory transporter ProP in Escherichia coli. *Mol Microbiol*. 64,1455-65.

20. Structure of YciI from Haemophilus influenza (HIO828) reveals a ferredoxin-like α/β-fold with a histidine/aspartate centered catalytic site (2005) Willis, M.A, Song, F., Zhuang,Z., Krajewski, W., Chalamasetty, V. R , Reddy, P., Howards, A. Dunaway-Mariano, D. Herzberg, O. *Proteins* 59, 648-652.

21. Santos, J. M, Freire P, Vincente, M. and Arraiano C. M. (1999) The stationary-phase morphogene *bolA* from *Escherichia coli* is induced by stress during early stages of growth. *Mol. Microbiology* 32, 789-798.

22. Santos, J. M., Lobo, M., Matos, A.P. De Pedro, M. A., and Arraiano C. M. (2002) The gene *bolA* regulates *dacA* (PBP5), *dacC* (PBP6) and *ampC* (AmpC), promoting normal morphology in *Escherichia coli*. *Mol. Microbiology* 45, 1729-1740.

23. Huynen, M.A., Spronk, C.A.E.M., Gabaldon, T, Snel, B. (2005) Combining data from genomes, Y2H and 3D structures indicates that BolA is a reductase interacting with

a glutaredoxin. *FEBS Lett* 579, 591-596.

24. Gully, D., Bouveret, E.A. (2006) Protein network for phospholipid synthesis uncovered by a variant of the tandem affinity purification method in Escherichia coli. Proteomics. 6,282-93.

25. Leduc, D., Battesti, A., Bouveret, E. (2007) The hotdog thioesterase EntH (YbdB) plays a role in vivo in optimal enterobactin biosynthesis by interacting with the ArCP domain of EntB. J Bacteriol. 189,7112-26.

26. Naggert J, Narasimhan ML, DeVeaux L, Cho H, Randhawa ZI, Cronan JE Jr, Green BN, Smith S. (1991) Cloning, sequencing, and characterization of Escherichia coli thioesterase II. J Biol Chem. 266, 11044-50

APPENDIX

A1: Structure of small molecules

Coenzyme A (CoA):
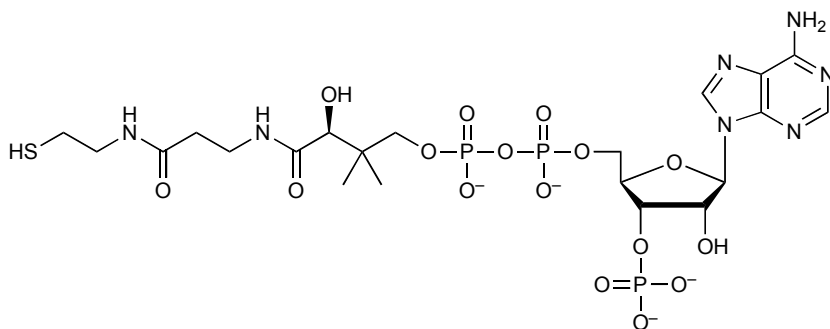
Acetyl-CoA:
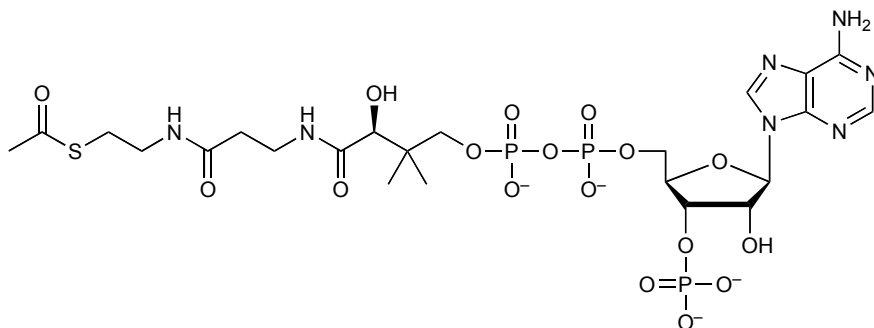
n-propionyl-CoA: CH_3CH_2CO-CoA

n-Butyryl-CoA: $CH_3CH_2CH_2CO$-CoA

Hexanoyl-CoA: $CH_3CH_2CH_2CH_2CH_2CO$-CoA

Octanoyl-CoA: $CH_3CH_2CH_2CH_2CH_2CH_2CH_2CO$-CoA

Decanoyl-CoA: $CH_3CH_2CH_2CH_2CH_2CH_2CH_2CH_2CH_2CO$-CoA

Lauroyl-CoA: CH_3-$(CH_2)_{10}$-CO-CoA

Myristoyl-CoA: CH_3-$(CH_2)_{12}$-CO-CoA

Palmitoyl-CoA: CH_3-$(CH_2)_{14}$-CO-CoA

Stearoyl-CoA: CH$_3$-(CH$_2$)$_{16}$-CO-CoA

Oleoyl-CoA: CH$_3$-(CH$_2$)$_7$-CH=CH-(CH$_2$)$_7$-CO-CoA

Arachidonoyl-CoA: CH3-(CH$_2$)$_4$-(CH=CH-CH$_2$)$_4$-CH$_2$CH$_2$CO-CoA
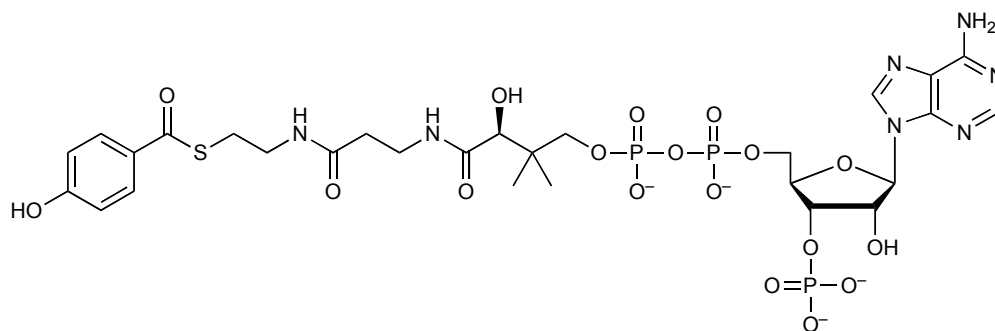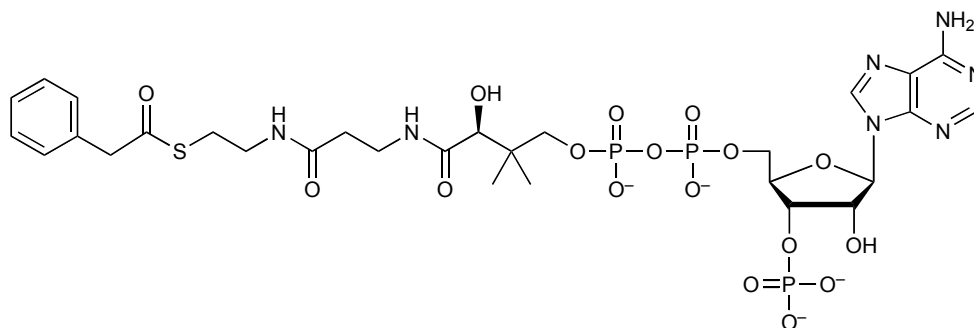
Isobutyryl-CoA:
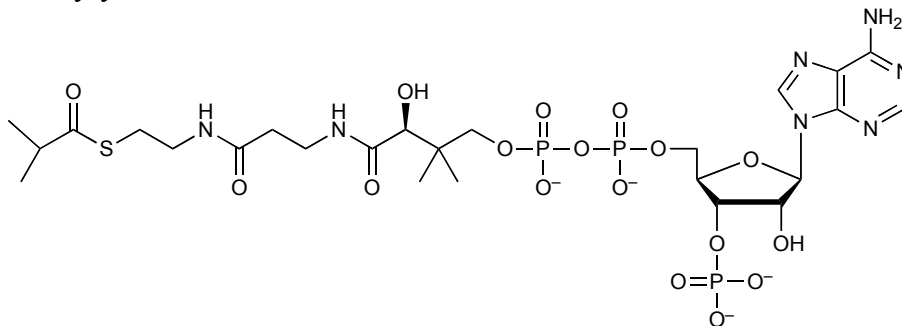
Succinyl-CoA:
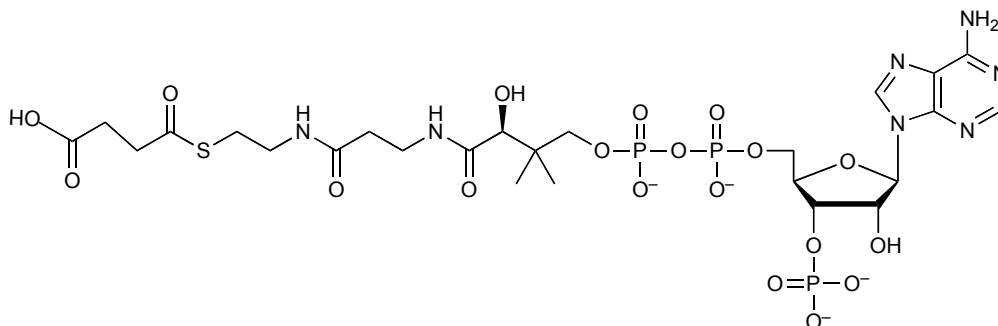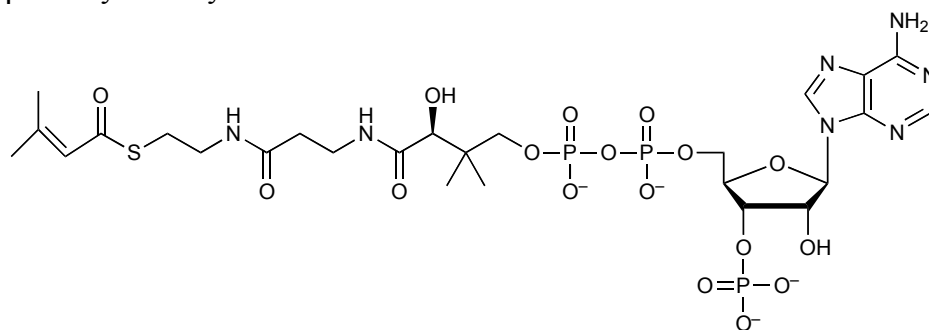
3-HPA-CoA:
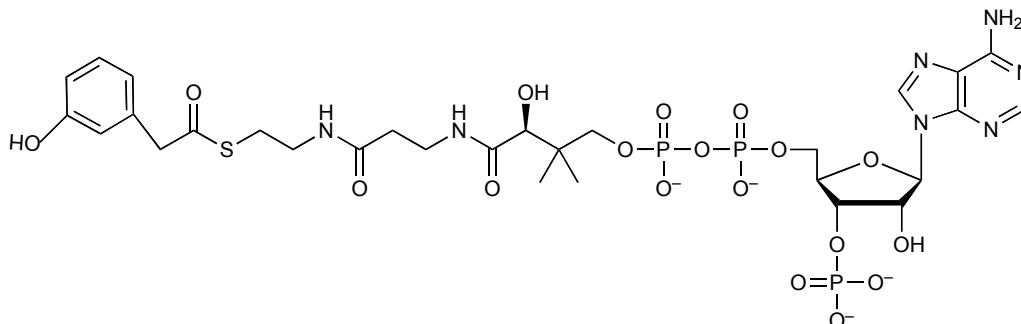
2-HBA-CoA:
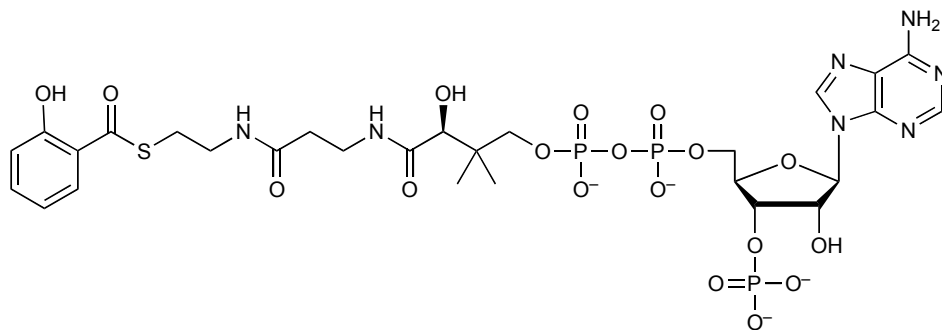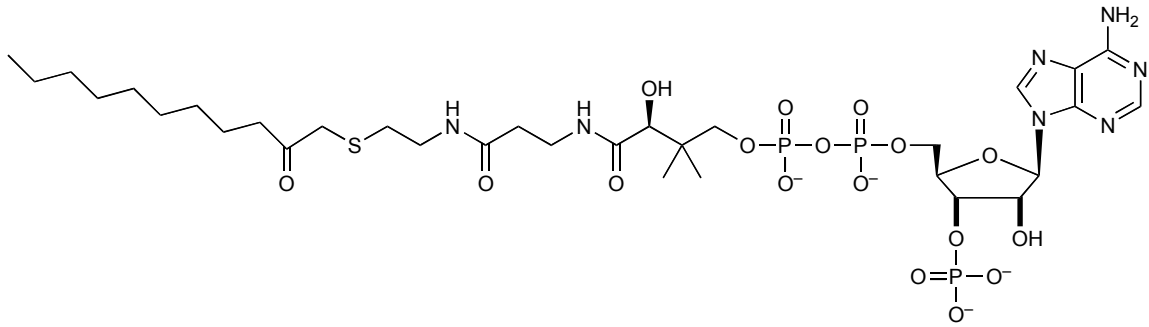

4-HBA-CoA:

Phenylacetyl-CoA:
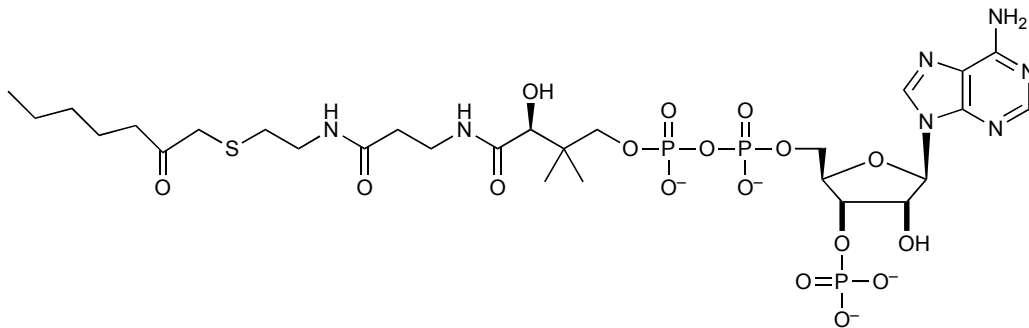

β-Methylcrotonyl-CoA:

Undecan-2-one-CoA:

Hexyl-CoA:

A2: List of Constructs

Full length hTHEM4: His$_6$-hTHEM4 (pET14b vector)

hTHEM4(Δ39): (-39)hTHEM4-His$_6$ (pET 23a vector)

Full length hTHEM5: hTHEM5-His$_6$ (pET 23b vector)

hTHEM5(Δ40): (-40)hTHEM5-His$_6$ (pET23a vector)

His$_6$-MBP-Akt1(pHM6g.TM1457 vector)

Human cell line expression:

hTHEM4-His$_6$ (pcDNA3.1 vector), hTHEM4(L17R)-His$_6$(pcDNA3.1 vector)

His-Xpress-hTHEM4(pcDNA4 vector), EGFP-hTHEM4(pEGFP-N1 vector)

hTHEM5-His6 (pcDNA3.1 vector), His-Xpress-hTHEM5 (pcDNA4 vector)

hTHEM5-GFP(pcDNA3.1 CT-GFP vector), hTHEM5(Δ32)-GFP